# BIOCHEMICAL AND SINGLE-MOLECULE FLUORESCENCE CHARACTERIZATION OF MUTS AND MUTS HOMOLOG PROTEIN-DNA INTERACTIONS

Vanessa Carolyn DeRocco

A dissertation submitted to the faculty of the University of North Carolina at Chapel Hill in partial fulfillment of the requirements for the degree of Doctor of Philosophy in the Department of Chemistry.

Chapel Hill
2012

Approved by:

Dr. Dorothy Erie

Dr. James Jorgenson

Dr. Chris Fecko

Dr. Tom Kunkel

Dr. Nancy Thompson

# ABSTRACT

VANESSA CAROLYN DEROCCO: Biochemical and single-molecule fluorescence characterization of MutS and MutS homolog protein-DNA interactions
(Under the direction of Dr. Dorothy A. Erie)

MutS and MutS homologs are the proteins within the prokaryote and eukaryote DNA mismatch repair pathways that are the responsible for recognizing single base-base mismatches or insertion/deletion errors in newly replicated DNA. Specific interactions between MutS and these DNA defects trigger a cascade of protein-protein interactions that ultimately results in repair of the DNA error. Mutations in the homologs of the MutS and MutL repair proteins involved the recognition and initiation of post replicative DNA mismatch repair are associated with ~80% of Hereditary Nonpolyposis Colorectal Cancer (HNPCC) occurrences. The mechanism by which MutS recognizes mismatch DNA and initiates of downstream repair is not well understood. In this dissertation, I present biochemical and single molecule fluorescence studies of *Thermus aquaticus (Taq)* MutS as well as human and yeast MutS heterodimer homologs (hMSH2-MSH6 and yMsh2-Msh6) protein-DNA interactions in an effort to better understand DNA mismatch recognition and repair.

Single molecule fluorescence methodologies were employed to compare the MutS-DNA interactions of wild type *Taq* MutS with a mutant of *Taq* MutS, E41A. Previous work has shown that *Taq* MutS adopts a complex series of conformations when interacting with mismatch DNA where a bent state and an unbent state being the

dominant states. In this work, the kinetics of interconversion among bending states was determined to vary widely for different mismatches. Further, the E41A mutant, which is known to have specific deficiencies in repair capability, demonstrates altered DNA bending kinetics on DNA mismatches that correlate with its repair deficiencies.

Despite structural similarities, the biochemical properties of prokaryotic MutS and eukaryotic MSH2-MSH6 (MutSα) have been shown to vary. Characterization of MutSα-DNA interactions has been limited. In order to compare the prokaryote and eukaryote, the protein-DNA interactions of wild type human MutSα (hMutSα) protein as well as two HNPCC separation-of-function mutants, $MSH2^{WT}$-$MSH6^{T1219D}$ and $MSH2^{G674A}$-$MSH6^{WT}$ were characterized. In contrast to *Taq* MutS-DNA interactions, I observed few hMutSα-DNA conformational changes suggesting a difference in the mechanism of MMR initiation between prokaryotes and eukaryotes. I further determined singular trapped conformational states for each HNPCC mutant that may be linked to MMR deficiency for each.

To my husband, Jason,
for all of his love, support, and understanding,

To Rose,
for her strength,

&

To my wonderful parents, Robert and JoAnn,
for opening my eyes to the world around me.

# ACKNOWLEDGEMENTS

First and foremost, I'd like to thank my advisor, Dorothy Erie. No one could ask for a better student-mentor relationship. She has always supported every scientific and professional decision I have made as her student. She has given me the freedom to pursue the questions that I thought were most interesting even if that meant brief and often fruitless obsessions or insane quests to figure out why yeast cells hate me. Dorothy has been there for some of the biggest, saddest, and scariest events of my life and remained supportive through all of it. Most importantly, she's taught me how to be a scientist. I cannot thank her enough for taking a chance on me. I'd like to think it has worked out for the both of us!

Enough cannot be said about the amazing people I have worked with in my graduate career. I'd like to thank my collaborators, Keith Weninger and Peggy Hsieh. Keith opened his lab to me and allowed me to monopolize his microscopes in my first few graduate years. I always felt that I had two advisors with Keith and Dorothy pushing me on. Peggy gave me the opportunity to collaborate with her on the human protein experiments. It has truly been a pleasure and a great learning experience working together.

Thank you to all of my coworkers – past and present- for their every contribution to my education. To Lauryn, Liz, Erika, and Scott – the four of you were central in my acclimating to life as a graduate researcher. You showed me the ropes and helped

establish the basis for everything I have learned. Thank you all for continuing to allow me bounce ideas and questions off of you regardless of where you have moved away to. I thank a special alumna of our lab, Hong, for taking the time to mentor me and do her best to advise me in my professional development. You are going to be an excellent PI in your own right, Hong! I thank Cherie for contributing her programming expertise at every turn. She made data analysis far less painful than it was when I first started this project and has always been ready to tweak programs based on analysis needs at the time. To Marc, Jackie, Dong, Dan, Matt, Kira, Jake, Zimeng, and Danielle- thank you for all of the Fridays. A special thanks to Jackie, Matt, Kira, and Jake for reading and editing manuscripts, chapters, CVs, and cover letters. Your input and discussions have been very much appreciated. I cannot thank you enough. You all have helped keep me sane.

Thank you to the Weninger Lab - particularly to Brandon, John, Trevor and Ruoyi – for making me feel a part of their lab and for all of their helpful discussions. I thank the Hsieh Lab – especially Hui and Chunwei – for being no more than an e-mail away for questions and requests.

Thank you to the many people who have contributed their time, expertise, and instrumentation to make this body of work possible. Dr. Keith Weninger and the Weininger Lab; Dr. Peggy Hsieh and the Hsieh Lab; Dr. Tom Kunkel and the Kunkel Lab; Dr. Ashtosh Tripathy and the UNC Macromolecular Interactions Facility where I spent many hours on the fluorimeter; Dr. Nancy Thompson and the Thompson Lab for showing me how to the make lipid membrane surfaces on my slides; Dr. Gary Pielak and the Pielak Lab; Dr. Kevin Weeks and the members of the Weeks lab; and the UNC Department of Chemistry.

A very special thank you to my friends on the eighth floor. To Jen, Phil, Jake, and Nate for your ever-constant moral support, cynic humor, and often needed comic relief. You have helped make the labors of graduate school that much more bearable. I have learned entirely too much about RNA and RNA structure from you all, and somehow I enjoyed it. How strange!

Kady-Ann, Kevin, Brent, and Brad – there are no words. It is not often one finds friends as wonderful as you. You are my family here in North Carolina.

My wonderful husband – I would fill pages with the number of thank yous that you are owed. You have supported me throughout my endeavors to earn my doctorate and the bachelor's degree before it. You have shared with me your family whose strength is infinite. You put up with the emotional roller coasters, the stress, the doubts, the fears, and the many, many tears. I cannot express how much I appreciate and love you. Thank you.

Lastly, I would like to thank my family without whose love and support I would not have even aspired to get this far. Thank you to my little brother, Gerrit, for being my constant friend and my hero in so many ways our entire lives. Thank you to my mother and father for instilling in me this need to learn. You have taught me so much about life, love, and the value of a strong, close-knit family. I could never thank you enough.

# TABLE OF CONTENTS

# LIST OF TABLES

# LIST OF FIGURES

# LIST OF ABBREVIATIONS

| | |
|---|---|
| ° | Degree |
| γ | Gamma correction factor |
| $\eta_A$ | Detection efficiency of an acceptor dye |
| $\eta_D$ | Detection efficiency of a donor dye |
| $\theta_1$ | Angle of incidence |
| $\theta_c$ | Critical angle |
| $\lambda$ | Wavelength |
| μM | micromolar |
| $\Phi_A$ | Quantum yield of an acceptor fluorophore |
| $\Phi_D$ | Quantum yield of a donor fluorophore |
| 8-oxo-G:A | 8-oxo-guanine to adenine mismatch |
| *a* | Anisotropy |
| Å | Angstrom |
| ABC | ATP binding cassette |
| ADP | Adenine diphosphate |
| AFM | Atomic force microscopy |
| Ala | Alanine |
| ATP | Adenine triphosphate |
| bp | Base pair |
| BSA | Bovine serum albumin |
| CC | Cytosine-cytosine mismatch |
| *d* | Evanescent field depth |
| dcrx | dichroic |
| DNA | Deoxyribonucleic acid |
| DTT | Dithiothreitol |
| *E* | FRET efficiency |
| *E. coli* | *Escherichia coli* |
| EA | Glutamic acid to alanine mutation |
| EDTA | Ethylenediaminetetraacetic acid |

| | |
|---|---|
| EMCCD | Electron-multiplying charge coupled device |
| Exo I | Exonuclease I |
| Exo VII | Exonuclease VII |
| Exo X | Exonuclease X |
| FA | Phenylalanine to alanine mutation |
| FRAP | Fluorescence recovery after photobleaching |
| FRET | Fluorescence resonance energy transfer |
| $G$ | Correction factor in anisotropy |
| G674A | $hMSH2^{G674A}$-$hMSH6^{WT}$ mutant |
| GG | Guanine-guanine mismatch |
| Glu | Glutamic acid |
| GT | Guanine-thymine mismatch |
| GUI | Graphic user interface |
| HCl | Hydrogen chloride |
| HEPES | 4-(2-hydroxyethyl)-1-piperazineethanesulfonic acid |
| his | Histidine |
| HNPCC | Hereditary non-polyposis colorectal cancer |
| Hz | Hertz |
| $I$ | Intensity |
| $I_{\parallel}$ | Intensity of emission parallel to excitation polarization |
| $I_{\perp}$ | Intensity of emission horizontal to excitation polarization |
| $I_A$ | Emission intensity of an acceptor fluorophore |
| $I_A^{\text{after bleach}}$ | Acceptor emission intensity after a bleach event |
| $I_A^{\text{before bleach}}$ | Acceptor emission intensity before a bleach event |
| $I_D$ | Emission intensity of a donor fluorophore |
| $I_D^{\text{after bleach}}$ | Donor emission intensity after a bleach event |
| $I_D^{\text{before bleach}}$ | Donor emission intensity before a bleach event |
| IDL | Insertion deletion loop |
| $I_{HH}$ | Horizontal polarization intensity after horizontally polarized excitation |
| $I_{HV}$ | Horizontal polarization intensity after vertically polarized excitation |
| $I_{VH}$ | Vertical polarization intensity after horizontally polarized excitation |

| | |
|---|---|
| $I_{VV}$ | Vertical polarization intensity after vertically polarized excitation |
| IRC | Initial recognition complex |
| $I_T$ | Total intensity |
| kcal | Kilocalorie |
| $k_{cat}$ | Catalysis rate constant |
| KCl | Potassium chloride |
| $K_d$ | Dissociation constant |
| m | Meter |
| M | Molar |
| MEF | Mouse embryonic fibroblasts |
| mg | Milligram |
| $MgCl_2$ | Magnesium chloride |
| min | Minute |
| mL | Milliliter |
| MLH1 | MutL homolog 1 |
| Mlh1 | Yeast MutL homolog 1 |
| MLH1-MLH3 | Heterodimer of MutL homologs 1 and 3 |
| Mlh1-Pms1 | Heterodimer of MutL homolog 1 and postmeiotic segregation increased 1 |
| MLH3 | MutL homolog 3 |
| mM | Millimolar |
| mmDNA | Mismatch DNA |
| MMR | Mismatch repair |
| MNNG | N-methyl-N'-nitro-N-nitrosoguanidine |
| mol | Mole |
| MSH2 | MutS homolog 2 |
| MSH2-MSH3 | Heterodimer of MutS homologs 2 and 3 |
| MSH2-MSH6 | Heterodimer of MutS homologs 2 and 6 |
| MSH3 | MutS homolog 3 |
| Msh4 | MutS homolog 4 |
| Msh5 | MutS homolog 5 |
| MSH6 | MutS homolog 6 |

| | |
|---|---|
| MSI | Microsatellite instability |
| MutLγ | Heterodimer of MutL homologs 1 and 3 |
| MutS(α) | MutS and MutSα |
| MutSα | Heterodimer of MutS homologs 2 and 6 |
| MutSβ | Heterodimer of MutS homologs 2 and 3 |
| mW | Milliwatt |
| *n* | Refractive index |
| NA | Numerical aperture |
| NaCl | Sodium chloride |
| NaOAc | Sodium acetate |
| ND | Neutral density filter |
| NHS | *N*-Hydroxysuccinimide ester |
| $Ni^{2+}$ | Nickel (II) |
| NIDDK | National Institute of Diabetes and Digestive and Kidney Diseases |
| NIH | National Institutes of Health |
| nm | Nanometer |
| nM | Nanomolar |
| No. | Number |
| NTP | Nucleotide triphosphate |
| NTR | N-terminal region |
| $O^6$-MeG | O6-methyl guanine |
| $O^6$-MeGT | O6-methyl guanine to thymine mismatch |
| OG | Oregon green |
| *P* | Polarization |
| PAGE | Polyacrylamide gel electrophoresis |
| PALM | Photoactivated light microscopy |
| PCNA | Proliferating cell nuclear antigen |
| PDB ID | Protein database identification |
| Phe | Phenylalanine |
| Phe-X-Glu | Phenylalanine-amino acid-glutamic acid motif |
| PIP box | PCNA interaction peptide |

| | |
|---|---|
| pM | Picomolar |
| Pms1 | Yeast postmeiotic segregation increased 1 |
| PMS2 | Postmeiotic segregation increased 2 |
| PMSF | Phenylmethylsulfonyl fluoride |
| Pol III | Polymerase III |
| Pol α | Polymerase α |
| Pol δ | Polymerase δ |
| r | Radius between donor and acceptor fluorophore |
| RFC | Replication factor C |
| $R_o$ | Förster distance |
| RPA | Replication factor A |
| s | Second |
| *S. cerevisiae* | *Saccharomyces cerevisiae* |
| SDS | Sodium dodecyl sulfate |
| $S_H$ | Detection efficiency of horizontally polarized light |
| smFRET | Single-molecule fluorescence resonance energy transfer |
| SNAP-25 | Soluble NSF Attachment Protein-25 |
| SNARE | Soluble NSF Attachment Protein Receptor |
| SSB | Single stranded DNA binding protein |
| ssDNA | Single stranded DNA |
| $S_V$ | Detection efficiency of vertically polarized light |
| T bulge | Single thymine insert |
| T1219D | $hMSH2^{WT}$-$hMSH6^{T1219D}$ mutant |
| TAMRA | Tetramethylrhodamine |
| *Taq* | *Thermus aquaticus* |
| TCEP | *tris*(2-carboxyethyl)phosphine |
| TDP | Transition density plot |
| TIR | Total internal reflection |
| TIRF | Total internal reflection fluorescence |
| TIRM | Total internal reflection microscopy |
| TMZ | Temozolomide |

| | |
|---|---|
| Tris | tris(hydroxymethyl)aminomethane buffer |
| tris-NTA | tris-nitrilotriacetic acid |
| TROLOX | 6-hydroxy-2,5,7,8-tetramethylchroman-2-carboxylic acid |
| URC | Ultimate recognition complex |
| UV | Ultra-violet |
| UvrD | *E. coli* helicase II |
| WT | Wild type |
| yMutSα | Yeast MSH2-MSH6 |
| *z* | Z direction |

# Chapter 1

## INTRODUCTION

### DNA mismatch repair and single-molecule fluorescence techniques.

## Introduction

The fidelity of any genome relies on the ability of the involved DNA polymerases to correctly replicate the genetic code. Despite the relatively high fidelity of the replicative DNA polymerases (Pol α and Pol δ in eukaryotes and Pol III in prokaryotes), approximately 1 in every $10^7$ base pairs synthesized result in an error being generated in the DNA per round of replication (Kunkel and Erie 2005; Iyer, Pluciennik et al. 2006; Kunz, Saito et al. 2009). These errors consist of base-base mismatches, insertion/deletion loops (IDLs) that result from polymerase slippages, and DNA lesions as a result of damaged templates and nucleotide triphosphate (NTP) pools (Schofield and Hsieh 2003; Iyer, Pluciennik et al. 2006; Hsieh and Yamane 2008; Kunz, Saito et al. 2009). Errors in the genetic code must be corrected to prevent carcinogenesis and disease. Fortunately, there are various repair pathways that post-replicatively repair DNA errors. DNA mismatch repair (MMR), base excision repair, and nucleotide excision repair are the three predominant pathways that deal with DNA mispairs, IDLs, and DNA base damage (Kunz, Saito et al. 2009). After post-replicative repair, the mutation rate of DNA

replication decreases 100 fold to about 1 in every $10^9$ bases synthesized (Schofield and Hsieh 2003; Kunkel and Erie 2005; Iyer, Pluciennik et al. 2006; Jiricny 2006; Kunz, Saito et al. 2009). The focus of this work is to characterize the initiation of one of the three mentioned DNA repair pathways, MMR.

## DNA Mismatch Repair

DNA mismatch repair is a bi-directional, post-replicative process that repairs the afore mentioned base-base mismatches and IDLs (Haber and Walker 1991; Schofield and Hsieh 2003; Kunkel and Erie 2005; Iyer, Pluciennik et al. 2006; Hsieh and Yamane 2008). MMR is a highly conserved process across both prokaryotes and eukaryotes (Table 1.1) (Kunkel and Erie 2005).

### *Prokaryotic Mismatch Repair*

In *Escherichia coli* (*E. coli*), MMR is performed by MMR proteins MutS, MutL, MutH, UvrD, SSB, an exonuclease (Exo I, Exo VII, RecJ, or Exo X), DNA polymerase III (Pol III), and DNA ligase. MutS recognizes an error in newly synthesized DNA and initiates the repair process via an ATP dependent interaction with MutL. Together, MutS and MutL (homodimers in prokaryotes) activate the latent endonuclease activity of MutH, which nicks the DNA at a hemi-methylated GATC site 5' or 3' from the mismatch. In *E. coli*, methylation serves as a strand discrimination signal, where the template DNA strand has been methylated and the daughter strand remains unmethylated until after replication. UvrD helicase unwinds the DNA and the single stranded DNA (ssDNA) binding protein (SSB) binds and stabilizes any ssDNA sections. Exonuclease excises the

**Table 1.1– Mismatch repair proteins and their eukaryotic homologs**

| *E. coli* Protein | Function | Eukaryotic Homolog | Function |
|---|---|---|---|
| **MutS** | Recognizes base-base mismatches and IDLs | MSH2-MSH6 (MutSα) | Recognizes base-base mismatches and 1-2 base IDLs and initiates MMR |
| | | MSH2-MSH3 (MutSβ) | Recognizes 2 or more base IDLs and initiates repair |
| | | MSH4-MSH5 | Involved in meiosis |
| **MutL** | Interacts in an ATP dependent manner with MutS once a mismatch has been identified.<br>Increases MutS specificity<br>Together, MutL and MutS initiate MMR. | MLH1-PMS2 (MutLα)<br>(yeast Mlh1-Pms1) | Interacts in an ATP dependent manner with MutSα once a mismatch has been identified.<br>Together, MutLα and MutSα initiate MMR. |
| | | MLH1-PMS1<br>(MutLβ)<br>(yeast Mlh1-Mlh2) | Human function unknown<br>Minor role in frameshift suppression |
| | | MLH1-MLH3 (MutLγ) | Involved in repair of some IDLs. Functions in meiosis |
| **MutH** | Nicks the daughter strand at a hemi-methylated GATC site | No known homolog | |
| **Helicase II (UvrD)** | Unwinds the DNA for MMR | No known homolog | |

**(Table Continued Next Page)**

| | | | |
|---|---|---|---|
| **β-clamp** | Participates in DNA replication and repair synthesis<br>Increases processivity of Pol III during replication | Proliferating cell nuclear antigen (PCNA) | Participates in DNA replication and repair synthesis<br>Has known interactions with MutSα, MutSβ, MutLα, Exo I, Pol δ, and Pol ε.<br>Recruits MMR proteins to DNA<br>Increases mismatch DNA binding specificity of Msh2-Msh6<br>Participates in DNA excision |
| **γ – δ complex** | Loads β clamp onto the DNA | Replication Factor C<br>(RFC complex) | Loads PCNA onto the DNA |
| **Exo I**<br>**Exo X** | Required for 3′ to 5′ excision | EXO 1 | 5′ to 3′ exonuclease involved in MMR excision<br>Deletion of EXO I results in only a mild mutator phenotype |
| **Exo VII,**<br>**RecJ** | Required for 5′ to 3′ excision | | |
| **Single stranded DNA Binding Protein (SSB)** | Binds ssDNA<br>Prevents self annealing of ssDNA<br>Participates in both DNA synthesis and repair | Replication Protein A (RPA) | Binds ssDNA in the gap<br>Prevents self annealing of ssDNA<br>Participates in both DNA synthesis and repair |
| **Pol III** | DNA polymerase required for DNA resynthesis after excision | Polδ/ε | DNA polymerase required for DNA resynthesis after excision |
| **Ligase** | Seals any nicks in the DNA after resynthesis | Ligase | Seals any nicks in the DNA after resynthesis |

DNA beyond the error. Pol III resynthesizes a new DNA strand to fill the DNA gap, and DNA ligase seals any nicks. This process is bidirectional, meaning that MMR proceeds in both the 5′ to 3′ and the 3′ to 5′ directions (Hsieh 2001; Schofield and Hsieh 2003; Kunkel and Erie 2005; Iyer, Pluciennik et al. 2006; Jiricny 2006; Hsieh and Yamane 2008).

*Eukaryotic Mismatch Repair*

Eukaryotic MMR is conserved from the prokaryotic system with almost every prokaryotic MMR protein having a eukaryotic homolog (Table 1.1). Unlike prokaryotic MMR, however, there is no known MutH or UvrD homologs in the eukaryotic repair pathway. Mismatch recognition responsibilities are shared by the MutS homolog heterodimers, MSH2-MSH6 (MutSα) and MSH2-MSH3 (MutSβ). MutSα is responsible for recognizing base-base mismatches as well as small (1-2 nucleotide) IDLs. MutSβ is responsible for recognizing larger IDLs comprised of up to 16 nucleotides. MMR is initiated by MutSα or MutSβ recognizing a base-base mismatch or IDL error in the newly synthesized DNA strand. MutSα then interacts with the MutL homolog heterodimer MutLα (MLH1-PMS2 in humans or Mlh1-Pms1 in yeast) in an ATP dependent manner. MutLα has been shown to have its own endonuclease activity that is mismatch dependent (Kadyrov, Dzantiev et al. 2006; Kadyrov, Holmes et al. 2007; Kadyrov, Genschel et al. 2009). MutLα nicks the daughter strand and the MutSα-MutLα complex initiates MMR. How the protein complex differentiates the nascent DNA strand from the newly replicated strand is yet unknown. Once the daughter strand has been identified and the MutSα-MutLα complex has initiated repair, the region of DNA containing the mismatch is excised by EXO I or other (unknown) nuclease. An SSB homolog, replication protein

A (RPA) binds and stabilizes the ssDNA-gapped region, and the DNA is resynthesized by Pol δ. Finally, DNA ligase seals any nicks in the new DNA strand.

*MutS in MMR Recognition and Initiation*

Unfortunately, there is no clearly defined mechanism by which MutS or MutSα (MutS(α) when referring to both the prokaryote and eukaryote) recognizes a mismatch and initiates repair of the DNA. Recognition of DNA mismatches is speculated to be related to the local flexibility of the DNA at the mismatch due to the local distortion effects of the incorrect pairing (Rajski, Jackson et al. 2000; Hsieh 2001; Schofield and Hsieh 2003; Kunkel and Erie 2005). The local flexibility of the DNA would differ at a mismatch versus homoduplex DNA. However, the thermodynamic stability of each mismatch does not correlate well with the relative repair efficiency of each mismatch. In fact, there is an apparent inverse correlation in the repair efficiency of a mismatch and the stability of that mismatch such that the more thermodynamically stable mismatches appear to be better repaired than the less stable mismatches (Peyret, Seneviratne et al. 1999; Wang, Yang et al. 2003; Kunkel and Erie 2005). The most stable mismatches, guanine-guanine (GG) or guanine-thymine (GT) mismatch, are the most efficiently repaired, with the least stable mismatch, cytosine-cytosine (CC) mismatch, being the least efficiently repaired (Su and Modrich 1986; Peyret, Seneviratne et al. 1999). This inverse correlation would suggest that structural factors must play role in mismatch discrimination.

An atomic force microscopy (AFM) study in our lab led to the suggestion of a DNA bending model for mismatch recognition. Wang *et al.* evaluated the DNA

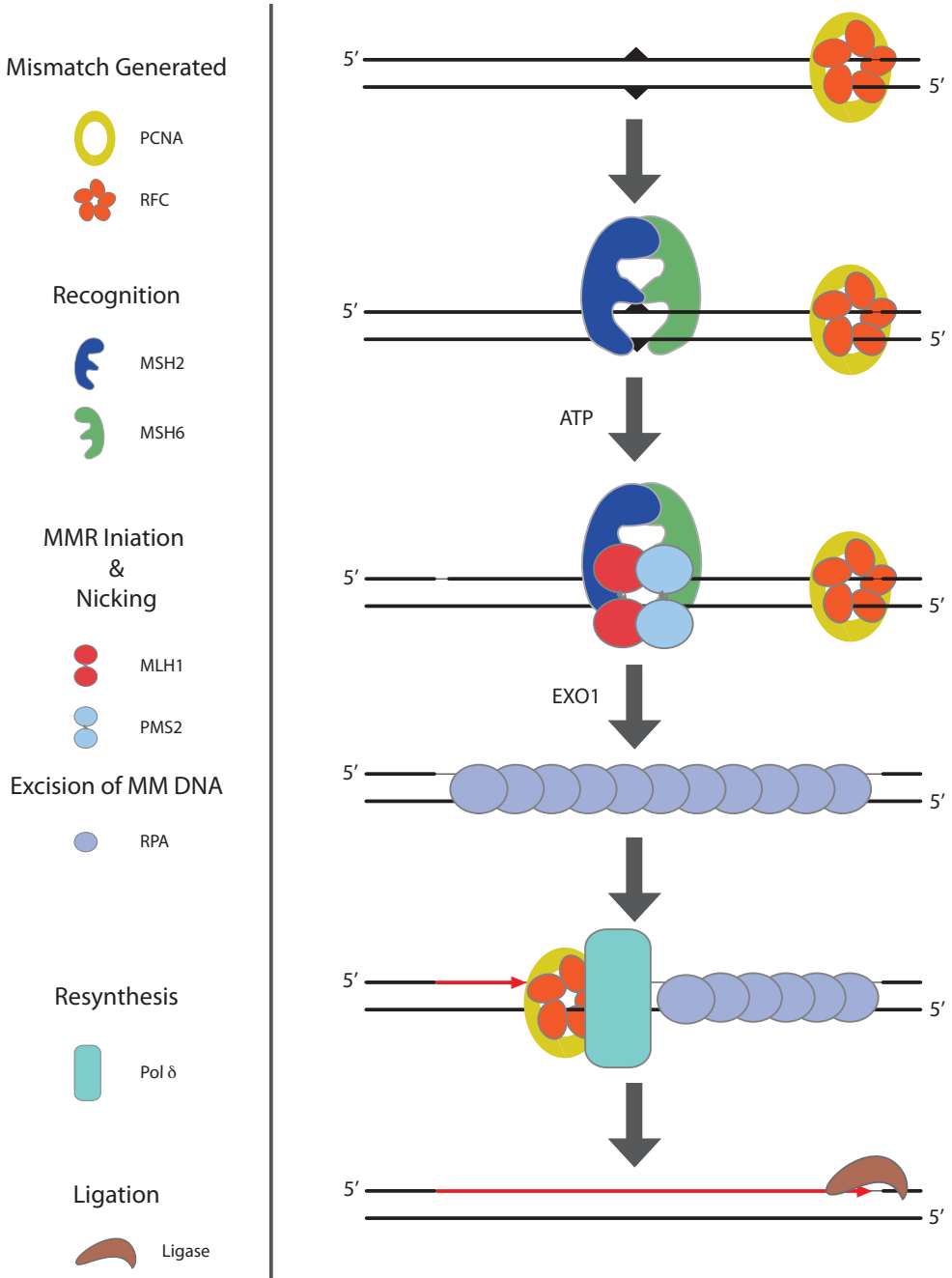
Mismatch Generated
PCNA
RFC
Recognition
MSH2
MSH6
MMR Iniation
&
Nicking
MLH1
PMS2
Excision of MM DNA
RPA
Resynthesis
Pol δ
Ligation
Ligase
5′
5′
ATP
EXO1

**Figure 1.1- Human DNA mismatch repair pathway.**

MSH2-MSH6 recognizes a mismatch in the DNA. MSH2-MSH6 interacts with MLH1-PMS2 in an ATP dependent manner. MLH1-PMS2 nicks the daughter strand. Together, MSH2-MSH6 and MLH1-PMS2 initiate the downstream mismatch repair process. EXO I excises the DNA beyond the mismatch. RPA binds all of the exposed ssDNA in the excised gap. Pol δ together with PCNA and RFC resynthesize the excised DNA section. The resynthesized DNA is noted as a red line. DNA ligase seals any nicks left in the DNA.

binding properties of *E. coli* and *Thermus aquaticus* (*Taq*) MutS in the presence of a single thymine insertion (T bulge), or a GT mismatch, and homoduplex DNA (Wang, Yang et al. 2003). The AFM results indicated the presence of both bent (~42° bend for *Taq* and ~74° bend for *E. coli*) and unbent (a ~0° bend for both *Taq* and *E. coli*) populations on heteroduplex DNA with MutS localized at the DNA bend (Wang, Yang et al. 2003). The unbent population was only observed at the position of the mismatch or IDL (Wang, Yang et al. 2003). The distribution of states in the presence of homoduplex DNA indicated the presence of a single bent population comparable to the bent population observed in the presence of heteroduplex DNA (a ~40-60° bend) (Wang, Yang et al. 2003). Given that there is no crystal structure of MutSα in complex with homoduplex DNA, this is one of the first structural insights into the interaction differences between MutSα and mismatch or homoduplex DNA.

The observation of the bent and unbent populations coupled with the kinked complex observed in the crystal structure led to a model in which MutSα bends the DNA as it searches for a mismatch. The searching conformation is represented by the bent population observed in AFM images of MutS bound to homoduplex DNA (Wang, Yang et al. 2003; Kunkel and Erie 2005). Upon interacting with a mismatch or IDL, MutS(α) kinks the DNA to form the initial recognition complex (IRC) (Wang, Yang et al. 2003; Kunkel and Erie 2005). This kinked IRC conformation is the observed conformation in the crystal structures. MutS(α) then unbends the DNA into the ultimate recognition complex (URC). The URC is the unbent DNA conformation observed in AFM studies that was specific for a mismatch or IDL (Wang, Yang et al. 2003; Kunkel and Erie 2005). From the URC, MutS(α) adopts the sliding clamp conformation and signals downstream

repair of the identified mismatch or IDL (Wang, Yang et al. 2003; Kunkel and Erie 2005). Recent fluorescence resonance energy transfer (FRET) studies of MutS DNA bending dynamics and their associated kinetics lends further support to this DNA bending model as the discriminatory mechanism between homoduplex and heteroduplex DNA (DeRocco, Anderson et al. 2010; Sass, Lanyi et al. 2010).

The steps following DNA error recognition remain unclear. Three models have been proposed to explain the MMR initiation mechanism. The translocation model suggests that upon recognizing a mismatch, ATP hydrolysis by MutS(α) drives the protein to travel along the DNA bidirectionally away from the mismatch (Allen, Makhov et al. 1997; Blackwell, Bjornson et al. 1998; Gradia, Subramanian et al. 1999; Blackwell, Bjornson et al. 2001; Acharya, Foster et al. 2003; Gorman, Chowdhury et al. 2007). The function of MutS traveling away from the mismatch is proposed to be the recruitment of other mismatch repair proteins and the coordination of downstream repair events (Allen, Makhov et al. 1997; Blackwell, Bjornson et al. 1998; Gradia, Subramanian et al. 1999; Blackwell, Bjornson et al. 2001; Acharya, Foster et al. 2003; Gorman, Plys et al. 2010). The molecular switch model suggests that a combination of factors must occur prior to MutS(α) initiated repair. MutS(α) must recognize a mismatch and then bind ATP into both subunits. The rate limiting exchange of ADP to ATP in Msh2 (or subunit 2 in *Taq* and *E.* coli) is the final step before MutS undergoes a conformational change to form a sliding clamp which would similarly recruit MMR proteins and coordinate downstream repair (Gradia, Acharya et al. 1997; Gradia, Subramanian et al. 1999; Gradia, Acharya et al. 2000; Acharya, Foster et al. 2003). The third model proposes that MutS(α) requires ATP binding and hydrolysis to control interactions with DNA while also remaining at the

mismatch site (Habraken, Sung et al. 1998; Wang, Lawrence et al. 1999; Junop, Obmolova et al. 2001; Schofield, Nayak et al. 2001; Selmane, Schofield et al. 2003; Geng, Sakato et al. 2012). There is evidence to support each of the proposed MMR initiation models. The mechanism of MutS(α) action remains an area of great interest in the MMR field.

**MutS and its Homologs: A Structural Comparison**

MutS exists as a homodimer in prokaryotes and a heterodimer of MSH2 and MSH6 (MutSα) or MSH2 and MSH3 (MutSβ) in eukaryotes. For the purpose of this work, we will exclude MutSβ from this discussion. MutS(α) contains a DNA binding domain at the N terminus and an ATPase domain at the C terminus of each subunit (Lamers, Perrakis et al. 2000; Obmolova, Ban et al. 2000; Natrajan, Lamers et al. 2003). The overall structure of the protein is conserved from *E. coli* to *Taq* (Figure 1.2) (Lamers, Perrakis et al. 2000; Obmolova, Ban et al. 2000; Warren, Pohlhaus et al. 2007). Human MSH2-MSH6 has also been crystallized (Figure 1.3) as a truncation mutant with a deletion of 341 residues at the N terminus of MSH6 (Warren, Pohlhaus et al. 2007). The truncated structure is remarkably similar to that of the prokaryotic protein structures. In all structures, the DNA is kinked in the DNA binding domains of the MutS(α) protein [$60^{o}$ angle in *Taq* (Obmolova, Ban et al. 2000) and *E. coli* (Lamers, Perrakis et al. 2000; Natrajan, Lamers et al. 2003), $45^{o}$ angle in human MutSα (Warren, Pohlhaus et al. 2007)].

There are five homologous domains within each subunit of the protein (Figure 1.2a). Domains I and IV of the protein act as the DNA binding region where the DNA is threaded through an open channel between the two domains. Domain I contains the only

residue contacts that are specific to a mismatch in the DNA. The mismatch interaction motif will be discussed in detail within the next section of this chapter. Domain IV is often referred to as the clamp region since it is the region that encircles the DNA. Domain III is considered the core of the protein, as it maintains direct contacts with domains II, IV, and V. Domain II connects domain I to the core domain, domain III. Domain V acts as the dimerization interface for the two subunits. Once the two subunits dimerize, domain V forms the ATPase domain of each subunit. The ATPase sites require the two domains to be interfaced to be active (Obmolova, Ban et al. 2000; Junop, Obmolova et al. 2001; Selmane, Schofield et al. 2003). Prior to DNA binding, domains I and IV exist as an unstructured globular region. Upon DNA binding, the domains I and IV form the structured DNA clamp region (Obmolova, Ban et al. 2000). Eukaryotic MutSα also has an additional 340 amino acid region located at the N-terminus of the MSH6 subunit. This additional region in MSH6 contains a PCNA interaction peptide motif (PIP box) (Gu, Hong et al. 1998; Clark, Valle et al. 2000; Bowers, Tran et al. 2001; Kleczkowska, Marra et al. 2001; Lau and Kolodner 2003; Lee and Alani 2006; Shell, Putnam et al. 2007; Iyer, Pohlhaus et al. 2008).

*MutS(α) Mismatch DNA Binding – The Phe-X-Glu Motif*

In all crystal structures, MutS(α) is shown to bind heteroduplex DNA in an asymmetric manner making specific contacts with the mismatch site only within a conserved phenylalanine-X-glutamic acid (Phe-X-Glu) DNA binding motif (Lamers, Perrakis et al. 2000; Obmolova, Ban et al. 2000; Warren, Pohlhaus et al. 2007). This specific interaction site is located in domain I of Chain A in the homodimer (Figure 1.2a

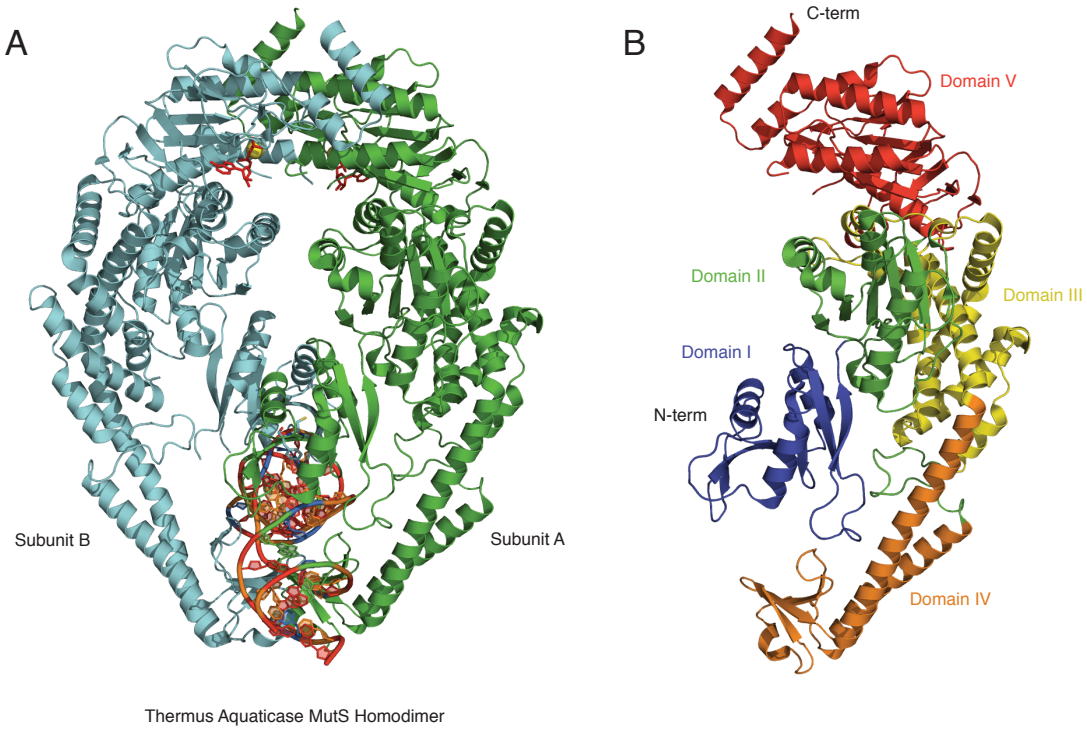


**Figure 1.2 - Crystal Structure of *T. aquaticus* MutS.**

(A) Front view of the MutS homodimer structure in complex with a single thymine insert (PDB ID: 1FW6). Subunit A contains the only specific contacts with the DNA mismatch. ADP is noted in the ATPase domains of each subunit in red stick representations. Magnesium ligands involved in coordinating ADP binding in the ATPase domains are represented as yellow spheres. (B) Structural representation of each domain within each subunit of the MutS homodimer. Domain I, II, III, IV, and V are noted in blue, green, yellow, orange, and red respectively.

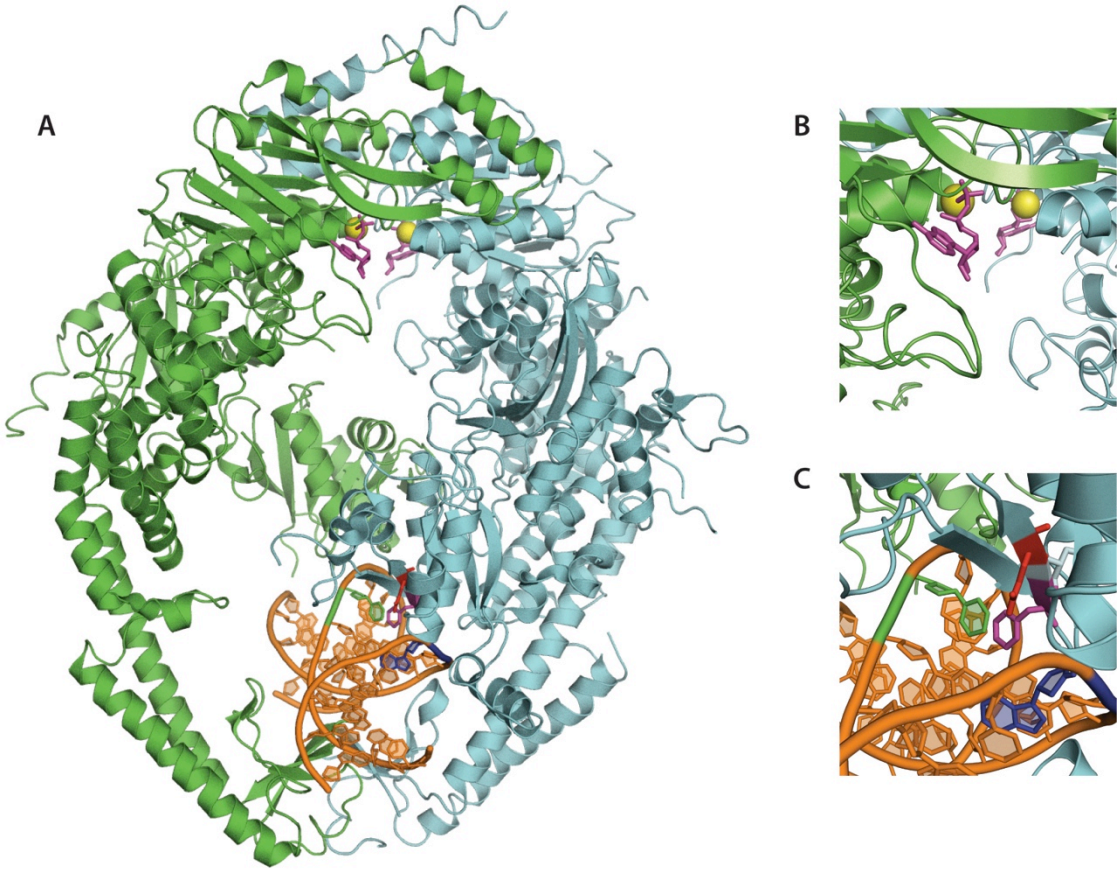


**Figure 1.3 - Crystal Structure of human Msh2-Msh6.**

(A) The crystal structure of the human heterodimer, MSH2 (in green) and MSH6 (in blue), is shown bound to a GT mismatched DNA and ADP (PDB ID: 2O8B). ADP is noted in the ATPase domains of each subunit in stick representation (pink). Magnesium ligands involved in coordinating ADP binding in the ATPase domains are represented as yellow spheres. (B) Inset of the ABC ATPase domain of MSH2-MSH6. (C) Inset of the DNA binding region of MSH6. The guanine and thymine that forms the GT mismatch are noted in blue and green respectively. The phenylalanine and glutamate residues in the Phe-X-Glu binding motif on MSH6 that forms the only specific contacts with the

mismatch are represented in pink and red respectively. Note the stacking of the phenylalanine with the mispaired thymine.

subunit shown in green) and in domain I of MSH6 in the heterodimer (Figure 1.3). The Phe-X-Glu motif is evolutionarily conserved in the N terminus of the MutS protein family with the exception of Msh2, Msh3, Msh4, and Msh5 (Sachadyn 2010). The lack of the motif in Msh2 and presence in Msh6 is consistent with the asymmetric DNA binding observed in the Msh2-Msh6 protein. The lack of the motif in the DNA binding domain of Msh3 suggests the Msh2-Msh3 recognition mechanism of large IDLs differs from that of MSh2-Msh6. Msh4 and Msh5 have been shown to be actively involved in the meiotic DNA repair pathway, homologous recombination (HR) (Malkov, Biswas et al. 1997; Sachadyn 2010). Therefore, Msh4 and Msh5 may not have evolutionarily conserved the Phe-X-Glu contact due to the nature of their roles in DNA repair.

The exact roles of each residue in the Phe-X-Glu motif have been the subject of debate within the MMR field. However, there is no refuting the conserved stacking of the phenylalanine upon the mismatched thymine observed in the crystal structures of *E. coli* MutS, *Taq* MutS, and human MSH2-MSH6 (Lamers, Perrakis et al. 2000; Obmolova, Ban et al. 2000; Warren, Pohlhaus et al. 2007). In each structure, the glutamate residue appears to form a hydrogen bond with the N3 of a mismatched thymine or the N7 of mismatched purines. Mutations in either Phe or Glu of the Phe-X-Glu motif result in significant changes in the MMR capabilities of each protein.

Mutation of the phenylalanine residue results in the elimination of both DNA binding by the protein and mismatch repair as a whole in *E. coli* (MutS F36A), *Taq* (MutS F39A), *S. cerevisiae* (Msh2-Msh6$^{F337A}$), and human (MSH2-MSH6$^{F432A}$) model systems (Malkov, Biswas et al. 1997; Bowers, Sokolsky et al. 1999; Das Gupta and Kolodner 2000; Dufner, Marra et al. 2000; Yamamoto, Schofield et al. 2000;

Drotschmann, Yang et al. 2001; Tessmer, Yang et al. 2008). Each phenylalanine to alanine (FA) mutant MutS(α) exhibits dimerization stability and ATPase activity in the absence of DNA that is consistent with wild type MutS. In each case, the overall DNA binding affinity of FA MutS(α) is significantly weaker than that of wild type MutS(α) for both hetero- and homoduplex DNA substrates. Interestingly, the weakened FA MutS(α) binding affinity for heteroduplex DNA is on the same order of the FA MutS(α) binding affinity for homoduplex DNA indicating that the FA mutant is unable to discriminate between hetero- and homoduplex DNA. The combination of weakened DNA binding and loss of specificity would explain the elimination of MMR as a whole. (Malkov, Biswas et al. 1997; Bowers, Sokolsky et al. 1999; Das Gupta and Kolodner 2000; Dufner, Marra et al. 2000; Yamamoto, Schofield et al. 2000; Drotschmann, Yang et al. 2001; Tessmer, Yang et al. 2008)

Similar mutational analyses of the glutamate residue in the *E. coli, Taq,* and *S. cerevisiae* yielded inconclusive results. The glutamate residue has been proposed to facilitate DNA kinking via electrostatic repulsion of the DNA phosphate backbone. Various mutations to abolish both hydrogen bonding and charge repulsion have resulted in genome-wide mutation rates similar to that of a MutS null system in prokaryotes (Holmes, Scarpinato et al. 2007) and a weak mutator phenotype in *S. cerevisiae* (Das Gupta and Kolodner 2000; Drotschmann, Yang et al. 2001; Holmes, Scarpinato et al. 2007).

Despite the striking phenotype in prokaryotes, glutamate to alanine (EA) mutants of *E. coli* (MutS E38A) and *Taq* (MutS E41A) exhibit little change in binding affinity for heteroduplex substrates as compared to wild type (WT) MutS (Schofield, Brownewell et

al. 2001; Lebbink, Georgijevic et al. 2006; Tessmer, Yang et al. 2008). Notably, DNA binding affinities of the EA mutants for homoduplex DNA show improvement to almost that of the heteroduplex substrates. Studies using DNA analogs that have no hydrogen bond capabilities indicate that hydrogen bonding at the glutamate residue is not required for DNA binding (Schofield, Brownewell et al. 2001; Drotschmann, Topping et al. 2004). MutS EA mutants in the presence of DNA containing base analogs exhibited similar binding affinities to that of typical heteroduplex DNA (Schofield, Brownewell et al. 2001; Drotschmann, Topping et al. 2004). This is consistent with a decreased discrimination between homo- and heteroduplex DNA similar to that observed with the FA mutants.

ATPase studies of EA mutants in the presence of homoduplex, T bulge, and GT mismatch DNA exhibit a loss of the biphasic ATPase activity profile that is characteristic of WT MutS in the presence of DNA. Typically, WT MutS pre-steady state ATPase activity includes an initial fast burst phase followed by a slower linear phase. The slow ATPase phase is believed to be a result of rate-limiting ADP exchange. The EA mutants only exhibit the fast ATPase phase. There is no inhibition of ATPase due to ADP exchange. This, coupled with the observation that the EA mutant dissociates from DNA faster than WT MutS, suggests that while the EA mutants are able to bind DNA with a near wild type affinity, they are unable to adopt a secondary signaling conformation (largely believed to be the sliding clamp) as a result of ATP hydrolysis or ADP release (Lebbink, Georgijevic et al. 2006; Tessmer, Yang et al. 2008).

To date, the only data on the function of the glutamate in the Phe-X-Glu motif in eukaryotes has been studies in yeast (Drotschmann, Topping et al. 2004; Holmes,

Scarpinato et al. 2007). The glutamate to alanine mutation in Msh2-Msh6 (Msh2-Msh6$^{E339A}$) exhibits a weak mutator phenotype such that the mutant results in only an 8-fold increase in mutation rate over WT as compared to the 1000 fold increase in mutation rate seen in the Msh6 null strain (Drotschmann, Topping et al. 2004). This is accompanied with both a slight loss in DNA binding affinity and a loss of mispair specificity (Drotschmann, Topping et al. 2004). In depth characterization of the mutation spectrum of Msh2-Msh6$^{E339A}$ indicates that the glutamate residue is dispensable for repair of IDLs while remaining important in the repair of base-base mismatches (Holmes, Scarpinato et al. 2007). Interestingly, evaluation of Msh2-Msh6$^{E339A}$ in an oxidative damage (8-oxo-guanine DNA damage) prone cell line indicates a specific role for the glutamate residue in recognizing 8-oxo-G:A mispairs (Holmes, Scarpinato et al. 2007). Overall, the differences in EA mutant phenotypes from prokaryotes to eukaryotes suggest a much more mismatch specific repair system is at work in the higher organism.

While the importance of phenylalanine in the Phe-X-Glu mismatch binding motif is not disputed, the role it plays in mismatch recognition remains a question. It has been suggested that the phenylalanine is involved in kinking the DNA as seen in each crystal structure and/or in stabilizing the MutS(α)-DNA or MutS(α)-DNA-ATP complex. An atomic force microscopy (AFM) study by Tessmer *et al.* may have shed some light on the role phenylalanine plays in DNA mismatch recognition. Tessmer *et al.* performed AFM on *Taq* WT MutS, MutS F39A, and MutS E41A in the presence of a GT mispairs and a single thymine insert (T Bulge) as well as homoduplex DNA (Tessmer, Yang et al. 2008). DNA binding affinities for each protein were similar to those previously published such that the F39A mutant exhibits a much weaker binding affinity for heteroduplex

DNA as compared to wild type while E41A exhibited comparable DNA binding affinities to wild type for homo- and heteroduplex DNA substrates (Malkov, Biswas et al. 1997; Yamamoto, Schofield et al. 2000; Tessmer, Yang et al. 2008). However, when the DNA conformations at a bound MutS protein were evaluated, differences between each mutant and wild type were observed.

As previously described in this chapter, wild type MutS bends homoduplex DNA into a single bend angle population (~60°) while MutS bends heteroduplex DNA into two populations (0° and ~40°). The unbent conformation is hypothesized to be the signaling conformation for downstream repair. In contrast, the bend angle distributions for F39A on homoduplex, GT mismatch, and T bulge DNA are each single populations centered on the same ~60° angle as is seen with WT MutS on homoduplex DNA. This result is consistent with the F39A mutant being unable to discriminate between homo- and heteroduplex DNA. Neither the F39A GT mispair distribution nor the T bulge distribution exhibits the 0° bend angle population seen with WT MutS on the same DNA substrates. The loss of the 0° bend angle suggests that the phenylalanine residue plays a role in either forming or stabilizing the unbent DNA conformation that is unique to MMR DNA substrates (Tessmer, Yang et al. 2008).

*MutS and DNA Damage Response*

Mutations in MMR proteins have been identified in HNPCC patients. Specifically, ~80% of HNPCC occurrences are related the MMR protein mutations. A majority of those occurrences are due to mutations in the factors that recognize and initiate repair (MSH2 and MLH1) (Peltomäki 2001).

MutSα is believed to play a role in the initiation of DNA damage induced apoptosis as a result of the presence of alkylated or cisplatinated nucleic acids in newly replicated DNA. Patients with mutations in the MMR protein alleles often display a resistance to the affectivity of certain chemotherapeutic agents such as N-methyl-N'-nitro-N-nitrosoguanidine (MNNG) and cisplatin.

MMR deficient cells were found to resist the effects of methylating agents used for chemotherapy while MMR proficient cells did not have the same resistive phenotype (Stojic, Brun et al. 2004). These methylating agents include such active components as temozolomide (TMZ), dacarbazine and procarbazine, and MNNG. MNNG exposure results in the most common DNA damage, $O^6$-methylguanine ($O^6$-MeG) (Stojic, Brun et al. 2004). In general, the presence of $O^6$-MeGT mismatches is believed to trigger apoptosis (Fishel 1999; Karran 2001; Kunkel and Erie 2005).

The mechanism by which apoptosis is signaled is not conclusively known. However, two theories have been proposed (Fishel 1999; Karran 2001). The "futile repair" hypothesis proposes that MutSα binds to the $O^6$-MeGT mismatch and signals MMR. If the parent strand contains the methylated base, MMR results in the removal of the thymine. DNA resynthesis results in a reinsertion of a thymine opposite to the $O^6$-MeG. This process continually repeats because the damaged portion of the DNA resides in the parent strand. Eventually, this excision and resynthesis leads to apoptosis triggered by double strand breaks formed in the DNA during replication. Alternately, the "signaling" hypothesis suggests that there is a mechanism by which the binding of MutS(α) transmits a damage signal to the checkpoint machinery that activates apoptosis. By characterizing the binding dynamics of MutSα on the $O^6$-MeG/T mismatch, the

mechanism by which MutS(α) signals apoptosis rather than repair may be better understood.

*MutS(α) ATPase activity and the sliding clamp*

The ATPase domains of MutS located in domain V of each subunit are essential for DNA repair (Haber and Walker 1991; Wu and Marinus 1994; Studamire, Quach et al. 1998; Drotschmann, Clark et al. 1999; Lamers, Perrakis et al. 2000; Biswas, Obmolova et al. 2001). Each ATPase site is comprised of a highly conserved Walker A and Walker B nucleotide binding motif as well as a set of six motifs that are a signature of ATP-binding cassette transporters (ABC transporters) at the C terminus of the subunit (Gorbalenya and Koonin 1990; Lamers, Perrakis et al. 2000; Obmolova, Ban et al. 2000; Junop, Obmolova et al. 2001; Alani, Lee et al. 2003). MutS and its homologs therefore belong to the ABC ATPase superfamily (Gorbalenya and Koonin 1990). The two ATPase regions of the protein exist at the interface between subunits as is characteristic of this superfamily. Each subunit of MutS(α) site contains five of the ABC motifs while the sixth ABC ATPase motif is provided by the interfacing subunit. The MutS(α) subunit dimerization results in two functional composite ATPase sites (Junop, Obmolova et al. 2001).

Many studies have shown that MutS(α) undergoes conformational changes in the presence of ATP (Allen, Makhov et al. 1997; Blackwell, Martik et al. 1998; Studamire, Quach et al. 1998; Gradia, Subramanian et al. 1999; Blackwell, Bjornson et al. 2001; Kato, Kataoka et al. 2001; Hess, Gupta et al. 2002; Joshi and Rao 2002; Jiang, Bai et al. 2005; Mendillo, Mazur et al. 2005; Gorman, Chowdhury et al. 2007; Pluciennik and Modrich 2007; Qiu, DeRocco et al. 2012). The ATPase activity and the nucleotide occupancy requirements for such a conformational change have been the focus of many

studies (Haber and Walker 1991; Gradia, Acharya et al. 1997; Blackwell, Bjornson et al. 1998; Blackwell, Martik et al. 1998; Gradia, Subramanian et al. 1999; Gradia, Acharya et al. 2000; Drotschmann, Hall et al. 2002; Joshi and Rao 2002; Antony and Hingorani 2003; Selmane, Schofield et al. 2003; Lamers, Georgijevic et al. 2004; Antony, Khubchandani et al. 2006; Mazur, Mendillo et al. 2006; Jacobs-Palmer and Hingorani 2007; Cyr 2008; Zhai and Hingorani 2010; Heinen, Cyr et al. 2011). Progress has been made in understanding the role of nucleotide occupancy in the formation of MutS(α)-MutL(α) ternary complexes and signaling downstream repair. Studies have shown that while the presence of ATP is a requirement for MutS(α)-MutL(α)-mismatch DNA (mmDNA) complex formation, ATP hydrolysis by either protein is not necessary (Selmane, Schofield et al. 2003). Given the importance of ATP binding and/or hydrolysis in the activation of the MMR process, it is not surprising to note that many types of mutations in the ATPase domain of either subunit are part of the human nonpolyposis colorectal cancer (HNPCC) (also referred to as Lynch Syndrome) mutation spectrum.

Interestingly, each ATPase domain of MutS(α) exhibits very different binding affinities for nucleotide. In yeast, Msh2 exhibits a stronger binding affinity for ADP while Msh6 preferentially binds ATP (Antony and Hingorani 2003; Bjornson and Modrich 2003; Antony, Khubchandani et al. 2006; Mazur, Mendillo et al. 2006; Hargreaves, Shell et al. 2010). Mutations in either ATPase site have varying results on the MMR activity of the protein. In fact, certain mutations in the Walker A and Walker B motifs that abolish the ATPase activity of the protein, result in deficient MMR. Such mutations involve the lysine residue of the Walker A motif (GXXGGK(S/T)) which is involved in coordinating the phosphate groups of the ATP in the ATPase active site.

Remarkably, MMR deficiency is not a result of loss of ATP hydrolysis or of a loss in ternary complex formation with MutL. Rather, MMR deficiency has been shown to be a result of loss of downstream signaling effects.

Other mutations in the ATPase domains result in separation-of-function mutant MutSα proteins which are deficient in MMR but are able to participate in apoptotic responses due to DNA damage. For example, a mutation of a glycine residue in the Walker A motif of Msh2 (GXXXGK(S/T)) ($MSH2^{G674A}$-$MSH6^{WT}$ in mouse and human systems) results in a deficiency in MMR while maintaining DNA damage response (Yang, Scherer et al. 2004; Geng, Sakato et al. 2012). Mouse embryonic fibrobalsts (MEFs) containing the $Msh2^{G674A}$-Msh6 protein exhibit the same mutagenic spectrum of cancer development as that of MutSα null cells (Yang, Scherer et al. 2004). However, the $Msh2^{G674A}$-Msh6 MEFs have a longer lifespan than that of the Msh2 null mice and exhibit the same susceptibility to chemotherapeutic treatment that WT Msh2-Msh6 mice had (Yang, Scherer et al. 2004) suggesting that the $Msh2^{G674A}$-Msh6 cells are inducing apoptosis in a similar manner to that of WT Msh2-Msh6 cells.

Another separation of function mutant of interest involves a mutation of an amino acid residue in Msh6 at the interface between Msh2 and Msh6 near the p-loop of the Msh2 ATPase site ($Msh2^{WT}$-$Msh6^{G1067D}$ in *S. cerevisiae* and the analogous mutations $MSH2^{WT}$-$MSH6^{T1219D}$ in humans and $Msh2^{WT}$-$Msh6^{T1217D}$ in mice) (Berends, Wu et al. 2002; Hess, Gupta et al. 2002; Yang, Scherer et al. 2004). Similar cell survival studies in MEFs to those performed with $Msh2^{G674A}$-$Msh6^{WT}$ yielded the same inability to activate MMR (observed in a higher occurrence of microsatellite instabilities (MSIs) which are a

hallmark of cancer susceptibility) while maintaining wild type-like cellular vulnerability to DNA damage (Yang, Scherer et al. 2004).

Interestingly, both separation-of-function mutants described above have been shown *in vitro* to be able to bind mmDNA like wild type protein, but are unable to form the ternary complex with MutLα that is required for MMR to proceed (Hess, Gupta et al. 2002; Hess, Mendillo et al. 2006; Geng, Sakato et al. 2012) suggesting a role for the MutSα-MutLα ternary complex in MMR signaling and some divergent function of MutSα in apoptotic response.

## Bulk and Single-Molecule Fluorescence Techniques – The Biophysical Tools

More and more, fluorescence-based techniques are being used to answer biological questions. The low-noise characteristic of fluorescence spectroscopy is attractive for use with complicated biological systems. The ability to use fluorescence at little to no risk to the integrity of the biological systems being probed is also highly appealing. The improvement of detection methods for fluorescence systems, in conjunction with the discovery of fluorescent proteins and the engineering of new, longer lifetime fluorescent proteins and organic dyes has pushed fluorescent technologies to the forefront of biological application. Technologies such as fluorescence resonance energy transfer (FRET), photoactivated light microscopy (PALM), fluorescence recovery after photobleaching (FRAP), and multi-photon fluorescence microscopy have allowed for high resolution of biological processes both *in vivo* and *in vitro*.

### *Single-Molecule Fluorescence Resonance Energy Transfer (smFRET)*

Often bulk techniques are utilized to study biochemical interactions like protein-protein and protein-DNA interactions. These techniques are very useful in gaining insight

about the average of all states present. However, bulk studies do not provide information about the individual characteristics of subpopulations of conformations which may be present but unresolvable within the ensemble average (Gell, Brockwell et al. 2006). Based on these same principles, if two states exist in approximately equal occurrence in bulk then both states are averaged to converge on a single mean value that may not actually represent either of the major states. These bulk experiments, therefore, disregard the heterogeneity of a sample by either assuming that the dominant states are the only states involved in a process or by not representing two equal states at all (Gell, Brockwell et al. 2006; Roy, Hohng et al. 2008). Single-molecule experiments allow an experimenter to distinguish between conformations that may be present at any given point in time given the time resolution of the technique being utilized.

Single-molecule fluorescence is a low noise technique that allows for detection limits on the order of $1.66 \times 10^{-24}$ mole (or molecule) of the analyte of interest (Gell, Brockwell et al. 2006; Lakowicz 2006). In addition to very low limits of detection, single-molecule fluorescence techniques allow for very high spatial resolution of the probe of interest and the environment surrounding that probe (Gell, Brockwell et al. 2006; Lakowicz 2006; Roy, Hohng et al. 2008). The combination of low limits of detection, high resolution, and current advances in nanotechnology and electronics has advanced techniques like single-molecule FRET (Gell, Brockwell et al. 2006).

Forster and Perrin first described FRET as being a non-radiative, long-range dipole-dipole transfer of energy from a donor molecule to an acceptor molecule over a 10-100Å range (Forster 1959; Gell, Brockwell et al. 2006; Lakowicz 2006; Roy, Hohng et al. 2008). FRET is typically reported in terms of FRET efficiency, which is defined as

the ratio of the energy transfer rate to the sum of all processes resulting in the relaxation of the donor molecule (Gell, Brockwell et al. 2006; Lakowicz 2006). Efficiency of energy transfer is dependent on several properties of the donor and acceptor dye pair selected: (1) the degree of spectral overlap between the donor emission spectrum and the acceptor absorption spectrum, (2) the quantum yield of the donor molecule, which is defined as the number of photons emitted relative to the number of photons absorbed by the molecule, (3) the relative orientation of the donor and acceptor transition dipoles, and (4) the physical distance between the donor and acceptor molecules (Lakowicz 2006). Energy transfer efficiency (FRET efficiency, E) is defined as Eq. 1.1:

$$E = \frac{1}{\left(1 + \frac{r^6}{R_o^6}\right)}$$

**Eq. 1.1**

where $r$ is the distance between the donor and acceptor probe and $R_o$ is the Forster distance (Gell, Brockwell et al. 2006; Lakowicz 2006). The Forster distance is the distance between the acceptor and donor chromophores at which 50% of the excitation energy from the donor is transferred to the acceptor (Forster 1959; Gell, Brockwell et al. 2006; Lakowicz 2006; Roy, Hohng et al. 2008). The Forster distance for every dye pair is unique given that it depends on the quantum efficiency of the donor dye, the spectral overlap of the two dyes involved, and the orientation of the dyes. Forster distance may also vary for the same dye pair from environment to environment as it is also dependent on the refractive index of the experimental system. Notably, FRET efficiency has a $1/r^6$ dependence on the distance between the acceptor and donor, which results in the technique being highly sensitive to relatively small changes in the positions of the donor

and acceptor dye (Figure 1.4). Measureable changes in positions are typically on the order of $10^{-9}$ m.

In single-molecule experiments, FRET efficiency can be expressed (Eq. 1.2) as an intensity ratio such that

$$E = \frac{I_A}{I_D + I_A}$$

**Eq. 1.2**

where $I_A$ is the intensity of fluorescence being emitted by the acceptor molecule and $I_D$ is the intensity of the donor fluorescence (Gell, Brockwell et al. 2006). In this case, only the donor molecule is excited and the transfer to the acceptor molecule is monitored in terms of fluorescence intensity. More correctly, experimental FRET efficiency is expressed as Eq. 1.3:

$$E = \frac{I_A}{\gamma I_D + I_A}$$

**Eq. 1.3**

where γ is a correction factor that accounts for quantum yields and detection efficiencies of each dye for a particular experimental system. The γ factor (Eq. 1.4) allows experimental normalization of results from microscope to microscope where

$$\gamma = \frac{\Phi_A \eta_A}{\Phi_D \eta_D}$$

**Eq. 1.4**

$\Phi_A$ and $\Phi_D$ are the quantum yields of the acceptor and donor respectively and $\eta_A$ and $\eta_D$ are the detection efficiencies of the acceptor and donor respectively (Gell, Brockwell et al. 2006; Mccann, Choi et al. 2010).

*Total Internal Reflection Fluorescence Microscopy – TIRFing For Single-molecule Detection*

Single-molecule detection has been made possible because of low noise excitation methods such as total internal reflection fluorescence (TIRF) as well as the improvement in electronic systems for detection. The increase in the number of researchers performing single-molecule fluorescence methodologies is due to the rise of commercially available (and relatively inexpensive) microscope systems for TIRF based excitation. There are two modes of TIRF excitation – through objective and through prism (Figure 1.5). Both utilize the same principle of total internal reflection to generate an evanescent wave in order to excite a sample. For the purpose of this work, I will describe TIR as it applies to the through prism instrument design shown in Figure 1.5.

Total internal reflection occurs when the angle of incidence ($\theta_1$) of a beam at the interface between two materials with different refractive indices ($n_1$ and $n_2$) is equal to or greater than the critical angle ($\theta_c$) (Figure 1.5) (Gell, Brockwell et al. 2006; Lakowicz 2006). The critical angle is defined as the angle at which all incident light is reflected and is calculated by Snell's law as (Eq. 1.5)

$$\theta_c = \sin^{-1}\left(\frac{n_2}{n_1}\right)$$

**Eq. 1.5**

The intensity of the reflected light is also somewhat dependent on the polarization of the incident light.

When $\theta_1$ is equal to or greater than $\theta_c$, TIR occurs and an electric field, called the evanescent field, is propagated through the side of the interface with the lower refractive

index ($n_2$ in Figure 1.5). The propagation intensity decay has a z direction dependence described by Eq. 1.6:

$$I(z) = I(0)exp\left(-\frac{z}{d}\right)$$

**Eq. 1.6**

where *I(z)* is the field intensity in the z direction into the lower refractive index material ($n_2$), *I(0)* is the intensity of the evanescent field at the interface, and *d* is the penetration depth of the evanescent field. The penetration depth of the field is dependent on the wavelength of the incident beam (λ), the angle of incidence, and the refractive indices of the two materials at the interface. This relationship is described by Eq. 1.7.

$$d = \frac{\lambda}{4\pi\sqrt{(n_1^2 \sin^2\theta_1 - n_2^2)}}$$

**Eq. 1.7**

It is therefore important to choose material of appropriate refractive indices in order to have optimum penetration depth of the evanescent field. For example, consider the diagram of through-prism TIRF shown in Figure 1.5. Typically, a quartz prism and slide are used ($n_1$=1.55) and a sample is in some aqueous environment (assume $n_2$ of water, $n_2$=1.33). The $\theta_c$ of such an experimental system would be ~60°. Now if you use an excitation wavelength of 532 nm at $\theta_c$, the penetration depth of the evanescent wave would be at most ~233 nm. The same experimental system using an excitation wavelength of 635 nm would yield a penetration depth of ~278 nm. However, only a fraction of the penetration depth is sufficiently excited due to the decay profile of the evanescent wave in the z direction.

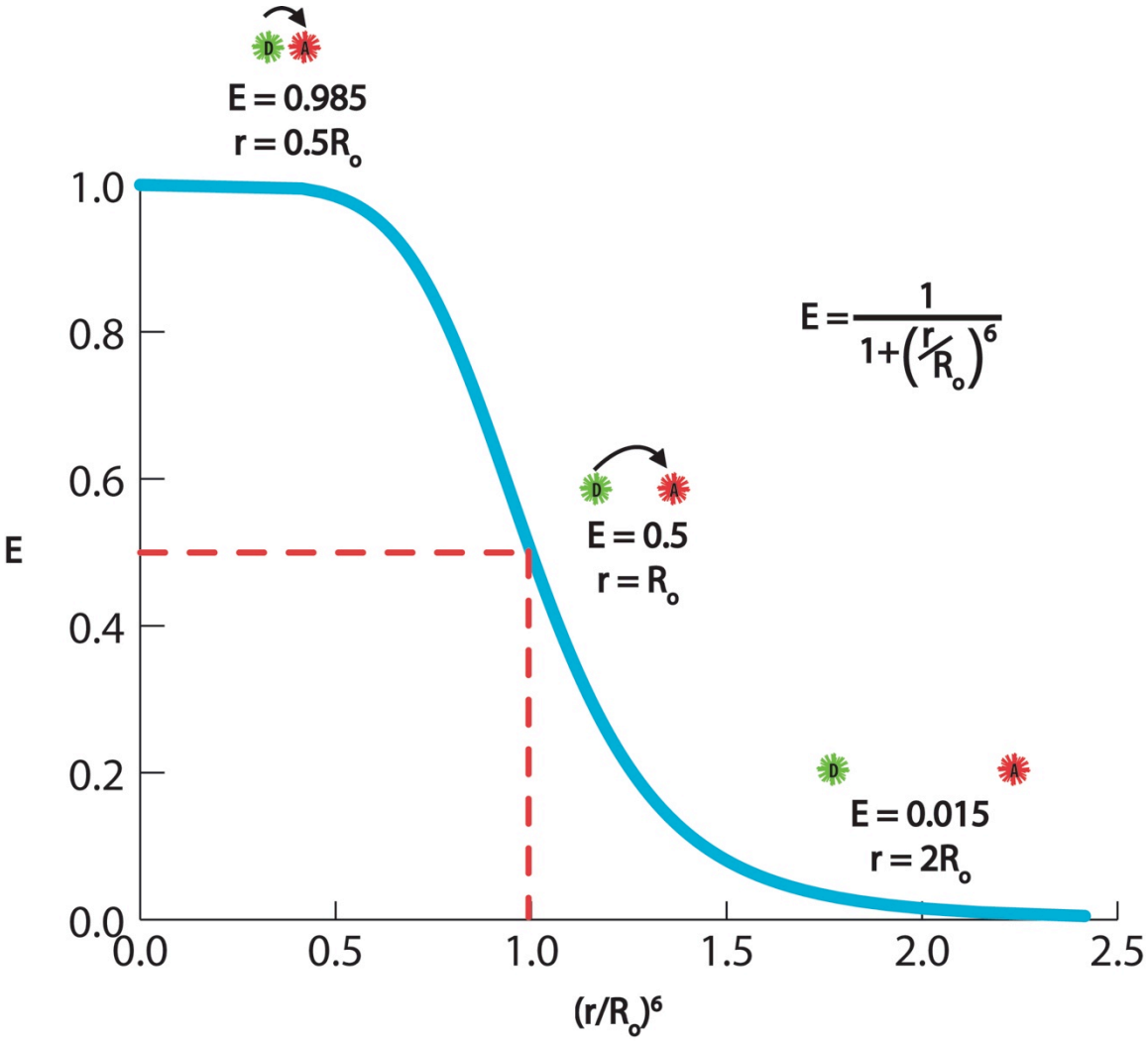


**Figure 1.4 - Distance dependence of donor to acceptor fluorescence resonance energy transfer.**

The dependence of the efficiency of fluorescence resonance energy transfer (E) on the distance (r) between the donor (D) and Acceptor (A) chromaphores and the Forster distance associated with the dye pair used ($R_o$) is demonstrated (blue line). The Förster distance or the distance at which the system has a 50% efficiency in energy transfer is noted (red dotted line). Adapted from (Lakowicz 2006)

Regardless of the excitation wavelength used, the overall sample excitation is restricted to ~200 nm at the interface between the two materials. This limited excitation range allows for low noise, single-molecule detection at the interface as only the fluorophores within this 200 nm range will be excited. The use of through-prism TIRF microscopy for smFRET excitation and detection of the DNA binding and bending properties of *Taq*, *S. cerevisiae*, and human MutS(α) for homoduplex, GT, T bulge, and $O^6$MeGT DNA will be extensively discussed in this dissertation.

*Fluorescence Anisotropy – Bulk Measurements at Their Best*

Fluorescence anisotropy is a standard bulk fluorescence technique capable of measuring the binding of a fluorescent ligand or substrate by biological macromolecules. The technique takes advantage of principles of light polarization. When a fluorescent sample is excited with a polarized light, the sample emission is also polarized. The degree of polarization of the sample emission is described as anisotropy. Changes in the degree of polarization of a sample emission result in changes in the sample anisotropy, which reflect the overall heterogeneity of that sample.

Measurement of anisotropy values in an L-format fluorimeter is depicted in Figure 1.6. Excitation with both vertically and horizontally polarized light yields two emission components, $I_{\parallel}$ (intensity of emission parallel to excitation polarization) and $I_{\perp}$(intensity of emission perpendicular to excitation polarization). Anisotropy is a ratiometric measurement of $I_{\parallel}$ and $I_{\perp}$ with respect to the total intensity ($I_T$) of the sample emission.

$$I_T = I_{\parallel} + 2I_{\perp}$$

**Eq. 1.8**

The $I_T$ term accounts for intensity of the sample in the x direction ($I_\perp$), the y direction ($I_\perp$), and the z direction ($I_\parallel$). Anisotropy is therefore expressed as shown in Eq. 1.9

$$a = \frac{I_\parallel - I_\perp}{I_\parallel + 2I_\perp}$$

**Eq. 1.9**

where *a* is the anisotropy of the sample. This is not the same as a polarization measurement. Polarization of a sample and anisotropy of a sample are related, but not directly interchangeable terms. Polarization of a sample is not measured with respect to the total sample emission intensity as it does not account for both x and y $I_\perp$ terms (Eq. 1.10).

$$P = \frac{I_\parallel - I_\perp}{I_\parallel + I_\perp}$$

**Eq. 1.10**

In terms of experimental measurements, anisotropy is calculated from four measureable intensities: $I_{VV}$ (excitation with vertically polarized light resulting in vertically polarized emission intensity), $I_{VH}$ (excitation with vertically polarized light resulting in horizontally polarized emission intensity), $I_{HV}$ (excitation with horizontally

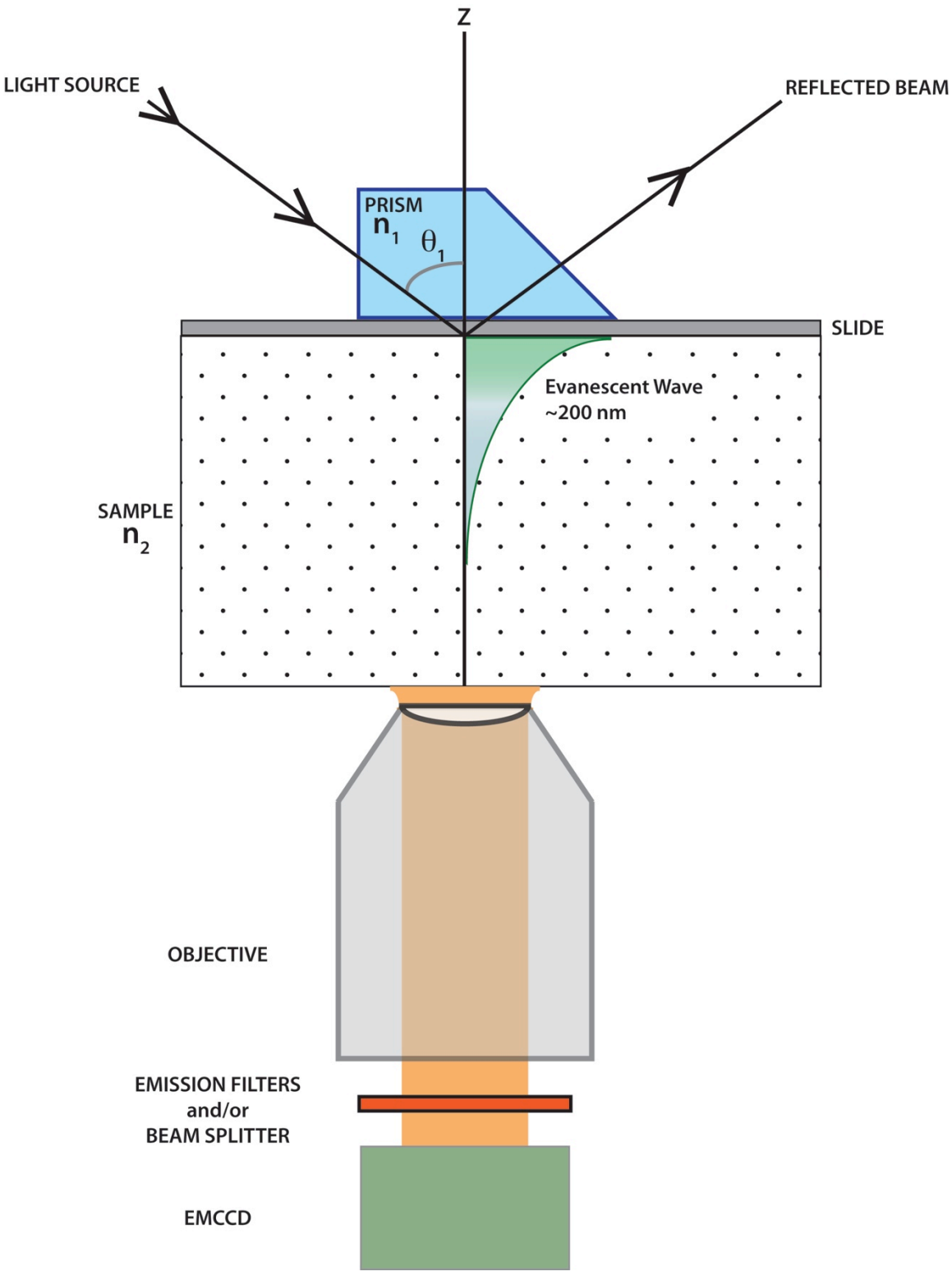
Z
LIGHT SOURCE
REFLECTED BEAM
PRISM
n1
θ1
SLIDE
Evanescent Wave
~200 nm
SAMPLE
n2
OBJECTIVE
EMISSION FILTERS
and/or
BEAM SPLITTER
EMCCD

**Figure 1.5 – Through Prism Total Internal Reflectance Fluorescence (TIRF) Microscopy.**

TIRF is generated at the interface between a quartz prism of refractive index, $n_1$, and a sample with refractive index, $n_2$. Upon TIR of a laser light source with an angle of incidence, $\theta_1$, an evanescent wave with an intensity dependent on the z direction is generated. The evanescent wave traverses through the sample with a typical depth of 200 nm. Surface immobilized fluorophores are excited by the evanescent wave. The emission of the fluorophore is transmitted through a water immersion objective followed by a series of dichroics and emission filters. The signal is finally recorded by an EMCCD camera. Figure adapted from (Lakowicz 2006)**.**

polarized light resulting in vertically polarized emission intensity), and $I_{HH}$ (excitation with horizontally polarized light resulting in horizontally polarized emission intensity) ( Figure 1.6). Experimental anisotropy is calculated as:

$$a = \frac{I_{VV} - GI_{VH}}{I_{VV} + 2GI_{VH}}$$

**Eq. 1.11**

where $G$ is a factor that accounts for differences in the efficiency of instrumental detection of vertical or horizontally polarized light.

$$G = \frac{S_V}{S_H} = \frac{I_{HV}}{I_{HH}}$$

**Eq. 1.12**

where $S_V$ and $S_H$ are the detection efficiencies of vertical and horizontal light respectively. The G factor can also be expressed in terms of $I_{HV}$ and $I_{HH}$ as shown in Eq. 1.12.

Changes in anisotropy values as one titrates protein into a sample containing a fluorescent ligand are due to differences in rotational diffusion of bound ligand molecules and unbound ligand. When a fluorescent ligand is excited with polarized light, the extent of excitation is dependent on the alignment of the dipole of the fluorescent molecule with that light. Each sample of fluorescent molecules therefore has an innate anisotropy value associated with it due to the rotational diffusion of that particular molecule. The rate of rotation of a fluorescent molecule will dictate the frequency at which the fluorescent dipole is aligned with the polarization of the excitation source, and therefore the average emission intensity of $I_{VV}$, $I_{VH}$, $I_{HV}$, and $I_{HH}$. As protein is titrated in, the rate of rotation of bound substrate is changed such that the frequency of dipole alignment with the excitation wavelength is increased resulting in changes in the anisotropy of the

population of protein-bound ligand. As the sample becomes a heterogeneous mixture containing protein-bound and unbound fluorescent ligand, the ensemble average anisotropy of the sample shifts away from the innate anisotropy of fluorescent ligand alone until the sample becomes a homogenous mixture of protein bound ligand. These changes in anisotropy can be used to construct a binding isotherm, which can be fit with the appropriate binding model to determine a protein binding affinity for the fluorescent ligand. We take advantage of this system to measure the DNA binding affinity of human MutSα for homoduplex DNA, a GT mismatch, and $O^6$MeGT damaged DNA substrate.

**Research Scope and Objectives**

The work described in this dissertation began as a follow-up to a previous study of the kinetics of the *Taq* MutS mismatch recognition mechanism. We wanted to explore the binding dynamics described for *Taq* MutS binding to a GT mismatch (Sass, Lanyi et al. 2010) as they related to the Phe-X-Glu mismatch binding motif, as well as expand upon the prokaryotic studies in similar analyses of a simple eukaryotic system in *S. cerevisiae*. The project evolved into the development of a multi-color TIRF detection

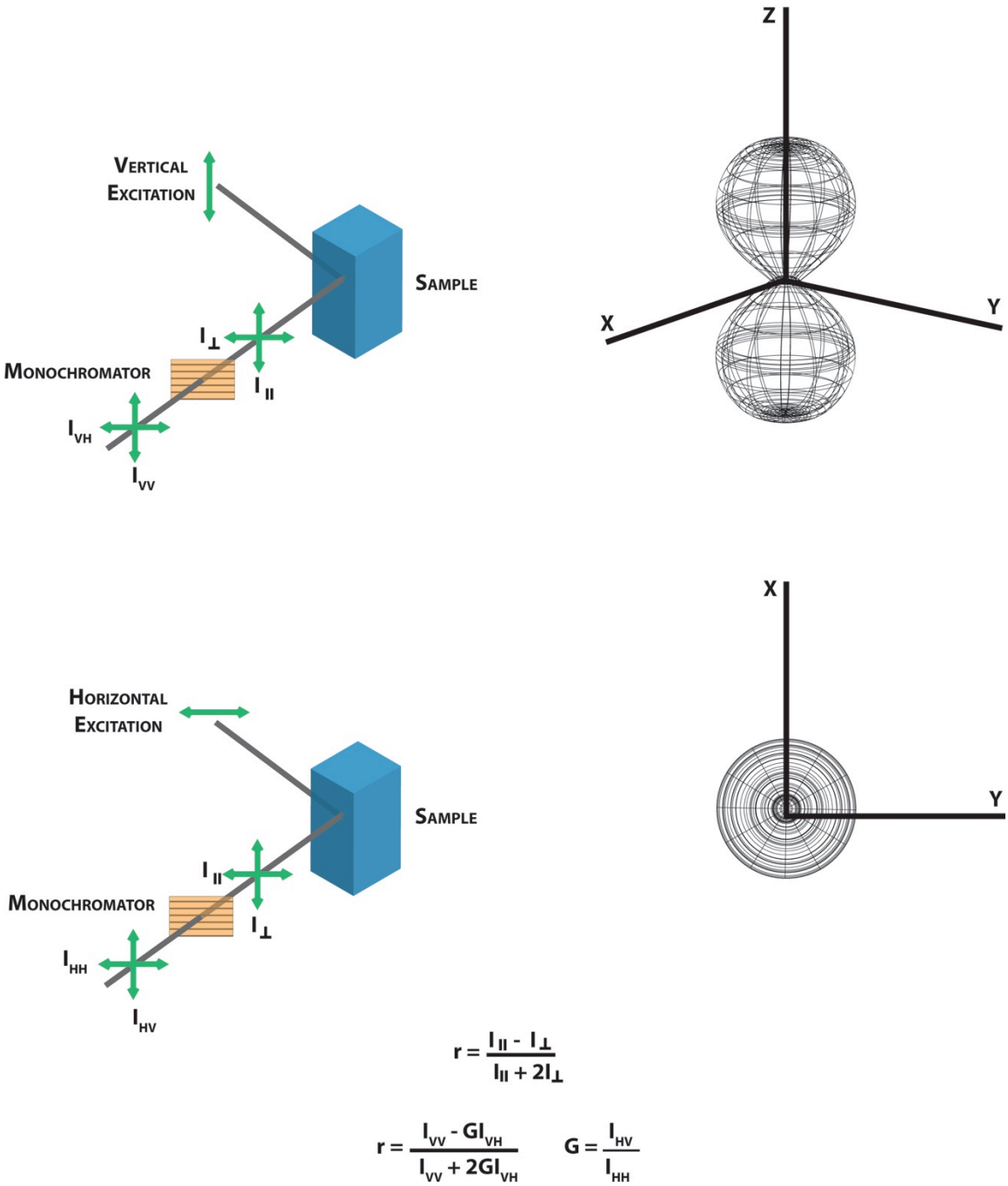


**Figure 1.6 - Bulk Fluorescence Anisotropy L-format Instrumentation.**

The instrumental diagrams indicated on the left display the experimental method used to measure $I_{VV}$, $I_{VH}$, $I_{HV}$, and $I_{HH}$. Insets depicted on the right are excitation direction profiles measured in the corresponding instrument design on the left. Adapted from (Lakowicz 2006)**.** Eq. 1.9, Eq. 1.11, and Eq. 1.12 are displayed for reference.

system partially due to the need to explore both DNA bending and protein colocalization at the mismatch simultaneously in the eukaryotic system. Finally, through a collaboration established with Peggy Hsieh at the NIDDK (NIH, Bethesda), we were given the opportunity to explore the DNA binding properties of higher eukaryotes in analyses of human MutSα for both base-base mismatched DNA and the damaged DNA substrate $O^6$MeGT. The latter work also includes analyses of two separation-of-function mutant proteins ($MSH2^{WT}$-$MSH6^{T1219D}$ and $MSH2^{G674A}$-$MSH6^{WT}$) that have been shown to be deficient in MMR but proficient in apoptotic response to DNA damage.

During my research tenure, I have used smFRET in conjunction with bulk fluorescence anisotropy to characterize the DNA binding and bending interactions of Taq (described in Chapter 2) and human MutS(α) (described in Chapter 5) with a variety of DNA substrates including homoduplex, GT mismatch, single thymine IDL, and $O^6$MeGT damaged DNA. I have optimized a multi-color TIRF microscope and dye labeling system for simultaneous excitation and detection of up to four laser lines (described in Chapter 3). I have disassembled and assembled a two-color TIRF and a four-color TIRF microscope system, and also re-designed the four-color system for use in both smFRET studies and epifluorescence studies *in vivo*. Finally, I have characterized the nucleotide binding properties of human MutSα in the absence of DNA and presence of homoduplex, GT, or $O^6$MeGT DNA (described in Chapter 4). Appendices A and B contain specific protocols for engineering a 500 base pair (bp) DNA substrate for smFRET and for performing smFRET data analysis respectively.

## References


Acharya, S., P. L. Foster, et al. (2003). "The coordinated functions of the E. coli MutS and MutL proteins in mismatch repair." Mol Cell **12**(1): 233-246.

Alani, E., J. Y. Lee, et al. (2003). "Crystal structure and biochemical analysis of the MutS.ADP.beryllium fluoride complex suggests a conserved mechanism for ATP interactions in mismatch repair." J Biol Chem **278**(18): 16088-16094.

Allen, D., A. Makhov, et al. (1997). "MutS mediates heteroduplex loop formation by a translocation mechanism." The EMBO journal **16**(14): 4467-4476.

Antony, E. and M. M. Hingorani (2003). "Mismatch recognition-coupled stabilization of Msh2-Msh6 in an ATP-bound state at the initiation of DNA repair." Biochemistry **42**(25): 7682-7693.

Antony, E., S. Khubchandani, et al. (2006). "Contribution of Msh2 and Msh6 subunits to the asymmetric ATPase and DNA mismatch binding activities of Saccharomyces cerevisiae Msh2-Msh6 mismatch repair protein." DNA repair **5**(2): 153-162.

Berends, M. J., Y. Wu, et al. (2002). "Molecular and clinical characteristics of MSH6 variants: an analysis of 25 index carriers of a germline variant." Am J Hum Genet **70**(1): 26-37.

Biswas, I., G. Obmolova, et al. (2001). "Disruption of the helix-u-turn-helix motif of MutS protein: loss of subunit dimerization, mismatch binding and ATP hydrolysis." J Mol Biol **305**(4): 805-816.

Bjornson, K. P. and P. L. Modrich (2003). "Differential and simultaneous adenosine di- and triphosphate binding by MutS." The Journal of biological chemistry **278**(20): 18557-18562.

Blackwell, L. J., K. Bjornson, et al. (1998). "DNA-dependent activation of the hMutSalpha ATPase." The Journal of biological chemistry **273**(48): 32049-32054.

Blackwell, L. J., K. P. Bjornson, et al. (2001). "Distinct MutS DNA-binding modes that are differentially modulated by ATP binding and hydrolysis." The Journal of biological chemistry **276**(36): 34339-34347.

Blackwell, L. J., D. Martik, et al. (1998). "Nucleotide-promoted release of hMutSalpha from heteroduplex DNA is consistent with an ATP-dependent translocation mechanism." The Journal of biological chemistry **273**(48): 32055-32062.

Bowers, J., T. Sokolsky, et al. (1999). "A mutation in the MSH6 subunit of the Saccharomyces cerevisiae MSH2-MSH6 complex disrupts mismatch recognition." J Biol Chem **274**(23): 16115-16125.

Bowers, J., P. T. Tran, et al. (2001). "MSH-MLH complexes formed at a DNA mismatch are disrupted by the PCNA sliding clamp." Journal of molecular biology **306**(5): 957-968.

Clark, A. B., F. Valle, et al. (2000). "Functional interaction of proliferating cell nuclear antigen with MSH2-MSH6 and MSH2-MSH3 complexes." The Journal of biological chemistry **275**(47): 36498-36501.

Cyr, J. (2008). "Hereditary cancer-associated missense mutations in hMSH6 uncouple ATP hydrolysis from DNA mismatch binding." Journal of Biological Chemistry.

Das Gupta, R. and R. D. Kolodner (2000). "Novel dominant mutations in Saccharomyces cerevisiae MSH6." Nat Genet **24**(1): 53-56.

DeRocco, V., T. Anderson, et al. (2010). "Four-color single-molecule fluorescence with noncovalent dye labeling to monitor dynamic multimolecular complexes." Biotechniques **49**(5): 807-816.

Drotschmann, K., A. B. Clark, et al. (1999). "Mutator phenotypes of yeast strains heterozygous for mutations in the MSH2 gene." Proc Natl Acad Sci U S A **96**(6): 2970-2975.

Drotschmann, K., M. C. Hall, et al. (2002). "DNA binding properties of the yeast Msh2-Msh6 and Mlh1-Pms1 heterodimers." Biol Chem **383**(6): 969-975.

Drotschmann, K., R. P. Topping, et al. (2004). "Mutations in the nucleotide-binding domain of MutS homologs uncouple cell death from cell survival." DNA Repair (Amst) **3**(7): 729-742.

Drotschmann, K., W. Yang, et al. (2001). "Asymmetric recognition of DNA local distortion. Structure-based functional studies of eukaryotic Msh2-Msh6." J Biol Chem **276**(49): 46225-46229.

Dufner, P., G. Marra, et al. (2000). "Mismatch recognition and DNA-dependent stimulation of the ATPase activity of hMutSalpha is abolished by a single mutation in the hMSH6 subunit." The Journal of biological chemistry **275**(47): 36550-36555.

Fishel, R. (1999). Signaling mismatch repair in cancer. Nature medicine. **5:** 1239-1241.

Forster, T. (1959). "Transfer Mechanisms of electronic excitation." Discussions of the Faraday Society **27**: 7-17.

Gell, C., D. Brockwell, et al. (2006). Handbook of Single Molecule Fluorescence Spectroscopy. New York, Oxford University Press.

Geng, H., M. Sakato, et al. (2012). "Biochemical Analysis of the Human Mismatch Repair Proteins hMutS  MSH2G674A-MSH6 and MSH2-MSH6T1219D." The Journal of biological chemistry **287**(13): 9777-9791.

Gorbalenya, A. E. and E. V. Koonin (1990). "Superfamily of UvrA-related NTP-binding proteins. Implications for rational classification of recombination/repair systems." Journal of molecular biology **213**(4): 583-591.

Gorman, J., A. Chowdhury, et al. (2007). "Dynamic basis for one-dimensional DNA scanning by the mismatch repair complex Msh2-Msh6." Mol Cell **28**(3): 359-370.

Gorman, J., A. J. Plys, et al. (2010). "Visualizing one-dimensional diffusion of eukaryotic DNA repair factors along a chromatin lattice." Nature structural & molecular biology **17**(8): 932-938.

Gradia, S., S. Acharya, et al. (1997). "The human mismatch recognition complex hMSH2-hMSH6 functions as a novel molecular switch." Cell **91**(7): 995-1005.

Gradia, S., S. Acharya, et al. (2000). "The role of mismatched nucleotides in activating the hMSH2-hMSH6 molecular switch." J Biol Chem **275**(6): 3922-3930.

Gradia, S., D. Subramanian, et al. (1999). "hMSH2-hMSH6 forms a hydrolysis-independent sliding clamp on mismatched DNA." Mol Cell **3**(2): 255-261.

Gu, L., Y. Hong, et al. (1998). "ATP-dependent interaction of human mismatch repair proteins and dual role of PCNA in mismatch repair." Nucleic Acids Research **26**(5): 1173-1178.

Haber, L. T. and G. C. Walker (1991). "Altering the conserved nucleotide binding motif in the Salmonella typhimurium MutS mismatch repair protein affects both its ATPase and mismatch binding activities." The EMBO journal **10**(9): 2707-2715.

Habraken, Y., P. Sung, et al. (1998). "ATP-dependent assembly of a ternary complex consisting of a DNA mismatch and the yeast MSH2-MSH6 and MLH1-PMS1 protein complexes." J Biol Chem **273**(16): 9837-9841.

Hargreaves, V. V., S. S. Shell, et al. (2010). "Interaction between the Msh2 and Msh6 Nucleotide-binding Sites in the Saccharomyces cerevisiae Msh2-Msh6 Complex." Journal of Biological Chemistry **285**(12): 9301-9310.

Heinen, C. D., J. L. Cyr, et al. (2011). "Human MSH2 (hMSH2) Protein Controls ATP Processing by hMSH2-hMSH6." The Journal of biological chemistry **286**(46): 40287-40295.

Hess, M. T., R. D. Gupta, et al. (2002). "Dominant Saccharomyces cerevisiae msh6 mutations cause increased mispair binding and decreased dissociation from mispairs by Msh2-Msh6 in the presence of ATP." The Journal of biological chemistry **277**(28): 25545-25553.

Hess, M. T., M. L. Mendillo, et al. (2006). "Biochemical basis for dominant mutations in the Saccharomyces cerevisiae MSH6 gene." Proc Natl Acad Sci U S A **103**(3): 558-563.

Holmes, S. F., K. D. Scarpinato, et al. (2007). "Specialized mismatch repair function of Glu339 in the Phe-X-Glu motif of yeast Msh6." DNA Repair (Amst) **6**(3): 293-303.

Hsieh, P. (2001). "Molecular mechanisms of DNA mismatch repair." Mutat Res **486**(2): 71-87.

Hsieh, P. and K. Yamane (2008). "DNA mismatch repair: molecular mechanism, cancer, and ageing." Mechanisms of ageing and development **129**(7-8): 391-407.

Iyer, R. R., A. Pluciennik, et al. (2006). "DNA mismatch repair: functions and mechanisms." Chem Rev **106**(2): 302-323.

Iyer, R. R., T. J. Pohlhaus, et al. (2008). "The MutSalpha-proliferating cell nuclear antigen interaction in human DNA mismatch repair." J Biol Chem **283**(19): 13310-13319.

Jacobs-Palmer, E. and M. M. Hingorani (2007). "The effects of nucleotides on MutS-DNA binding kinetics clarify the role of MutS ATPase activity in mismatch repair." J Mol Biol **366**(4): 1087-1098.

Jiang, J., L. Bai, et al. (2005). "Detection of high-affinity and sliding clamp modes for MSH2-MSH6 by single-molecule unzipping force analysis." Molecular cell **20**(5): 771-781.

Jiricny, J. (2006). "The multifaceted mismatch-repair system." Nature reviews Molecular cell biology **7**(5): 335-346.

Joshi, A. and B. J. Rao (2002). "ATP hydrolysis induces expansion of MutS contacts on heteroduplex: a case for MutS treadmilling?" Biochemistry **41**(11): 3654-3666.

Junop, M., G. Obmolova, et al. (2001). "Composite Active Site of an ABC ATPase:: MutS Uses ATP to Verify Mismatch Recognition and Authorize DNA Repair." Molecular cell.

Kadyrov, F. A., L. Dzantiev, et al. (2006). "Endonucleolytic function of MutLalpha in human mismatch repair." Cell **126**(2): 297-308.

Kadyrov, F. A., J. Genschel, et al. (2009). "A possible mechanism for exonuclease 1-independent eukaryotic mismatch repair." Proceedings of the National Academy of Sciences of the United States of America **106**(21): 8495-8500.

Kadyrov, F. A., S. F. Holmes, et al. (2007). "Saccharomyces cerevisiae MutLalpha is a mismatch repair endonuclease." The Journal of biological chemistry **282**(51): 37181-37190.

Karran, P. (2001). "Mechanisms of tolerance to DNA damaging therapeutic drugs." Carcinogenesis **22**(12): 1931-1937.

Kato, R., M. Kataoka, et al. (2001). "Direct observation of three conformations of MutS protein regulated by adenine nucleotides." Journal of molecular biology **309**(1): 227-238.

Kleczkowska, H. E., G. Marra, et al. (2001). "hMSH3 and hMSH6 interact with PCNA and colocalize with it to replication foci." Genes & Development **15**(6): 724-736.

Kunkel, T. A. and D. A. Erie (2005). "DNA mismatch repair." Annu Rev Biochem **74**: 681-710.

Kunz, C., Y. Saito, et al. (2009). "DNA Repair in mammalian cells: Mismatched repair: variations on a theme." Cell Mol Life Sci **66**(6): 1021-1038.

Lakowicz, J. R. (2006). Principles of fluorescence spectroscopy. New York, Springer.

Lamers, M. H., D. Georgijevic, et al. (2004). "ATP increases the affinity between MutS ATPase domains. Implications for ATP hydrolysis and conformational changes." The Journal of biological chemistry **279**(42): 43879-43885.

Lamers, M. H., A. Perrakis, et al. (2000). "The crystal structure of DNA mismatch repair protein MutS binding to a G x T mismatch." Nature **407**(6805): 711-717.

Lau, P. J. and R. D. Kolodner (2003). "Transfer of the MSH2.MSH6 complex from proliferating cell nuclear antigen to mispaired bases in DNA." The Journal of biological chemistry **278**(1): 14-17.

Lebbink, J. H. G., D. Georgijevic, et al. (2006). "Dual role of MutS glutamate 38 in DNA mismatch discrimination and in the authorization of repair." The EMBO journal **25**(2): 409-419.

Lee, S. D. and E. Alani (2006). "Analysis of interactions between mismatch repair initiation factors and the replication processivity factor PCNA." Journal of molecular biology **355**(2): 175-184.

Malkov, V. A., I. Biswas, et al. (1997). "Photocross-linking of the NH2-terminal region of Taq MutS protein to the major groove of a heteroduplex DNA." J Biol Chem **272**(38): 23811-23817.

Mazur, D. J., M. L. Mendillo, et al. (2006). "Inhibition of Msh6 ATPase activity by mispaired DNA induces a Msh2(ATP)-Msh6(ATP) state capable of hydrolysis-independent movement along DNA." Molecular cell **22**(1): 39-49.

Mccann, J. J., U. B. Choi, et al. (2010). "Optimizing Methods to Recover Absolute FRET Efficiency from Immobilized Single Molecules." Biophysical Journal **99**(3): 961-970.

Mendillo, M. L., D. J. Mazur, et al. (2005). "Analysis of the interaction between the Saccharomyces cerevisiae MSH2-MSH6 and MLH1-PMS1 complexes with DNA using a reversible DNA end-blocking system." The Journal of biological chemistry **280**(23): 22245-22257.

Natrajan, G., M. H. Lamers, et al. (2003). "Structures of Escherichia coli DNA mismatch repair enzyme MutS in complex with different mismatches: a common recognition mode for diverse substrates." Nucleic Acids Research **31**(16): 4814-4821.

Obmolova, G., C. Ban, et al. (2000). "Crystal structures of mismatch repair protein MutS and its complex with a substrate DNA." Nature **407**(6805): 703-710.

Peltomäki, P. (2001). "Deficient DNA mismatch repair: a common etiologic factor for colon cancer." Human Molecular Genetics **10**(7): 735.

Peyret, N., P. A. Seneviratne, et al. (1999). "Nearest-neighbor thermodynamics and NMR of DNA sequences with internal A.A, C.C, G.G, and T.T mismatches." Biochemistry **38**(12): 3468-3477.

Pluciennik, A. and P. Modrich (2007). "Protein roadblocks and helix discontinuities are barriers to the initiation of mismatch repair." Proceedings of the National Academy of Sciences of the United States of America **104**(31): 12709-12713.

Qiu, R., V. C. DeRocco, et al. (2012). "Large conformational changes in MutS during DNA scanning, mismatch recognition and repair signalling." The EMBO journal.

Rajski, S. R., B. A. Jackson, et al. (2000). "DNA repair: models for damage and mismatch recognition." Mutat Res **447**(1): 49-72.

Roy, R., S. Hohng, et al. (2008). "A practical guide to single-molecule FRET." Nature Methods **5**(6): 507-516.

Sachadyn, P. (2010). "Conservation and diversity of MutS proteins." Mutation Research/ … **694**(1-2): 20-30.

Sass, L. E., C. Lanyi, et al. (2010). "Single-molecule FRET TACKLE reveals highly dynamic mismatched DNA-MutS complexes." Biochemistry **49**(14): 3174-3190.

Schofield, M. J., F. E. Brownewell, et al. (2001). "The Phe-X-Glu DNA binding motif of MutS. The role of hydrogen bonding in mismatch recognition." J Biol Chem **276**(49): 45505-45508.

Schofield, M. J. and P. Hsieh (2003). "DNA mismatch repair: molecular mechanisms and biological function." Annu Rev Microbiol **57**: 579-608.

Schofield, M. J., S. Nayak, et al. (2001). "Interaction of Escherichia coli MutS and MutL at a DNA mismatch." J Biol Chem **276**(30): 28291-28299.

Selmane, T., M. J. Schofield, et al. (2003). "Formation of a DNA mismatch repair complex mediated by ATP." J Mol Biol **334**(5): 949-965.

Shell, S. S., C. D. Putnam, et al. (2007). "The N terminus of Saccharomyces cerevisiae Msh6 is an unstructured tether to PCNA." Molecular cell **26**(4): 565-578.

Stojic, L., R. Brun, et al. (2004). "Mismatch repair and DNA damage signalling." DNA Repair (Amst) **3**(8-9): 1091-1101.

Studamire, B., T. Quach, et al. (1998). "Saccharomyces cerevisiae Msh2p and Msh6p ATPase activities are both required during mismatch repair." Molecular and Cellular Biology **18**(12): 7590-7601.

Su, S. S. and P. Modrich (1986). "Escherichia coli mutS-encoded protein binds to mismatched DNA base pairs." Proc Natl Acad Sci U S A **83**(14): 5057-5061.

Tessmer, I., Y. Yang, et al. (2008). "Mechanism of MutS searching for DNA mismatches and signaling repair." J Biol Chem **283**(52): 36646-36654.

Wang, H., C. W. Lawrence, et al. (1999). "Specific binding of human MSH2.MSH6 mismatch-repair protein heterodimers to DNA incorporating thymine- or uracil-containing UV light photoproducts opposite mismatched bases." The Journal of biological chemistry **274**(24): 16894-16900.

Wang, H., Y. Yang, et al. (2003). "DNA bending and unbending by MutS govern mismatch recognition and specificity." Proc Natl Acad Sci U S A **100**(25): 14822-14827.

Warren, J. J., T. J. Pohlhaus, et al. (2007). "Structure of the Human MutSalpha DNA Lesion Recognition Complex." Mol Cell **26**(4): 579-592.

Wu, T. H. and M. G. Marinus (1994). "Dominant negative mutator mutations in the mutS gene of Escherichia coli." Journal of bacteriology **176**(17): 5393-5400.

Yamamoto, A., M. J. Schofield, et al. (2000). "Requirement for Phe36 for DNA binding and mismatch repair by Escherichia coli MutS protein." Nucleic Acids Res **28**(18): 3564-3569.

Yang, G., S. J. Scherer, et al. (2004). "Dominant effects of an Msh6 missense mutation on DNA repair and cancer susceptibility." Cancer Cell **6**(2): 139-150.

Zhai, J. and M. M. Hingorani (2010). "Saccharomyces cerevisiae Msh2-Msh6 DNA binding kinetics reveal a mechanism of targeting sites for DNA mismatch repair." Proceedings of the National Academy of Sciences of the United States of America **107**(2): 680-685.

# Chapter 2

## DISTINCT DNA BENDING DYNAMICS ALLOW MUTS TO DISTINGUISH DIFFERENT DNA MISMATCHES

### Introduction

The DNA mismatch repair (MMR) pathway plays a critical role in prevention of undesirable genomic drift during cell division. The importance of this process has led to strong evolutionary conservation of the proteins that initiate MMR throughout both prokaryotes and eukaryotes (Au, Welsh et al. 1992; Drummond, Li et al. 1995; Buermeyer, Deschenes et al. 1999; Jiricny and Marra 2003). Mutations of this family of genes in humans are associated with a proclivity toward tumor development. In particular, such mutations have been linked to more than 80% of hereditary non-polyposis colorectal cancer (HNPCC) as well as other sporadic cancers (Modrich 1989; Loeb, Loeb et al. 2003; Peltomaki 2003).

The specific molecular events that initiate DNA MMR have not been determined. The first enzymes in the MMR pathway, MutS homodimers in prokaryotes and the eukaryotic homologs Msh2-Msh6 (MutSα) and Msh2-Msh3 (MutSβ), have the particularly difficult task of locating a single Watson-Crick base-base mismatch or base insertion/deletion over the millions of DNA base pairs in the cell. Moreover, mismatches do not significantly distort the DNA, and often the difference in the stability of a normal

Watson-Crick base pairing (for example, a GC base pair) and a mismatch (for example, a GT mismatch) is small (~3 kcal/mol) (Isaacs, Rayens et al. 2002; Natrajan, Lamers et al. 2003).

Crystal structures of *Thermus aquaticus (Taq)* MutS and human MutSα bound to a number of different mismatched DNA bases and base insertion/deletions (Lamers, Perrakis et al. 2000; Obmolova, Ban et al. 2000; Natrajan, Lamers et al. 2003; Warren, Pohlhaus et al. 2007) reveal that only two specific amino acid contacts are made between MutS or MutSα and the mismatched base. These contacts are located in a conserved phenylalanine-X-glutamate (Phe-X-Glu) motif at the DNA binding domain (F36/E38 in *E. coli,* F39/E41 in *Taq* MutS, F337/E339 in yeast Msh6, and F432/E434 in human MSH6) where the phenylalanine stacks with the mismatched base and the glutamate forms a hydrogen bond with the N3 of the mismatched thymine or N7 of the mismatched purine (Lamers, Perrakis et al. 2000; Obmolova, Ban et al. 2000; Natrajan, Lamers et al. 2003; Warren, Pohlhaus et al. 2007). All other interactions between MutS and the DNA are nonspecific backbone contacts. The primary observation in these structures is that the DNA is sharply bent at the mismatch site, stabilized both by the specific amino acid interactions with the mismatch as well as the nonspecific contacts along the backbone.

Structural heterogeneity in mismatched DNA-MutS complexes was revealed by atomic force microscopy (AFM) measurements. Two unique DNA conformations were induced by MutS at the mismatched base: bent and unbent (Wang, Yang et al. 2003; Tessmer, Yang et al. 2008). This finding inspired the proposal that MutS first locates a mismatch in a configuration with sharp DNA bending (Wang, Yang et al. 2003; Kunkel and Erie 2005), and then undergoes a conformational change to generate an unbent DNA-

MutS conformation. The unbent DNA conformation was proposed to permit ATP hydrolysis or nucleotide exchange and generate a new state that signals downstream repair processes (Wang, Yang et al. 2003).

Further structural studies using AFM and crystallography examining mutations of the Phe-X-Glu motif have suggested connections between some of these MutS-DNA interactions and degrees of DNA bending. A series of nonspecific contacts along the DNA backbone combined with the electrostatic repulsion of the glutamate residue in the DNA binding domain is suggested to facilitate smooth bending in the DNA while MutS 'scans' homoduplex DNA in search of a mismatch (Wang, Yang et al. 2003; Kunkel and Erie 2005; Tessmer, Yang et al. 2008). Upon locating a mismatch base pair, smooth bending in the DNA is converted to a sharp kink due to the local flexibility in the DNA at the mismatch, which allows Phe to stack and the Glu to form a hydrogen bond with the mismatched base (Lamers, Perrakis et al. 2000; Obmolova, Ban et al. 2000; Junop, Obmolova et al. 2001; Schofield, Brownewell et al. 2001; Selmane, Schofield et al. 2003; Wang, Yang et al. 2003; Kunkel and Erie 2005; Tessmer, Yang et al. 2008). The importance of the conserved Phe in mismatch recognition is underscored by studies indicating that a mutation of this residue to alanine reduces mismatch binding specificity by three orders of magnitude (Malkov, Biswas et al. 1997; Yamamoto, Schofield et al. 2000; Drotschmann, Yang et al. 2001; Tessmer, Yang et al. 2008) and increases mutation frequency *in vivo* to that of an MMR null (Das Gupta and Kolodner 2000; Drotschmann, Yang et al. 2001).

The role of the Glu contact is less clear. The Glu hydrogen bonding has been proposed to stabilize the formation of MutS-DNA complexes, to stabilize the kinked

DNA conformation observed in crystal structures (Drotschmann, Yang et al. 2001; Schofield, Brownewell et al. 2001), and also to facilitate unbending of the DNA at the mismatch (Wang, Yang et al. 2003; Tessmer, Yang et al. 2008). Studies *in vivo* using mutations of the conserved Glu in MutS point to functional roles for this residue in signaling for repair after mismatch identification. In *E. coli,* mutation of Glu38 to alanine resulted in complete loss of repair of both base-base mismatches and insertion/deletion loop mismatches (Schofield, Brownewell et al. 2001; Lebbink, Georgijevic et al. 2006; Holmes, Scarpinato et al. 2007). In contrast, mutating E339 to alanine in Msh6 of *Saccharomyces cerevisiae* (*S. cerevisiae*) conferred a mutator phenotype for base-base mismatches, but the residue appeared to be expendable for repair of single base insertion/deletion mismatches (Holmes, Scarpinato et al. 2007). Structural observations of *Taq* MutS (E41A)-mismatched DNA complexes with AFM in conjunction with ATPase assays determined wild type binding and bending at an insertion/deletion mismatch (T bulge) but non-wild type behavior at GT mismatches (Tessmer, Yang et al. 2008), suggesting the yeast and *Taq* systems could share a common phenotype.

Based on this accumulated evidence, DNA bending at the mismatch has been proposed to play a fundamental role in mismatch recognition or subsequent repair signaling (Jiricny and Marra 2003; Kunkel and Erie 2005), yet a mechanistic connection between DNA bending and DNA MMR initation remains elusive. The hypothesis connecting DNA bending and repair initiation is challenged by the observation that each crystal structure reveals the same contacts and approximately the same degree of DNA bending at every type of mismatch even though different mismatches are repaired with different efficiencies *in vivo* (Kramer, Kramer et al. 1984). In addition, there seems to be

an inverse correlation between the facility for a mismatch to bend and its repair efficiency (Wang, Yang et al. 2003). In fact, the DNA mismatches most efficiently repaired in the cell induce the least amount of distortion in the DNA (Kunkel and Erie 2005).

Single-molecule fluorescence resonance energy transfer (smFRET) measurements of MutS induced DNA bending have suggested a kinetic aspect of DNA bending may be involved in MutS MMR function (DeRocco, Anderson et al. 2010; Sass, Lanyi et al. 2010). These studies found that MutS-GT mismatched DNA complexes are significantly dynamic and sample a number of different conformations with a variety of kinetic rates (Sass, Lanyi et al. 2010). The smFRET measurements found that MutS bound GT mismatched DNA initially in the sharply bent state (similar to that seen in the crystal structures) and then proceeded into an equilibrium conformational landscape with several bent and unbent states that is significantly more complex than a simple two state equilibrium (Sass, Lanyi et al. 2010).

Here we report smFRET studies of conformational dynamics for MutS bound to a number of different DNA mismatches. These studies are discussed in conjunction with data acquired by Dr. Lauryn E. Sass of our laboratory. We also investigated how the DNA conformations sampled and the dynamics between these conformations are affected by removal of the conserved Glu residue in the DNA binding motif of MutS. We have found that the kinetics of switching between distinct DNA bending states varies over orders of magnitude for MutS bound to different mismatched substrates. Despite the distinct equilibrium kinetics, we determined, by direct observation, that the first DNA conformation sampled upon MutS binding a mismatch is a bent state for all mismatches. The unbent state is sampled later for wild type MutS:DNA complexes, but the E41A

mutant does not progress to the unbent state. These observations support a model in which the initial recognition complex is a bent DNA-MutS conformation and that the Glu residue facilitates the formation of an unbent MutS-DNA complex. Further, we suggest that the varied dynamics for MutS bound to different mismatches may control its ability to signal repair and thus influence the relative differences in the ability of MutS to repair certain types of mismatches.

**Results**

We used smFRET to study the DNA conformations sampled when *Taq* MutS, both wild type and E41A, binds three different DNA lesions: a single thymine insertion (T bulge), a GT mismatch (repaired efficiently *in vivo*), and a CC mismatch (deficient repair *in vivo)*. Similar to the method we used to previously measure DNA bending dynamics of MutS bound to GT mismatched DNA (Sass, Lanyi et al. 2010), we created 50 base pair double stranded DNA substrates that were labeled with an acceptor dye (Cy5) on one end and a donor dye (TAMRA) 19 bases 3′ of the acceptor dye. A mismatch was located midway between the dyes and the 5′ end of the DNA was biotinylated to allow immobilization on a quartz substrate (see Fig. 2C and methods for additional details). smFRET signals were obtained from MutS bound to these complexes as described previously, as DNA bending results in smaller dye separation and increased FRET (Sass, Lanyi et al. 2010).

*Wild type MutS-DNA conformations and conformational dynamics vary significantly from mismatch to mismatch*

FRET signals reporting DNA bending from individual MutS-mismatched DNA complexes were dramatically different in both FRET efficiency, indicating bending, as

well as in kinetic switching among efficiencies for the three mismatches we examined: T bulge, GT, and CC. The differences between substrates are shown in individual smFRET traces (Figure 2.1), histograms representing distributions of all DNA conformations sampled (Figure 2.2), and transition density plots (TDPs) (Figure 2.3) displaying transitions between different conformational states.

Figure 2.1 shows representative FRET traces for T bulge, GT, and CC DNA mismatches in the presence of wild type MutS (top panel) and E41A MutS (bottom panel). MutS-T bulge smFRET traces display a dominant population of single, long-lived FRET efficiencies (or DNA conformations) (Figure 2.1). Conformational changes were observed in a subset of molecules (~ 20% of the thousands of molecules measured), but transitions appeared to be infrequent compared to other mismatches. Overall, T bulge transitions proceeded from a lower FRET state (~0.36) to the higher FRET state (~0.46) (Figure 2.1).

As previously described, the conformational profile of MutS-GT complexes is very intricate (Sass, Lanyi et al. 2010). A number of different conformational states are sampled and are readily interchanged during a single MutS binding event at the GT mismatch (Sass, Lanyi et al. 2010). In MutS-GT complexes, although six conformations are isolated, the dominant conformational pathway is between a stable bent state (FRET ~ 0.65) and a stable unbent state (FRET ~ 0.30) (Sass, Lanyi et al. 2010) The majority of

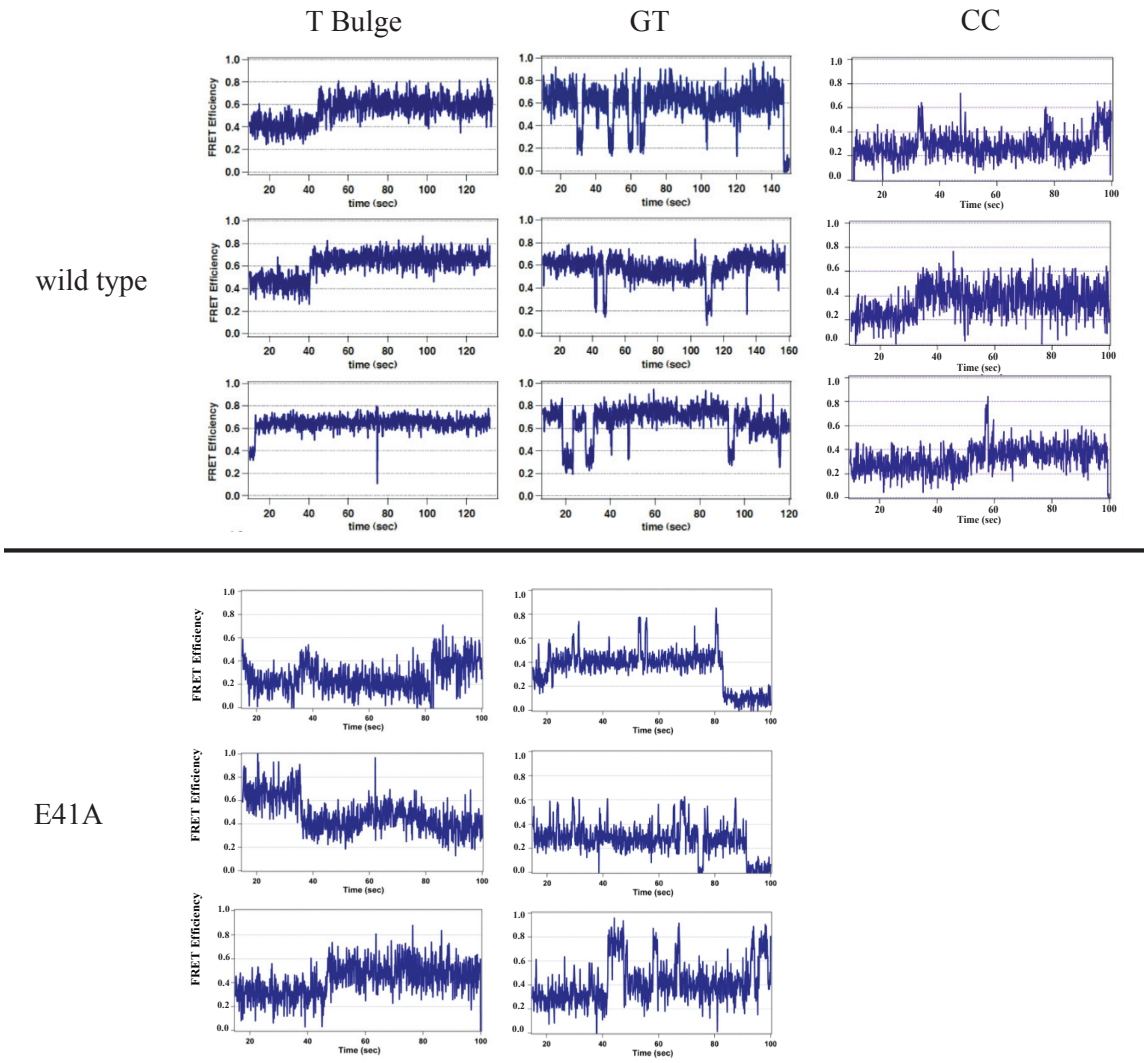


**Figure 2.1 – Example WT MutS and E41A MutS FRET traces in the presence of DNA substrates.**

Example FRET traces for T Bulge (left column), GT mispair (middle column), and CC mispair (right column) DNA in the presence of either wild type *Taq* MutS (top row) or E41A *Taq* MutS (bottom row) are shown in their respective panels. (T-bulge and GT wild type experiments performed by Lauryn Sass.)

these transitions proceed from the more stable high FRET state (~0.65) to the shorter-lived lower FRET state (~0.30) (Figure 2.1).

Of the three mismatches studied, the most extensive difference is observed when looking at the conformations of CC mismatch DNA in the presence of MutS. When MutS does bind the CC, the bound state is short-lived and is typically an intermediately bent conformational state. Representative MutS-CC mismatch FRET traces reveal that MutS-CC complexes proceed from the lower FRET state (~0.21) to the intermediate FRET state (~0.5) and back (Figure 2.1). Due to the rapid dynamic change between the lower FRET state to the intermediate FRET state, a subset of smFRET data was collected at a faster collection rate of 15 $ms^{-1}$ (rather than the 100 $ms^{-1}$ rate used with GT and T bulge) in order to better resolve the short lived states (Figure 2.1 – top right)[15 $ms^{-1}$ data collected by Ruoyi Qiu]. Analysis of the 15 $ms^{-1}$ data reveals a short-lived (83 ms), intermediately bent state (data not shown). The faster collection rate allowed the resolution of the intermediately bent state centered at FRET ~0.42 using the Cy3-Cy5 dye pair. Although we cannot make direct quantitative comparisons between the 100 $ms^{-1}$ Cy5-TAMRA used with the other mismatches described here and the 15 $ms^{-1}$ Cy5-Cy3 data, we can identify a general trend regarding the MutS-CC interaction. The MutS-CC complex rapidly samples an intermediate FRET state consistently and, based on the TDP generated (discussed below), we can say that the MutS-CC complex transitions between unbound DNA and the intermediate FRET state directly.

Histograms of the populations of FRET states sampled for MutS-homoduplex, MutS-T bulge, MutS-GT, and MutS-CC complexes are shown in Figure 2.2. Each

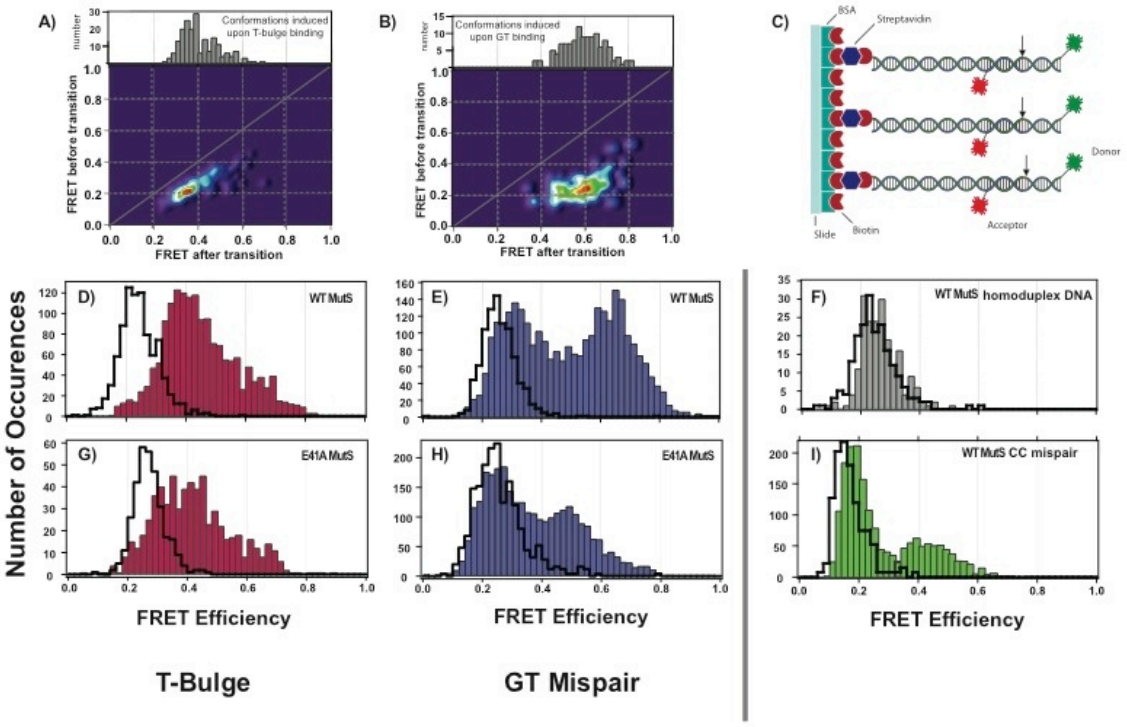


**Figure 2.2 – WT MutS and E41A MutS smFRET histogram distributions**

Binding data acquired by flowing protein for wild type *Taq* MutS on a T Bulge insertion/deletion (A) and a GT mispair (B). Each binding TDP is accompanied by its respective histogram of FRET states (above). A cartoon representation of the DNA substrate and slide functionalization is shown (C). Histogram distributions of observed FRET states for T Bulge DNA in the presence of wild type *Taq* MutS (D) and E41A MutS (G), for GT mispair DNA in the presence of wild type *Taq* MutS (E) and E41A MutS (F), for homoduplex DNA in the presence of wt MutS (F), and for CC mispair DNA in the presence of wild type MutS (I). For each histogram, black cityscapes indicate the distribution of the observed innate FRET state of DNA in the absence of protein and colored bars represent the distribution of FRET states in the presence of the indicated protein. Due to the rapid nature of the transitions on the CC mispair, the data shown (I) is

collected at a 50 ms frame rate using the Cy3-Cy5 dye pair.

histogram displays the innate FRET states associated with the unbound (free) DNA in cityscape and the FRET states associated with the formation of MutS-DNA complexes in shaded bars. The MutS-homoduplex DNA complexes do not exhibit a significant shift away from the innate DNA FRET distribution (shown in black cityscape) consistent with the low binding affinity and low specificity for MutS to homoduplex DNA.

The histogram distributions of FRET states vary widely between MutS-T bulge, MutS-GT, and MutS-CC complexes (Figure 2.2 panels D, E, and I). MutS-T bulge complexes sample FRET values centered around ~0.41 resulting in a single peak significantly shifted away from the free DNA distribution. Note the limited amount of overlap between the free DNA and MutS-T bulge distributions. The majority of the T bulge DNA is bound by MutS, where as free, unbound DNA is very infrequently observed. This result is not surprising given that *Taq* MutS binds T bulge with an affinity of 5 nM, vs. 40 nM $K_d$ for *Taq* MutS to a GT mismatch (Jiricny, Su et al. 1988; Yang, Sass et al. 2005; Sass, Lanyi et al. 2010). The overall distribution spans a wide FRET range from 0.14 to 0.82. The breadth of this distribution is indicative of multiple populations.

The distribution of MutS-GT FRET states has been extensively discussed previously (Sass, Lanyi et al. 2010). However, it is important to note two clear peaks centered at FRET ~0.30 and FRET ~0.65. Unlike the MutS-T bulge complex, there is a more significant overlap of the MutS-GT distribution with the free DNA. This observation is consistent with the lower binding affinity of MutS for a GT mismatch (40 nM) versus a T bulge (5 nM) (Yang, Sass et al. 2005).

In the case of the CC mismatch, there is a higher presence of free DNA in the majority of smFRET traces, which is not surprising given the low affinity of MutS for a CC mismatch (Brown, Brown et al. 2001; Cho, Chung et al. 2007). The overlap of the MutS-CC distribution with the free DNA profile is greater than that seen in either the T bulge or the GT mismatch distributions. The overall distribution is shifted toward higher FRET states with a median FRET at ~ 0.53, which is a more bent FRET state than that observed in the binding of MutS to T bulge. However, the MutS-GT bent states tend to sample even higher FRET.

To better explain the populations of FRET levels observed in the FRET efficiency histograms and the role each level might play in mismatch binding dynamics, it is necessary to evaluate not only the FRET level but also the transitions to and from each level. Transition density plots (TDPs) are three-dimensional histograms displaying a matrix of populations for each transition from FRET value Y to FRET value X and vice versa. Histogram distributions of the FRET states sampled in the presence of protein (Figure 2.2 panels D, E, G, H, and I), in conjunction with the TDPs (Figure 2.3), showing the conformational changes from one state to another determined from a population of smFRET trajectories, reveal distinct conformational states and dynamics between those states for MutS bound to different mismatches. MutS-T bulge, MutS-GT, and MutS-CC complexes differ in the extremity of the bent and unbent states, where the differences between the bent and unbent states are more exaggerated in the MutS-GT complexes (at opposite ends of the FRET histogram) and more subtle in the MutS-T bulge complexes and the MutS-CC complexes (closer in the mid-range of the FRET histogram).

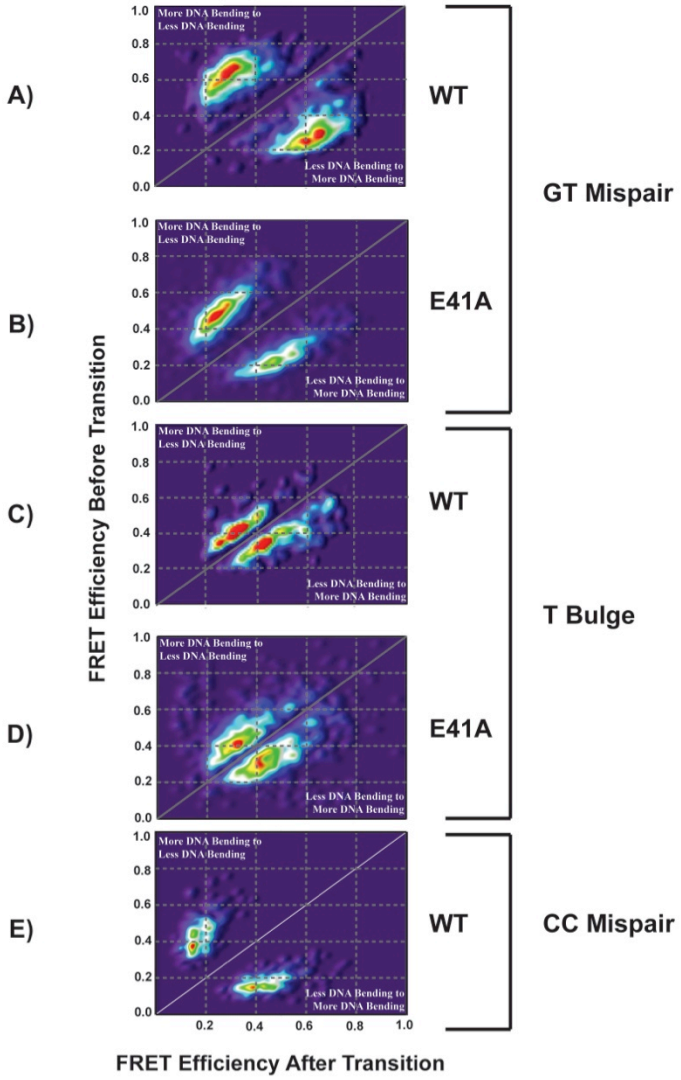


**Figure 2.3 - Transition density plots for WT MutS and E41A MutS in the presence of GT, T bulge, and CC mismatch DNA.**

TDPs of observed conformational or binding/unbinding FRET changes for wild type *Taq* MutS in the presence of a GT mispair (A), a T bulge IDL (C), or a CC mispair (E), and for E41A MutS in the presence of a GT mispair (B) or a T bulge IDL (D). Due to the rapid nature of the transitions on the CC mispair, the TDP shown (E) is collected at a 50 ms frame rate using the Cy3-Cy5 dye pair.

The relative stabilities of these states are significantly different between the mismatches, where the unbent state is stable but has a short lifetime in MutS-GT complexes, but is significantly stable in MutS-T bulge complexes (lifetimes were longer than could be identified in the experiments). In contrast, the MutS-CC complexes exhibit a stable, long lived unbent state and short, intermediate bent states. TDPs reveal interesting conformational differences in the dynamics of a MutS-T bulge complex versus a MutS-GT complex. Notably, the binding of MutS to a T bulge mismatch results in a conformational "walk" from the lower observed FRET state (~0.36) to the higher observed FRET state (0.46).

MutS-T bulge complexes preferentially sampled two FRET states centered at FRET ~ 0.36 and FRET ~ 0.46 (Figure 2.2D). Two additional conformations are isolated at higher FRET levels, indicating higher degrees of DNA bending, although these are less frequently sampled and are not the dominant states in these complexes. This result is in contrast to the MutS-GT complex whose most frequently sampled states are at FRET ~0.30 and FRET ~0.65 (Figure 2.2E). MutS-CC complexes sampled from a less bent state (FRET ~ 0.2) coinciding with the innate FRET of the free DNA to a medium bent state (FRET ~0.41) (Figure 2.2I) with a low relative stability of the bent state.

### *MutS binds the mismatch and directly induces unique conformational changes in the DNA*

All of the conformational dynamics observed and shown in Figure 2.1 were determined from steady-state studies, where MutS was pre-incubated with the DNA prior to single-molecule imaging. As a result, embedded in these data are all DNA binding, DNA unbinding, and MutS-DNA bound conformational transitions. We performed MutS

flow experiments to directly measure the first DNA conformation induced at the mismatch upon MutS binding by imaging immobilized DNA in a flow chamber while adding MutS in real-time. This allowed direct measurement of the change in FRET signal upon immediate MutS binding. These results for two mismatches, T bulge and GT, are shown in Figure 2.2 panels A and B.

The overall distribution of FRET states for MutS binding T bulge (Figure 2.2A) is consistent with the distribution of all states observed in the steady state experiments (Figure 2.2D). A dominant peak is observed at FRET ~0.36 with a secondary shoulder at FRET ~0.46. The overall shift away from the free DNA (FRET ~ 0.2) is consistent with that observed in the steady state experiments. A TDP of MutS binding to T bulge indicates that two distinct conformations are induced immediately upon binding. These two states are the two most stable states at FRET ~ 0.46 and FRET ~ 0.36. The lesser bent state at FRET ~ 0.36 is the more likely binding state. Binding of MutS to form the MutS-T bulge complex in the lower FRET state (~ 0.36) is consistent with the observed conformational progression from low FRET (unbent or mildly bent DNA) to high FRET (bent DNA).

In contrast, the distribution of FRET states adopted upon MutS binding to the GT mismatch (Figure 2.2B) indicates a preferential binding directly into the higher FRET ~0.65 observed in the steady state experiments (Figure 2.2E). The MutS-GT binding distribution indicates very little observed overlap with the region associated with free DNA. The TDP reveals more specifically that when MutS binds the GT mismatch, at least three or more different unique conformations may be induced. The most frequently observed DNA conformations are the stably bent state at FRET ~ 0.65 and the

intermediately bent state at FRET ~ 0.50. These two states being the most stable binding states are consistent with the steady state observations (Sass, Lanyi et al. 2010). The distribution of FRET states observed upon MutS binding the GT is overall very broad, supporting the idea that at least three unique FRET states are induced in these complexes, as previously described (Sass, Lanyi et al. 2010).

*Taq E41A MutS-DNA complex adopts wild type-like conformations on a T bulge and intermediately bent conformations on a GT mismatch*

smFRET reveals similarities between the observed conformational states of E41A MutS bound to a T bulge and the conformational states observed for wild type MutS-T bulge complexes. For the E41A MutS-T bulge complexes (Figure 2.2G), there is a higher population of free DNA than compared to the wt MutS-T bulge complexes (Figure 2.2D); however, the E41A-T bulge complexes have a similar distribution of FRET states (Figure 2.2G) in comparison to the wt MutS-T bulge complexes (Figure 2.2D). Interestingly, the E41A MutS-T bulge complexes are more dynamic (observed in FRET traces of individual molecules (Figure 2.1)) and sample the higher level bent states with a greater frequency than observed in the wt MutS-T bulge complexes. However, the overall distribution of FRET states and transition density plots for wild type (Figure 2.3C) and E41A MutS (Figure 2.3D) bound to the T bulge are very similar.

In contrast, differences in the conformational states of *Taq* E41A MutS and wild type MutS bound to a GT mismatch are observed. The results for the E41A-GT complexes provide a very different conformational profile in comparison to wt MutS-GT complexes. Like the E41A-T bulge complex, there is a higher percentage of free GT DNA in the presence of E41A MutS than wild type MutS, consistent with the reduced

binding affinity previously reported (Tessmer, Yang et al. 2008). When E41A MutS does bind the GT mismatch, there is a reduced population of the two most frequently sampled FRET states observed with wild type MutS (the bent and unbent states previously mentioned), and there is an increased population of the intermediately bent states. Most of the transitions observed in GT-E41A molecules are binding and unbinding transitions directly into these intermediately bent conformational states similar to those observed in the wild type MutS-CC complexes.

**Discussion**

Overall, using smFRET, we are able to observe that the conformational states for MutS-T bulge, MutS-GT, and MutS-CC complexes exhibit very different general trends in observed states, in relative stabilities of each state, and in time-scales for transitions from state to state. MutS-T bulge complexes exhibit a single broad FRET population centered around FRET efficiency of 0.4 with a general step-wise walk transitioning from lower to higher FRET states. The time scales of transitions from lower to higher FRET states are slower than those observed in either MutS-GT or MutS-CC complexes and each resulting state sampled by the MutS-T bulge complex is long-lived suggesting a greater relative stability of the higher FRET state. MutS-GT complexes exhibit dynamic behaviors already discussed elsewhere (Sass, Lanyi et al. 2010) not observed in either MutS-T bulge or MutS-CC complexes. The most dominant state in MutS-GT complexes is a stable bent conformation (FRET ~ 0.65), and the primary conformational pathway is an equilibrium between this state and a stable unbent state (FRET ~ 0.30), although at least 4 other DNA conformations were identified (Sass, Lanyi et al. 2010). In contrast, when MutS is bound at a T bulge base-insertion or a CC mismatch, the DNA

conformational profile, including the number of DNA conformational states sampled, the kinetic exchange between those states, and the overall lifetime of MutS bound to the DNA, are significantly different from those observed in MutS-GT complexes.

This difference in transition trends between those observed for the MutS-T bulge complex and the MutS-GT complex can be explained by the relative stabilities of the different conformational states uniquely sampled by each complex upon DNA binding (Figure 2.2 panels D and E). Based on the long lifetime of the MutS-T bulge complex (we rarely observed dissociation transitions of MutS unbinding the DNA in steady state studies (Figure 2.1)), we estimate that this MutS-DNA complex is ~ 2.4 kcal/mol more stable than the MutS-GT complex. The lifetime of the unbent MutS-T bulge complex (FRET ~ 0.36) is significantly longer than the relative lifetime of the comparable state in the GT-MutS complex (stable unbent state at FRET ~ 0.30). In fact, the two stable MutS-T bulge conformations appear to have similar relative stabilities (roughly based on the long lifetimes of both states). As a result, there is a lower energy barrier for the transition between the bent state and the unbent state in MutS-T bulge complexes than those observed in MutS-GT complexes.

This suggestion is supported by a study with Uracil DNA Glycosylase, where it was noted that the energy barrier for a transition from a bent DNA state to an unbent DNA state at an unpaired base is ~ 3 kcal/mol lower than for paired DNA bases (Krosky, Song et al. 2005). This result is not surprising given the inherent differences in the local properties of a base-base mismatch which contains intact base pairing and hydrogen bonding versus those of an unpaired base which has little to no interactions with the surrounding residues in the DNA. It is likely that MutS is binding the T bulge directly

into the stable bent state, but the transition to the unbent state is faster than our data acquisition rate in these experiments. The ease in which the unbent state is formed, particularly here for *Taq* MutS-T bulge complexes, supports a model that DNA unbending signals repair, particularly in line with the high repair efficiency of base insertion and deletion mismatches in prokaryotes.

### *Glu41 stabilizes the MutS-mismatch DNA complex and also stabilizes DNA bending and unbending*

An intermediately bent state observed in E41A MutS-GT complex dynamics was observed as an unstable, briefly sampled state in the wt MutS-GT FRET traces (Sass, Lanyi et al. 2010). These observations are also consistent with AFM observations that showed a shift in the unbent DNA population to a more intermediately bent state (Tessmer, Yang et al. 2008). However, what are lost in the AFM data are the rapid transitions observed into and out of this intermediately bent state. Near exclusive formation of this intermediately bent state in the E41A-GT complexes suggests that the Glu residue is essential in the formation of a bent DNA conformation. However, the rapid transitions observed suggest that the Glu residue is also essential in driving the DNA to an unbent state and stabilizing the unbent state once formed. *In vivo* studies indicate that the glutamate to alanine mutation in *E. coli* (E38A) results in mutation rates similar to a MutS null cell line and a deficiency in repair of both single base-base mismatches and single base IDLs (Holmes, Scarpinato et al. 2007). However, the homologous mutation in *S. cerevisiae* (yMsh2-Msh6$^{E339A}$) results in competent *in vivo* repair of single base insertion/deletion and a loss of *in vivo* repair of single base-base mismatches (Holmes, Scarpinato et al. 2007).

Interestingly, while the conformational dynamics of the MutS-T bulge and the MutS-GT complexes differ so greatly, the opposite can be said of the MutS-CC and the E41A-GT complexes. Both MutS-CC and E41A-GT complexes sample rapid conformational transitions from a low, long lived FRET state corresponding with free DNA (~0.3) into short-lived, medium FRET states (~0.6-0.8). The histogram distribution of these sampled conformational states indicates an increase in overlap with the free DNA distribution for both complexes as a well as a decrease in the number of times a high FRET value (FRET 0.65) corresponding with the bent state observed for MutS-GT complexes is observed. In both data sets we observe a dominance of those FRET states associated with intermediate transition states in the MutS-GT complexes.

Overall, the FRET results for the E41A mutant on both the base-base mismatch and the insertion/deletion mismatch and the results for wild type MutS on a CC mismatch have interesting implications regarding the differential *in vivo* mutator phenotypes of the homologous yMsh2-Msh6$^{E339A}$ for repair of base-base mismatches versus repair of base insertions/deletions in (Holmes, Scarpinato et al. 2007). Our results suggest a requirement for MutS-DNA complexes to undergo specific conformational sampling of states to signal repair. It is likely that it is necessary to sample both a stable bent state and a stable unbent state with some frequency in order for the MutS-DNA complexes to get on to proper conformational path to signal repair. Because the MutS-DNA complexes for the E41A mutant bound to a GT mismatch and wt MutS bound to a CC mismatch are unable to induce the necessary conformations to initiate the downstream repair effects, these systems cannot efficiently undergo MMR.

*DNA bending and unbending are essential in the ability for MutS to signal repair*

The DNA conformational dynamics studied for wild type MutS and E41A MutS, in comparison with *in vivo* repair of different mismatches by the wild type and mutated MutS proteins, support a dynamic DNA bending and unbending mechanism necessary to signal mismatch repair. There is a high degree of correlation between particular DNA conformations sampled in these dynamic studies and the ability for specific mismatches to be repaired. The T bulge and GT mismatches, in the presence of wild type MutS, sample several different DNA conformations, but do exhibit two dominant states that are clearly more stable than the others and interchange directly between each other as the prevalent conformational transitions in the complexes. The CC mismatch is poorly bound by wild type MutS in general, but when binding occurs, an intermediately bent state is formed, and unbinding is not far behind. The inability for MutS to induce appropriate DNA conformations at this mismatch is consistent with this mismatch being deficiently repaired *in vivo*.

The conformational dynamics of *Taq* E41A MutS are especially interesting and also support a dynamic kinetic sampling mechanism for mismatch repair initiation by MutS. Specifically, E41A MutS-T bulge complexes behave very similar to the wild type MutS-T bulge complexes, sampling identical bent and unbent states and exhibiting similar transitions between those states. The E41A MutS-T bulge complexes are certainly more dynamic, supporting the role of the Glu residue in the binding motif to stabilize these states. However, the complexes are able to sample the proposed conformations essential for repair. On the contrary, the E41A MutS-GT complexes behave differently from the wild type MutS-GT complexes. The E41A MutS-GT complex is not very stable, and the most stable state is an intermediately bent state

considered to be off of the preferred bent to unbent conformational pathway. These results support the necessity of the Glu residue to stabilize both bending and unbending at a base-base mismatch. These results are supported by the *in vivo* observations in yMutSα that the Glu-to-Ala mutation only displays a mutator phenotype for repair of base-base mismatches (Holmes, Scarpinato et al. 2007). All of these results combined support the DNA bending model and the hypothesis that the delicate balance of conformational dynamics and transitions between stable bent and stable unbent states is necessary for the signaling of repair.

*Can DNA bending dynamics tell us something about mismatch repair in vivo?*

Genetic studies revealed that *S. cerevisiae* MutSα (yMutSα) maintains nearly complete functionality in frameshift repair (represented by the T bulge substrate) with loss of repair of base-base mismatches with the Msh2-Msh6$^{E339A}$ mutation (Holmes, Scarpinato et al. 2007). Our results reveal that this mutant in *Taq* behaves differently when bound to base-base mismatches in comparison to base insertion/deletions. There are two elements, the stability of the MutS-DNA complex itself and the conformational dynamics of these DNA-MutS complexes. It has been previously suggested that the stability of the MutS-mismatched DNA complex itself does not necessarily dictate repair efficiency because even mismatches bound weakly by MutS are repaired *in vivo* (Sass, Lanyi et al. 2010). The work presented here evokes questions regarding the role DNA conformational dynamics may serve in DNA mismatch repair.

The DNA bending model hypothesizes that DNA bending and unbending serve as signaling strategies employed by MutS to get repair underway (Wang, Yang et al. 2003). Detailed results of MutS-GT complexes, combined with the results presented here for

MutS bound to two other mismatches, leads to the proposition that dynamic conformational sampling of MutS-DNA complexes could also have a part in governing mismatch repair initiation, and perhaps significant occupancy in a stable unbent conformation is necessary for efficient signaling of mismatch repair.

Although E41A-T bulge complexes frequently occupy bent DNA conformations, these complexes are very dynamic and continue to sample the unbent DNA conformation with reasonable frequency (for several seconds or longer). If similar conformational dynamics occur for the homologous mutation in yMutSα, this observation may explain why this Glu-to-Ala mutation does not eliminate repair of frameshifts *in vivo* (Holmes, Scarpinato et al. 2007).

We observe very different DNA conformational dynamics for E41A-GT complexes. These complexes were very unstable and did not appear to occupy the unbent conformation that we observe in the wild type MutS-GT complexes. Once again, if we hypothesize that similar conformational dynamics occur for the homologous mutation in yMutSα, this observation may explain why the Glu-to-Ala mutation eliminates repair of base-base mismatches *in vivo* (Holmes, Scarpinato et al. 2007).

Lebbink and coworkers suggested that the hydrogen bond between the glutamate and the GT mismatch in *E. coli* was essential in inducing a conformational change in MutS to an ATP-bound sliding clamp MutS conformation that functions in signaling repair (Sass, Lanyi et al. 2010). The DNA bending model suggests that DNA unbending also facilitates the formation of this MutS sliding clamp, thus signaling the ATPase activity of MutS and repair initiation. Therefore, the inability of *Taq* MutS (E41A)-GT complexes to sample the unbent DNA conformation is consistent with all of these

previous *in vitro* and *in vivo* observations (Wang, Yang et al. 2003; Lebbink, Georgijevic et al. 2006; Holmes, Scarpinato et al. 2007; Sass, Lanyi et al. 2010).

**Conclusions**

We used smFRET to measure mismatched DNA binding and bending by MutS at multiple mismatches and to determine what effect, if any, the mutation of a conserved Glu in the DNA binding motif would have on mismatch recognition and DNA conformational flexibility and dynamics. The results revealed that DNA conformations, and the dynamics between them, play an important role in mismatch recognition and the ability to signal repair. Well-repaired mismatches sample a number of different states but follow a clearly preferred pathway between a stable bent and a stable unbent state. Mismatches that are poorly repaired, such as the CC mismatch here, are not able to form these stable on-path states.

Studies of the E41A MutS mutant and its interactions with both an insertion/deletion mismatch and a base-base mismatch reveal that the Glu residue helps to form a stable MutS-GT complex but is less necessary in stabilizing the MutS-T bulge complex given the lifetime of the mutated protein on the DNA for both of these mismatches. These results complement *in vivo* observations (Lebbink, Georgijevic et al. 2006; Holmes, Scarpinato et al. 2007) and suggest that formation of a stable MutS-mismatch complex, while important to in mismatch recognition, cannot be the only factor in initiating DNA mismatch repair *in vivo* (Jiricny, Su et al. 1988).

Our results show that mismatched E41A MutS-DNA complexes are very dynamic, with DNA conformational fluctuations increased considerably relative to the wild type MutS-DNA complexes. The dynamics of mismatched DNA-MutS complexes

may govern mismatch repair signaling and offer a link between MutS-DNA structures and mismatch repair efficiency that is not revealed in crystal structures alone. We propose, in line with the DNA bending model, that the ability to sample an unbent DNA conformation may be fundamental in initiating mismatch repair. As a result, more dynamic MutS-DNA complexes may sample the unbent conformation less frequently and still be repaired (e.g. E41A-T bulge) while others are incapable of sampling the unbent conformation and are less able to signal repair efficiently (e.g. E41A-GT), resulting in refractory or decreased mismatch repair *in vivo*.

If protein-DNA dynamics play an essential role in signaling important downstream effects like DNA MMR, what other protein-DNA systems may also utilize such a dynamic system? Static techniques like AFM and X-ray crystallography give researchers an insightful snapshot of protein-DNA interactions in potentially the most stable of conformations, but dynamic techniques such as smFRET are excellent tools in revealing the dynamic nature in which these interactions actually exist. We can potentially gain insight into intermediate conformational states such as the states described in this work, the kinetics of conformational state transitions, and conformational state transition pathways. The results described here lead one to speculate about the potential dynamics associated with other known dynamic systems such as the DNA base-flipping systems like the MutY system or transcription factor binding.

## Experimental Procedures

*Protein and DNA substrates*

Wild type MutS and E41A MutS from *Thermus aquaticus* were over-expressed in *Escherichia coli* and purified as previously described (Biswas and Hsieh 1996). HPLC-purified labeled and unlabeled single-stranded oligonucleotides were purchased from Integrated DNA Technologies. DNA substrates contained a TAMRA-labeled oligonucleotide (5′-Biotin-TGT CGG GGC TGG CTT AAG GTG TGA AAT ACC TCA TCT CGA GCG TGC CGA TA-TAMRA-3′) annealed to a Cy5-labeled oligonucleotide (5′-TAT CGG CAC GTT CGA GATG-Cy5-3′) to create a duplex DNA fragment containing a GT base-base mismatch (Figure 2.2C). Oligonucleotides were annealed in buffer containing 20 mM Tris-HCl pH 7.8, 100 mM sodium acetate, and 5 mM magnesium chlordie in a 1:1 ratio at 65°C for 20 minutes followed by slow cooling. When the temperature reached 55°C, an additional complementary strand (5′-AGG TAT TTC ACA CCT TAA GCC AGC CCC GACA-3′) was added and annealed to complete the duplex DNA substrate. The substrate was allowed to slowly cool to room temperature and was stored on ice or at 4°C.

*Fluorescence microscopy*

Quartz microscope slides and flow channels were prepared as previously described (Li, Augustine et al. 2007). Slides were thoroughly cleaned by 15 minute incubations in a bath sonicator in the following series of solvents: $H_2O$/detergent (Alconox), acetone, ethanol, 1 M potassium hydroxide, ethanol, 1 M potassium hydroxide. Slides were rinsed and stored in water and flamed under a propane torch to dry immediately before use. Flow channels were created in the slides by adhering a No.

1.5 coverslip to the slide using Scotch double-sided tape as a spacer. Edges were sealed with epoxy. DNA samples were inserted into the channels through small holes drilled in the quartz slide prior to cleaning.

The quartz surface was treated first with biotinylated-BSA (Sigma, 1 mg/mL, 5 minute incubation) followed by streptavidin (Invitrogen, 0.1 mg/mL, 5 minute incubation), similar to methods previously described (McKinney, Freeman et al. 2005). Annealed, biotinylated, fluorescently-labeled, mismatched DNA was added to the treated surfaces at a concentration ranging between 10 and 30 pM for 5 minutes, and the unbound DNA was removed by rinsing with chilled buffer (20 mM Tris-HCl pH 7.8, 100 mM NaOAc, and 5 mM $MgCl_2$). Samples were imaged at room temperature in the above rinsing buffer with the addition of enzymatic oxygen scavenging components (2% glucose (Sigma), 1% β-mercaptoethanol (Fluka), 0.1 mg/mL glucose oxidase (Sigma), and 0.025 mg/mL catalase (Sigma)) to enhance fluorophore lifetime and with the addition of triplet state quencher cyclooctatetraene (Aldrich) (~50 μM) to reduce dye blinking. Images were collected both in the presence and absence of MutS. Protein was allowed to bind the DNA for at least 5 minutes prior to image collection for steady state experiments. Protein was added through a flow-cell apparatus for flow-binding experiments, with imaging in real-time.

Data were collected using a prism-type total internal reflection fluorescence (TIRF) laser microscope as described (Li, Augustine et al. 2007). Two lasers were directed onto the prism, one at 532 nm to directly excite the donor dye (TAMRA) and one at 635 nm in an alternating sequence to directly excite the acceptor dye (Cy5) at the quartz-solution interface. Fluorescence emission was collected through a 60x 1.2 NA

water immersion objective and split by a 645dcrx dichroic mirror (Chroma) into short and long wavelength paths. These paths were filtered for TAMRA and Cy5 emissions using HQ 585/70 and HQ 700/75 bandpass filters (Chroma), respectively. The spectrally-resolved emissions were relayed as side-by-side images onto a charge-coupled device camera (Cascade 512B, Roper Scientific). Images were exposed at 10 frames per second and collected using software written in-house.

Observed intensities of single molecules were integrated with software written in-house to obtain individual fluorescence emission time traces as described previously (Li, Augustine et al. 2007). Emission traces were background subtracted and corrected for leakage of the donor signal into the acceptor channel (~ 5%). Molecules not confirmed to contain exactly one donor and one acceptor fluorophore were excluded from further analysis. FRET efficiencies were calculated from the respective donor and acceptor emissions as $E = (I_A)/(I_D + I_A)$, where $I_D$ and $I_A$ are the corrected intensities of the donor fluorophore and acceptor fluorophore, respectively.

*FRET data analysis*

We apply a Gaussian derivative kernel algorithm to isolate FRET transitions in single-molecule traces (Canny 1986). This algorithm (as previously described and available at http://www.cs.unc.edu/~nanowork/cismm/download/edgedetector/index.html) yields each FRET efficiency sampled in a given FRET trace as well the time the molecule spends at that FRET efficiency ('dwell time', or $\Delta t$) and the transition sequence (Sass, Lanyi et al. 2010). FRET transitions are used to generate transition density plots (TDPs) and lifetimes are used to assess the kinetics of the different conformations sampled for a

given MutS-DNA complex. Details of this analytical approach have been previously described (Sass, Lanyi et al. 2010).

## References


Au, K. G., K. Welsh, et al. (1992). "Initiation of methyl-directed mismatch repair." J Biol Chem **267**(17): 12142-12148.

Biswas, I. and P. Hsieh (1996). "Identification and characterization of a thermostable MutS homolog from Thermus aquaticus." J Biol Chem **271**(9): 5040-5048.

Brown, J., T. Brown, et al. (2001). "Affinity of mismatch-binding protein MutS for heteroduplexes containing different mismatches." Biochem J **354**(Pt 3): 627-633.

Buermeyer, A. B., S. M. Deschenes, et al. (1999). "Mammalian DNA mismatch repair." Annu Rev Genet **33**: 533-564.

Canny, J. (1986). "A computational approach to edge detection." IEEE Trans. Pattern Anal. Mach. Intell. **8**(6): 679-698.

Cho, M., S. Chung, et al. (2007). "A simple fluorescent method for detecting mismatched DNAs using a MutS-fluorophore conjugate." Biosens Bioelectron **22**(7): 1376-1381.

Das Gupta, R. and R. D. Kolodner (2000). "Novel dominant mutations in Saccharomyces cerevisiae MSH6." Nat Genet **24**(1): 53-56.

DeRocco, V., T. Anderson, et al. (2010). "Four-color single-molecule fluorescence with noncovalent dye labeling to monitor dynamic multimolecular complexes." Biotechniques **49**(5): 807-816.

Drotschmann, K., W. Yang, et al. (2001). "Asymmetric recognition of DNA local distortion. Structure-based functional studies of eukaryotic Msh2-Msh6." J Biol Chem **276**(49): 46225-46229.

Drummond, J. T., G. M. Li, et al. (1995). "Isolation of an hMSH2-p160 heterodimer that restores DNA mismatch repair to tumor cells." Science **268**(5219): 1909-1912.

Holmes, S. F., K. D. Scarpinato, et al. (2007). "Specialized mismatch repair function of Glu339 in the Phe-X-Glu motif of yeast Msh6." DNA Repair (Amst) **6**(3): 293-303.

Isaacs, R. J., W. S. Rayens, et al. (2002). "Structural differences in the NOE-derived structure of G-T mismatched DNA relative to normal DNA are correlated with differences in (13)C relaxation-based internal dynamics." J Mol Biol **319**(1): 191-207.

Jiricny, J. and G. Marra (2003). "DNA repair defects in colon cancer." Curr Opin Genet Dev **13**(1): 61-69.

Jiricny, J., S. S. Su, et al. (1988). "Mismatch-containing oligonucleotide duplexes bound by the E. coli mutS-encoded protein." Nucleic Acids Res **16**(16): 7843-7853.

Junop, M. S., G. Obmolova, et al. (2001). "Composite active site of an ABC ATPase: MutS uses ATP to verify mismatch recognition and authorize DNA repair." Mol Cell **7**(1): 1-12.

Kramer, B., W. Kramer, et al. (1984). "Different base/base mismatches are corrected with different efficiencies by the methyl-directed DNA mismatch-repair system of E. coli." Cell **38**(3): 879-887.

Krosky, D. J., F. Song, et al. (2005). "The origins of high-affinity enzyme binding to an extrahelical DNA base." Biochemistry **44**(16): 5949-5959.

Kunkel, T. A. and D. A. Erie (2005). "DNA mismatch repair." Annu Rev Biochem **74**: 681-710.

Lamers, M. H., A. Perrakis, et al. (2000). "The crystal structure of DNA mismatch repair protein MutS binding to a G x T mismatch." Nature **407**(6805): 711-717.

Lebbink, J. H., D. Georgijevic, et al. (2006). "Dual role of MutS glutamate 38 in DNA mismatch discrimination and in the authorization of repair." Embo J **25**(2): 409-419.

Lebbink, J. H. G., D. Georgijevic, et al. (2006). "Dual role of MutS glutamate 38 in DNA mismatch discrimination and in the authorization of repair." The EMBO journal **25**(2): 409-419.

Li, Y., G. J. Augustine, et al. (2007). "Kinetics of complexin binding to the SNARE complex: correcting single molecule FRET measurements for hidden events." Biophys J **93**(6): 2178-2187.

Loeb, L. A., K. R. Loeb, et al. (2003). "Multiple mutations and cancer." Proc Natl Acad Sci U S A **100**(3): 776-781.

Malkov, V. A., I. Biswas, et al. (1997). "Photocross-linking of the NH2-terminal region of Taq MutS protein to the major groove of a heteroduplex DNA." J Biol Chem **272**(38): 23811-23817.

McKinney, S. A., A. D. Freeman, et al. (2005). "Observing spontaneous branch migration of Holliday junctions one step at a time." Proc Natl Acad Sci U S A **102**(16): 5715-5720.

Modrich, P. L. (1989). "Methyl-directed DNA mismatch correction." Journal of Biological Chemistry.

Natrajan, G., M. H. Lamers, et al. (2003). "Structures of Escherichia coli DNA mismatch repair enzyme MutS in complex with different mismatches: a common recognition mode for diverse substrates." Nucleic Acids Res **31**(16): 4814-4821.

Obmolova, G., C. Ban, et al. (2000). "Crystal structures of mismatch repair protein MutS and its complex with a substrate DNA." Nature **407**(6805): 703-710.

Peltomaki, P. (2003). "Role of DNA mismatch repair defects in the pathogenesis of human cancer." J Clin Oncol **21**(6): 1174-1179.

Sass, L. E., C. Lanyi, et al. (2010). "Single-molecule FRET TACKLE reveals highly dynamic mismatched DNA-MutS complexes." Biochemistry **49**(14): 3174-3190.

Schofield, M. J., F. E. Brownewell, et al. (2001). "The Phe-X-Glu DNA binding motif of MutS. The role of hydrogen bonding in mismatch recognition." J Biol Chem **276**(49): 45505-45508.

Selmane, T., M. J. Schofield, et al. (2003). "Formation of a DNA mismatch repair complex mediated by ATP." J Mol Biol **334**(5): 949-965.

Tessmer, I., Y. Yang, et al. (2008). "Mechanism of MutS searching for DNA mismatches and signaling repair." J Biol Chem **283**(52): 36646-36654.

Wang, H., Y. Yang, et al. (2003). "DNA bending and unbending by MutS govern mismatch recognition and specificity." Proc Natl Acad Sci U S A **100**(25): 14822-14827.

Warren, J. J., T. J. Pohlhaus, et al. (2007). "Structure of the Human MutSalpha DNA Lesion Recognition Complex." Mol Cell **26**(4): 579-592.

Yamamoto, A., M. J. Schofield, et al. (2000). "Requirement for Phe36 for DNA binding and mismatch repair by Escherichia coli MutS protein." Nucleic Acids Res **28**(18): 3564-3569.

Yang, Y., L. E. Sass, et al. (2005). "Determination of protein-DNA binding constants and specificities from statistical analyses of single molecules: MutS-DNA interactions." Nucleic Acids Res **33**(13): 4322-4334.

# Chapter 3

## FOUR-COLOR SINGLE MOLECULE FLUORESCENCE WITH NONCOVALENT DYE LABELING TO MONITOR DYNAMIC MULTIMOLECULAR COMPLEXES



### Introduction

Single molecule fluorescence techniques, including single-molecule Förster resonance energy transfer (smFRET), allow measurements of molecular associations and conformational changes during protein-protein and protein-nucleic acid interactions (Ha, Ting et al. 1999). Many important biological processes are amenable to single molecule studies by fluorescently labeling the molecules of interest and recording fluorescence emissions. Detection of three distinct single molecule fluorescence signals for multimeric colocalization or multiple FRET couplings have been demonstrated (Bowen, Weninger et al. 2004; Hohng, Joo et al. 2004; Clamme and Deniz 2005; Friedman, Chung et al. 2006; Lee, Kapanidis et al. 2007; Ross, Buschkamp et al. 2007; Roy, Kozlov et al. 2009; Munro, Altman et al. 2010). Discrimination of single molecule fluorescence from 4 distinct dyes is used in a commercial DNA sequencing instrument employing zero mode waveguide sample chambers and prism-based spectral dispersion (Lundquist, Zhong et al.

---

[1] DeRocco, V., T. Anderson, et al. (2010). "Four-color single-molecule fluorescence with noncovalent dye labeling to monitor dynamic multimolecular complexes." BioTechniques **49**(5): 807-816.

2008; Eid, Fehr et al. 2009). This sophisticated instrument has not quantified FRET efficiency at single molecule level for four dyes. FRET interactions among four dyes on DNA have been recorded with a confocal microscope employing photodiodes for single point detection (Heilemann, Tinnefeld et al. 2004). Here, we present a simple modification of the typical two-color total internal reflection microscope (TIRM) that provides detection of single molecule fluorescence in four distinct spectral channels simultaneously using wide-field imaging, and we demonstrate its capabilities for quantitative FRET studies (Figure 3.1). Instrument construction is related to that used to characterize polarization and two-color FRET simultaneously (Webb, Rolfe et al. 2008). We combine this instrument with a tris-nitrilotriacetic acid (tris-NTA) dye-labeling to introduce a flexible approach for studying dynamics of multimeric complexes.

To dye-label proteins while preserving function, we use the recently developed tris-NTA-fluorophores (Lata, Reichel et al. 2005; Lata, Gavutis et al. 2006). Ensemble FRET studies (Kapanidis, Ebright et al. 2001) used similar mono- and bis-NTA dyes, which bind 6-histidine tagged (6-his) proteins with micromolar affinities. In contrast, tris-NTA- fluorophores have subnanomolar to nanomolar binding constants for 6-his-proteins and dissociation rates on the order of $10^{-3}$ to $10^{-4}$ $s^{-1}$ (Lata, Reichel et al. 2005). The dye-bound state lifetimes of thousands of seconds are sufficient for most single molecule fluorescence experiments. A fluorescent dye is attached to the tris-NTA moiety via a 6-carbon linker (Lata, Reichel et al. 2005) similar to the linker in commonly used covalently-linked dyes. This linker allows rotational flexibility for the dye, which is important for quantitative FRET applications. The non-covalent labeling is versatile, easily performed, and allows labeling proteins that do not tolerate more common labeling

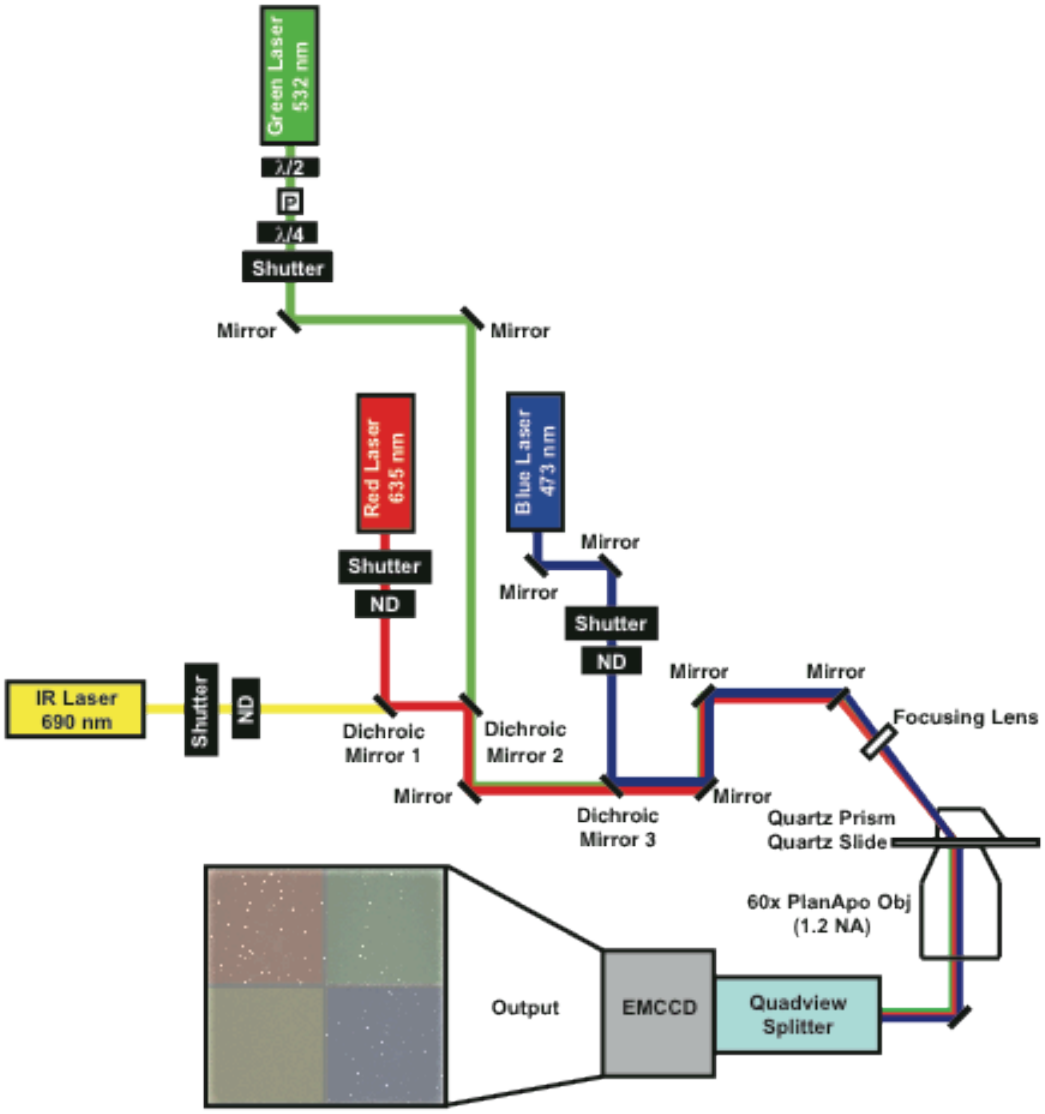


**Figure 3.1 – Four-color single molecule TIRF microscope schematic.**

Simultaneous FRET and colocalization experiments were performed using the prism-type total internal reflection configuration. An Olympus IX51 inverted microscope with a 60x PlanApo water immersion objective and a Quadview image splitter (550dcxr, 645dcxr, 750 dcxr) relayed the emitted fluorescence to a Cascade 512B emCCD camera. Laser

excitation was shutter controlled. ND = neutral density filter; P= polarization dependent beamsplitter; λ/2 = half wave plate; λ/4=quarterwave plate.

approaches. We demonstrate colocalization of a transient binding partner via its tris-NTA-fluorophore while simultaneously measuring conformational changes in the substrate using a FRET pair spectrally distinct from the tris-NTA dye with single molecule sensitivity for two different biological systems: one monitoring protein-induced DNA bending (yMutSα-mismatched DNA complexes) and the other monitoring protein-induced conformational changes in another protein (SNARE complexes). Both of these systems involve protein-induced conformational changes in the substrate that can be monitored by smFRET; however, independently colocalizing the binding partner confirms assembly of the complex.

## Materials and Methods

### *Oligonucleotides*

We purchased dye- and biotin-labeled oligonucleotides from Integrated DNA Technologies (Coralville, IA). The 50-bp Biotin/TAMRA-labeled oligonucleotide was 5′-Biotin-TGTCGGGGCTGGCTTAAGGTGTGAAATACCTCATCTCGAGCGTGCCGATA-TAMRA–3′. The Cy5-labeled 19-bp complement was 5′-TATCGGCACCCTCGAGATG-Cy5-3′ (underlined indicates CC base-base mispair). The unlabeled 31-bp complement was 5′-AGGTATTTCACACCTTAAGCCAGCCCC GACA–3′. The 50-bp and 19-bp oligonucleotides were annealed at ~65 $^{o}$C for 20 min and slowly cooled to 55 $^{o}$C. At 55 $^{o}$C, the 31 bp complement was added and the mixture was cooled to room temperature (Figure 3.2A,B).

### *yMsh2-Msh6 protein*

Expression and purification of 6-his tagged yMsh2-Msh6 (yMutSα) was performed as described (Clark, Cook et al. 1999). Dr. Thomas Kunkel (NIEHS, Research Triangle Park, NC) provided yMsh2 (pAC12 His-Msh2) and yMsh6 (yEpspGal Msh6) plasmids.

*SNARE proteins*

Expression and purification of full-length syntaxin-1A, soluble syntaxin-1A (1-263), SNAP-25, and soluble synaptobrevin(1-96) were as described (Weninger, Bowen et al. 2003; Bowen, Weninger et al. 2004; Weninger, Bowen et al. 2008). Unless indicated that 6-his tags were retained, 6-his tags were removed with thrombin as verified by SDS-PAGE. Munc-18 was expressed and purified as described (Weninger, Bowen et al. 2008) without 6-his tag removal.

SNARE proteins with combinations of indicated cysteine mutations introduced into cysteine free templates (syntaxin- e35c, s249c; synaptobrevin-s61c, a72c; SNAP-25-q20c-n139c) and Munc-18 (containing all native cysteines) were labeled by mixing with 10-fold excess maleimide dyes (Alexa Fluors 488, 555 and 647; all Invitrogen, Carlsbad, CA) in 20 mM phosphate, 200 mM NaCl, 100 μM TCEP, pH 7.4, overnight at 4°C. Labeling efficiencies were 30% (syntaxin), 50% (synaptobrevin), >80% (SNAP-25) and 200% (Munc-18). Wild-type synaptobrevin(1-96) was labeled with Cy7-NHS (GE Healthcare, Piscataway, NJ) by incubating with equimolar dye in 20 mM Phosphate, 200 mM NaCl, pH 8, overnight at 4°C, yielding 50% labeling. Synaptobrevin contains 2 central lysines (residues 52 and 59) and 5 C-terminal lysines (residues 83,85,87,91 and 94). Thus, we expect >70% of the Cy7-synaptobrevin to carry a C-terminally located

dye. Note, optimization of labeling is important because the total four-color labeling efficiency of a multimeric complex is the product of individual efficiencies.

Parallel SNARE complex was formed from SNAP-25, $His_6$-synaptobrevin, and syntaxin as described elsewhere, including the 7M urea-buffer wash (Weninger, Bowen et al. 2003).

*DNA Sample Preparation*

Biotinylated dsDNA was incubated for 10 min at 10 pM on biotinylated-BSA (Sigma-aldrich, St. Louis, MO)-streptavidin (Invitrogen) coated quartz slides as described elsewhere (Li, Augustine et al. 2007; Sass, Lanyi et al. 2010). All experiments were performed at room temperature in 20 mM Tris HCl, 100 mM sodium acetate, 5 mM magnesium chloride, 2% glucose, 0.1 mg $mL^{-1}$ glucose oxidase, 0.025 mg $mL^{-1}$ catalase, 2 mM 6-hydroxy-2,5,7,8-tetramethylchroman-2-carboxylic acid (Trolox) and 50 μM cyclooctotetraene all at pH 7.8 (all Sigma-Aldrich). No reducing agents were used to preserve the 6-His-$Ni^{2+}$-NTA complex.

*SNARE Sample Preparation*

Soluble SNARE complex was encapsulated at 33 nM per 3 mg $ml^{-1}$ lipids in 100 nm egg phosphatidylcholine liposomes with 5% biotin-phosphatidylethanolamine lipids (Rhoades, Gussakovsky et al. 2003; Choi, Strop et al. 2010) (Avanti Polar Lipids, Alabaster, AL). The liposomes were formed with a syringe mini-extruder using 100 nm filters. The protein-containing liposomes were separated from free protein using gel filtration (SepharoseCL-4B) (GE Healthcare). Liposomes were tethered to biotinylated-BSA/streptavidin-coated quartz slides as described for the DNA samples. SNARE

complex containing full-length syntaxin was reconstituted into supported bilayers as detailed elsewhere (Weninger, Bowen et al. 2008).

*tris-NTA-Oregon Green Labeling*

tris-NTA fluorescent dye conjugates were prepared as described elsewhere (Lata, Reichel et al. 2005; Lata, Gavutis et al. 2006). We dye-labeled yMsh2-Msh6 by first incubating 10 nM tris-NTA-Oregon Green (NTA-OG) with 30 nM $NiCl_2$ for ~1 hr at room temperature. yMsh2-Msh6 (5 nM) was then incubated with 5 nM NTA-OG/15 nM $NiCl_2$($Ni_3$NTA-OG) for ~1 hr on ice. Protein was not purified from unbound dye. 6His SNARE complexes were labeled with Tris-NTA-OG (Figure 3.3) as described in the results and discussion section below.

*Microscope*

Fluorescence experiments were performed using a prism-type TIRM (Figure 3.1) consisting of an IX51 microscope with a 60x 1.2 NA PlanApo water immersion objective (Olympus, Tokyo, Japan) and four collinear lasers for illumination (blue-473nm-50mW exciting OG or Alexa488; green-532nm – 50mW exciting TAMRA or Alexa555; red-635nm-40mW exciting Cy5 or Alexa647; infrared-690nm-50mW exciting Cy7). The lasers were individually shuttered to allow all combinations of simultaneous and sequential illumination. The microscope image was split into four distinct spectral bands by a Quadview imager (Photometrics, Tucson, AZ) and relayed onto quadrants of a Cascade 512B/emCCD (Photometrics). The Quadview contained three dichroic mirrors (550dcxr, 645dcxr, 750dcxr, Chroma, Brattleboro, VT) and band pass filters to define the spectral bands: blue channel (513x17, Semrock, Rochester, NY), green channel (585x70, Chroma), red channel (685x70, Chroma), and infrared channel (794x160, Chroma).

When the 690 nm laser was used, a 640x100 nm filter (Chroma) was added to the red channel. Movies were collected at 10 Hz. A mapping function to align the four distinct spectral images was derived from images of TetraSpeck fluorescent microspheres (Invitrogen), which were visible in all channels. This mapping function was used to extract the other three dye emission intensities from locations pre-identified to contain the acceptor. Data was analyzed with custom MatLab routines (Mathworks, Inc. Natick, MA).

Backgrounds and leakages between channels were corrected during analysis as described elsewhere (Hohng, Joo et al. 2004; Clamme and Deniz 2005; Lee, Kapanidis et al. 2007; Ross, Buschkamp et al. 2007). Traces in Figure 3.2C-E were corrected for background and leakage but not for gamma. We determined gamma factors from anti-correlated donor and acceptor photobleaching events using $\gamma=\Delta I_A/\Delta I_D$ (where $\Delta I_A=I_A^{\text{before bleach}} - I_A^{\text{after bleach}}$, and $\Delta I_D=I_D^{\text{after bleach}} - I_D^{\text{before bleach}}$) as described elsewhere (Ha, Ting et al. 1999; Choi, Strop et al. 2010; McCann, Choi et al. 2010). Gamma was determined from the data for Figure 3.2F to be 2.16 for the Quadview. We confirmed that the same sample when measured with our 2-color single molecule FRET microscope yielded consistent FRET efficiency results (0.31) when using gamma specific for that instrument (0.94). Emission leakage between spectral channels was measured using single-labeled DNA samples. Transmission efficiencies of the blue, green, red, red with an extra 640x100 filter, and infrared channels in our Quad-view system are 60%, 49%, 66%, 50%, and 65%, respectively of their value without the Quad-view dichroics and filters in place (bypass mode). Forty percent of Alexa488 signal level leaked into the green channel, 9% leaked into the red channel and none leaked into the infrared channel. No TAMRA signal

was detected in the blue or infrared channels, and 15% of the TAMRA signal leaked into the red channel. No Alexa555 emission was detected in the blue or infrared channels but 9% leaked into the red channel. There was no detectable emission from Alexa 647 in the blue, green, and infrared channels or from Cy7 in the blue, green, and red channels.

*Observation protocols*

Because blue dye photobleaching was limiting, we sometimes used a time-lapsed, shuttered blue illumination. This illumination scheme simplified interpretation of FRET between Alexa555 (or TAMRA) and Alexa647 because we could calculate FRET when the blue laser was not active. Undesired direct excitation of TAMRA and Alexa555 by blue light can complicate FRET measurements (Hohng, Joo et al. 2004; Clamme and Deniz 2005; Lee, Kapanidis et al. 2007; Ross, Buschkamp et al. 2007).

Figure 3.4 illustrates several excitation patterns. Sequential excitation is used first to excite Alexa647 (635 nm) followed by the excitation of Alexa488 (473 nm) to colocalize the acceptor and the auxiliary molecule (Figure 3.4B). Next, the donor Alexa555 is excited (532 nm) to observe FRET between the SNARE domains of Syntaxin 1A as reported by the high Alexa647 emission. In Figure 3.4C, a laser sequence that allows for semi-continuous monitoring of Alexa488 labeled Munc-18 is used. The 635 nm laser is used to identify the acceptor Alexa647 dye and then is shuttered off at frame 5. The donor Alexa555 dye is excited (532 nm) at frame 10 and FRET to the acceptor is observed. The 473 nm laser is shuttered on for one frame at every 15$^{th}$ frame. The flashing laser pattern allows periodic monitoring of the Munc-18 colocalization while both prolonging the life of the blue dye and leaving frames for FRET calculation that are unaffected by the blue laser. The frames with 473 nm illumination are omitted

from display in the red and green signals. Note the bleaching of Alexa488 after 8 seconds.

**Results and Discussion**

The sequential and simultaneous FRET and colocalization experiments were performed with a prism-type TIRM, a Quadview splitter containing three dichroic mirrors, and an emCCD, allowing the simultaneous excitation and detection of the fluorescence from 4 dyes with emission spectra characteristic of Cy2, Cy3, Cy5 and Cy7 (Figure 3.1 and methods). We first demonstrated this instrument by examining DNA bending induced by yMutSα. MutS homologs are responsible for recognizing and signaling repair of base-base mismatches and insertion-deletions in newly replicated DNA (Kunkel and Erie 2005). MutS-mismatch complexes adopt multiple conformations with different degrees of DNA bending (from unbent to bend angles of ~ 90°) (Wang, Yang et al. 2003; Tessmer, Yang et al. 2008; Sass, Lanyi et al.). It has been suggested that each bending state may have a different repair signaling potential (Kunkel and Erie 2005; Tessmer, Yang et al. 2008; Sass, Lanyi et al.).

Biotinylated DNA (50 base pairs) labeled with a FRET donor (TAMRA) and acceptor (Cy5) separated by 19 base pairs with a CC mismatch approximately halfway between the two fluorophores was tethered to a streptavidin-coated quartz surface (Figure 3.2A,B). Because yMutSα contains over 30 cysteines, site-specific labeling using maleimide dye methodology is not feasible. Consequently, 6His-tagged-yMutSα (tagged on the N-terminus of Msh2) was non-covalently labeled using tris-NTA-OG (OG-yMutSα) (Lata, Gavutis et al. 2006). OG-yMutSα complexes were prepared before

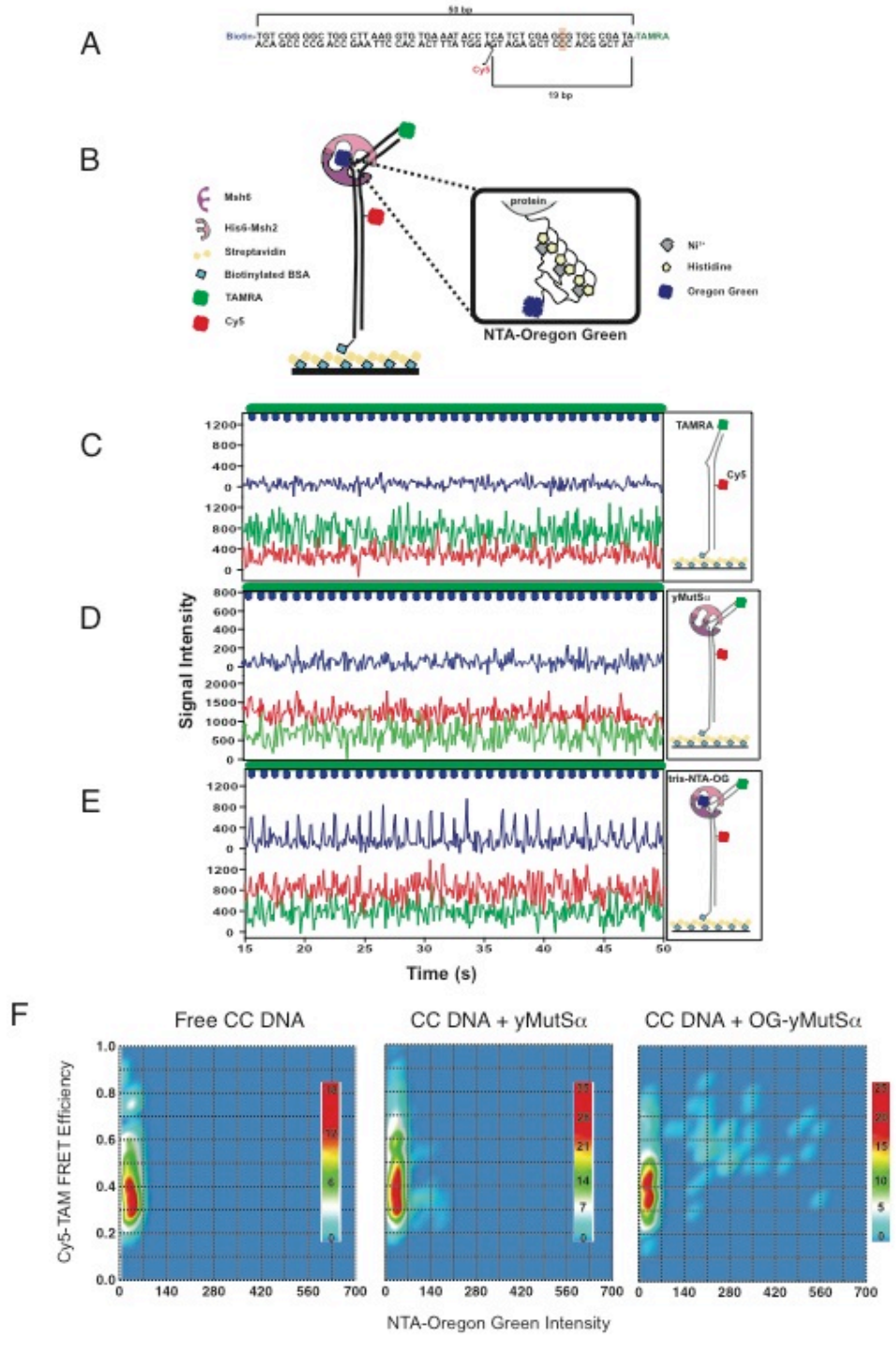
A
B
C
D
E
F
Msh6
His6-Msh2
Streptavidin
Biotinylated BSA
TAMRA
Cy5
protein
NTA-Oregon Green
Ni++
Histidine
Oregon Green
Signal Intensity
Time (s)
yMutSα
tris-NTA-OG
Free CC DNA
CC DNA + yMutSα
CC DNA + OG-yMutSα
Cy5-TAM FRET Efficiency
NTA-Oregon Green Intensity

**Figure 3.2 - yMutSα smFRET experiments.**

**(A**) DNA sequence of CC mismatch DNA containing a biotin tag, Cy5 label, and TAMRA label. **(B**) Cartoon describing the DNA functionalized quartz surface in the presence of tris-NTA Oregon Green labeled MutSα. **(C**) Emission from surface immobilized CC DNA labeled with Cy5 (red trace) and TAMRA (green trace). No colocalization is observed in the blue channel. **(D)** Emission from Cy5-TAMRA CC DNA exposed to unlabeled yMutSα. No colocalization is observed in the blue channel. **(E)** Emission from Cy5-TAMRA CC DNA bound by NTA-OG labeled yMutSα (blue trace). **(F)** Three-dimensional histograms of Cy5-TAM FRET efficiency versus yMutSα-OG intensity in the presence and absence of 5 nM unlabeled yMutSα or tris-NTA-OG labeled yMutSα. The z-axis is the number of occurrences. Laser illumination pattern is indicated above each graph (blue=473nm, green=532nm, red=635nm).

addition to CC-mismatch-DNA coated surfaces (methods**)**. DNA bending was monitored by continuously exciting TAMRA with 532 nm illumination and measuring FRET to Cy5. The presence of OG-yMutSα was monitored by measuring OG emission under either continuous (data not shown) or pulsed (Figure 3.2C-E) 473 nm illumination. Despite using an oxygen scavenging system, a shutter-pulsed scheme was required to allow longer observation intervals before OG photobleached.

After leakage subtraction and gamma correction (Methods), free CC-mismatch DNA molecules exhibit constant FRET efficiencies **(**Figure 3.2C**)**, with an average FRET ~ 0.35 (Figure 3.2F). Unlabeled yMutSα binding increases FRET between TAMRA and Cy5, but yields no blue emission (Figure 3.2D); whereas, binding of OG-yMutSα increases both FRET and the blue emission, consistent with the presence of the NTA-OG moiety (Figure 3.2E). In addition, using a shuttered excitation (Figure 3.2E), the presence of OG-yMutSα can be observed for long times indicating that the OG-NTA moiety remains stably bound to MutSα during the time course of the experiment. These long bound state lifetimes for tris-NTA dyes are consistent with ensemble experiments using NTA-dyes (Lata, Gavutis et al. 2006). In the absence of MutSα, the histogram of CC-DNA FRET efficiency *vs*. OG-yMutSα emission intensity for many molecules (Figure 3.2F) shows FRET efficiencies around 0.35 and OG emission near zero. In the presence of OG-MutSα, one FRET emission peak overlaps with free DNA and another population shifted to higher FRET values (~0.6 gamma corrected) indicating yMutSα-induced DNA bending. A significant population of DNA without bound protein is expected because yMutSα is present at 5 nM, well below the 54 nM $K_D$ (determined by fluorescence anisotropy). The higher FRET population can be divided into those with

low or high OG emission. Those higher FRET events with low blue intensities suggest that unlabeled yMutSα is bound, and those with higher blue (15% of molecules) intensities confirm bound OG-yMutSα. To assess if tris-NTA-dye-labeling affects DNA bending, we compared DNA bending distributions for labeled and unlabeled MutSα and found no significant differences (Figure 3.2F). These data demonstrate that fluorescently tagged yMutSα is active.

To demonstrate the method's flexibility, we examined interactions among neuronal SNARE proteins, which mediate membrane fusion (Rizo and Rosenmund 2008). For neuronal SNAREs, two membrane proteins (syntaxin and synaptobrevin) on distinct cellular compartments assemble with a third SNARE protein (SNAP-25) to form a heteromeric complex of 4 parallel α-helices called the SNARE complex, which crosslinks the fusing membranes through the transmembrane domains of the proteins (Figure 3.3A).

Noncovalent labeling allows dyes to be added to samples in situ, as we demonstrated for membrane-incorporated SNARE complexes. 30 nM $Ni_3$-tris-NTA-OG was introduced above a phosphatidylcholine bilayer that contained SNARE complexes tethered by syntaxin's transmembrane domain (Figure 3.3B). The complexes were tagged before assembly with Alexa647-maleimide covalently linked to S61C of synaptobrevin. We used simultaneous 473 nm and 635 nm illumination to identify individual Alexa647 labeled complexes by red emission, while NTA-OG binding was assessed by blue emission (Figure 3.3C). NTA-OG colocalized with over 25% of SNARE complexes when the 6His was present on synaptobrevin, and was reduced to background levels (1-4%) in controls (Figure 3.3D).

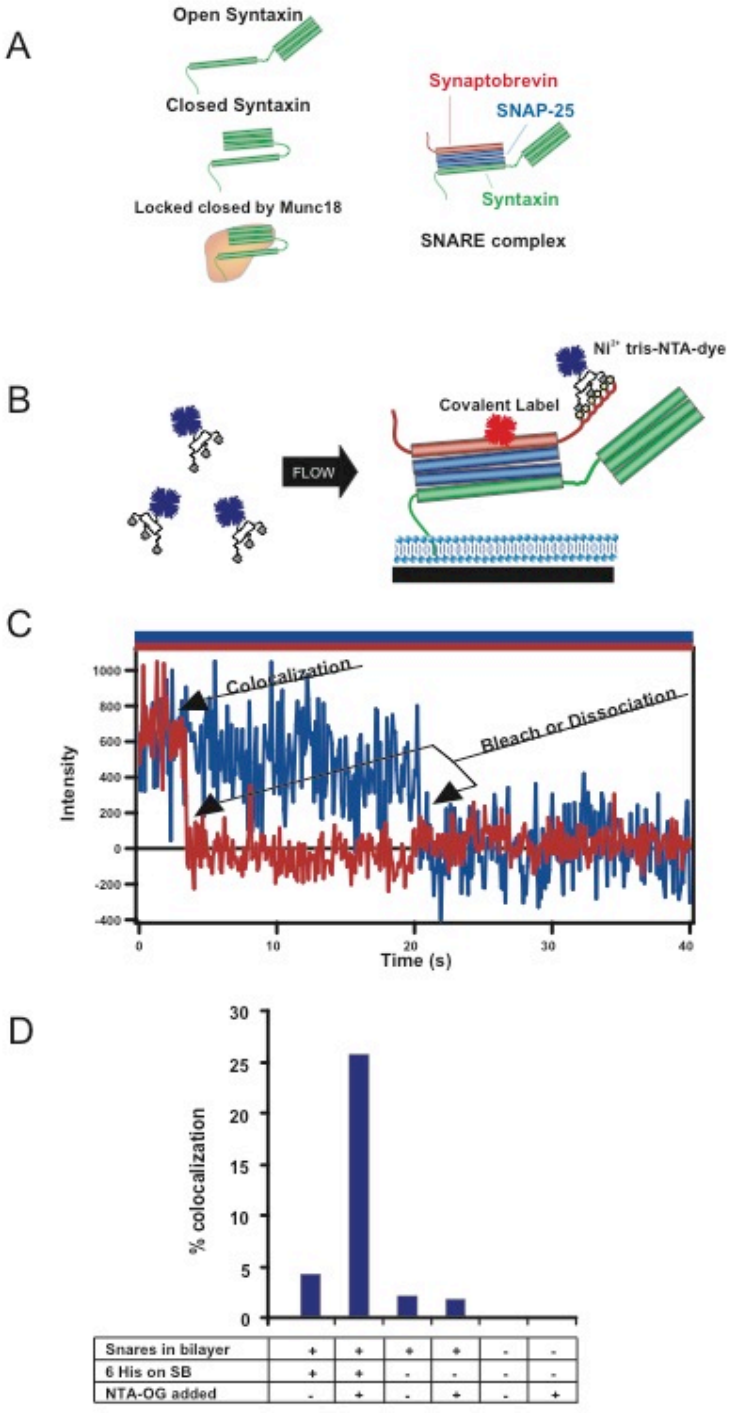
A
Open Syntaxin
Closed Syntaxin
Locked closed by Munc18
Synaptobrevin
SNAP-25
Syntaxin
SNARE complex
B
Ni2+ tris-NTA-dye
Covalent Label
FLOW
C
Colocalization
Bleach or Dissociation
Intensity
Time (s)
D
% colocalization
Snares in bilayer + + + + - -
6 His on SB + + - - - -
NTA-OG added - + - + - +

Figure 3

**Figure 3.3 - In situ labeling of SNARE proteins reconstituted in a supported lipid bilayer using tris-NTA dyes.**

(A) Schematic descriptions of syntaxin and the SNARE complex. (B) SNARE complex labeled by Alexa 647 at a cysteine mutation in synaptobrevin (s61c) is reconstituted into a 100% phosphatidylcholine supported lipid bilayer by the transmembrane domain of syntaxin. Tris-NTA-OG dye is added above the bilayer. (C) Simultaneous 473nm and 635nm illumination is used to colocalize the OG dye on synaptobrevin's 6-His tag with the covalently attached Alexa647. Synaptobrevin (1-96) is required to be incorporated in SNARE complex with SNAP-25 and syntaxin in order for it to localize to the bilayer. (D) Population analysis of colocalization (percentages) of Ni:NTA-OG from solution at sites preidentified to contain membrane incorporated SNARE complexes labeled with Alexa 647 (synaptobrevin a72c). Experiments using 6His-tagged synaptobrevin are compared to controls omitting the 6His-tag, Ni:NTA-OG, or SNARE complex as indicated.

Alternately, covalent labeling with four dyes can be used to structurally characterize this multiprotein complex. We prepared SNARE complexes with one donor-acceptor pair (Alexa 488/Alexa 555) at the N-terminal end of the α-helical bundle and a distinct donor-acceptor pair (Alexa 647/Cy7) at the C-terminal end. The SNARE complex is a 2 nm x 10 nm rod-like structure, so high FRET is expected from each pair, but little coupling is expected between the two pairs. Under continuous illumination with both blue and red lasers, we simultaneously observed two independent FRET pairs on individual complexes (Figure 3.4A).

The SNARE complex is also a binding platform for other proteins that regulate membrane fusion. We investigated Munc-18 binding to both syntaxin and to the SNARE complex (Dulubova, Khvotchev et al. 2007; Rizo and Rosenmund 2008). In the first SNARE experiment (Figure 3.3A), syntaxin was covalently labeled with dyes at cysteine mutations in the C-terminal end of the SNARE domain and the N-terminal end of the 3-helix bundle that were designed to yield low (but non-zero) FRET (Margittai, Widengren et al. 2003) when the two domains connected by a flexible linker are unbound (open syntaxin) and high FRET when they bind (closed syntaxin). Syntaxin was reconstituted into supported lipid bilayers and Alexa488 labeled Munc-18 was added in solution above the bilayer. Using sequential red-blue-green laser illumination (top axis, Figure 3.4B), we observed complexes where blue emission indicated the presence of Munc-18 and FRET in the green and red channels reported the conformational state of syntaxin. We confirmed that Munc18 binds to syntaxin in the closed conformation, as expected (Margittai, Widengren et al. 2003) (Figure 3.4B).

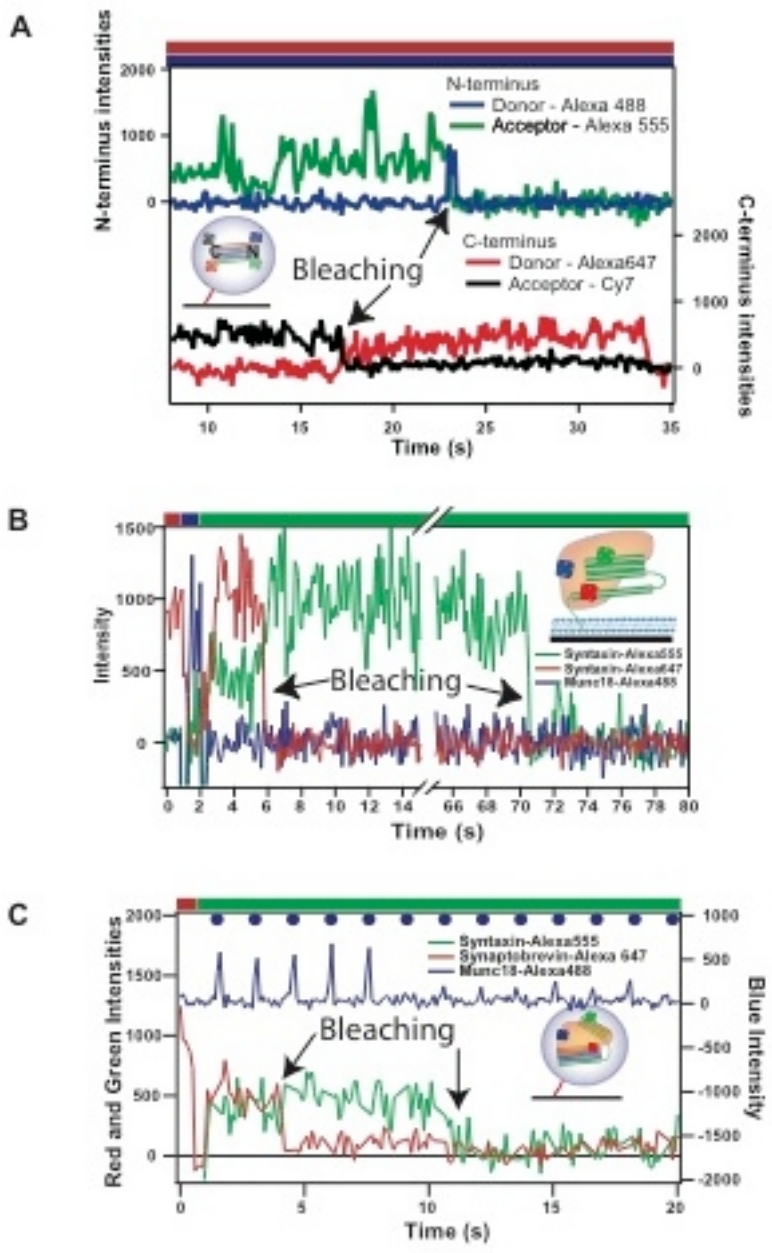


**Figure 3.4 - SNARE smFRET experiments.**

**(A)** SNARE complex lacking transmembrane domains was immobilized inside tethered liposomes and labeled with Alexa488 and Alexa555 on SNAP-25 (residues 20 and 139 – both near the SNARE complex N-terminus), Alexa 647 on syntaxin (residue 249 – near the SNARE complex C-terminus) and Cy7 on synaptobrevin (on a lysine,

~70% near the C-terminus). Two distinct FRET pairs on the same protein complex are simultaneously measured. **(B)** Emission from bilayer reconstituted, full-length syntaxin labeled with Alexa555 (green trace) and Alexa647 (red trace) (labels at residues 35 and 249) co-localized with Alexa488 labeled Munc-18 (blue trace). **(C)** Emission from liposome encapsulated SNARE complex lacking transmembrane domains labeled with Alexa555 (syntaxin-e35c) and Alexa647 (synaptobrevin-a72c) is co-localized with Alexa488 labeled Munc-18 (blue). Note, the 473 nm laser is pulsed. In all panels, traces were selected to show anticorrelated bleaching events to confirm single molecule FRET interactions. Laser illumination pattern is indicated above the graphs (blue=473nm, green=532nm, red=635nm, black=690nm).

We also observed Munc-18 interacting with the full SNARE complex (Dulubova, Khvotchev et al. 2007). Soluble SNARE complex was co-encapsulated with Alexa488-Munc-18 in surface-tethered, 100 nm liposomes (Fig. 4C). The structure of this 4-protein complex is as yet undetermined. For this experiment, the SNARE complex was labeled with a donor dye (Alexa 555) in the 3-helix bundle of syntaxin and with an acceptor dye on synaptobrevin in the central region of the SNARE bundle. We screened liposomes for the presence of Alexa488-Munc-18 through blue dye emission under pulsed illumination and then used FRET in only those liposomes to examine the spacing between syntaxin's 3-helix bundle and the core SNARE complex (Figure 3.4C). Measuring FRET from additional label attachment locations will allow us to put constraints on the overall conformation of the Munc18:SNARE complex.

Our development of a 4-color, single molecule fluorescence instrument for measurements on immobilized biomolecules with wide-field imaging will allow single molecule studies of increasingly complex systems. The ability to colocalize binding partners at complexes while also monitoring conformational changes in other parts of the complex via FRET, or to simultaneously monitor two FRET pairs on a single complex, will enable studies of more complicated molecular assemblies than current approaches. This ability to directly correlate transient accessory binding to dynamic conformational transitions provides a new avenue for studies of biological signaling pathways. Simultaneous quantification of fluorescence emission from four dyes interacting through FRET has the potential to report six distinct distances on a single molecular complex.

Furthermore, the demonstration that tris-NTA dye conjugates can label 6His-tagged proteins for single molecule studies significantly expands the capability for

labeling proteins. Non-covalent labeling at a terminally located affinity tag can minimize the possibility of destroying function in proteins that are susceptible to structural perturbation by point mutations for dye attachment. The tris-NTA labeling approach also avoids the long incubation times required for most covalent labeling strategies and allows *in situ* labeling. The bound state lifetimes of the tris-NTA dyes to the 6His-tagged proteins are sufficiently long to permit monitoring of many protein-protein and protein-DNA interactions.

The ease of modifying an existing two-color TIRM by using a commercially available four color splitting device and its affordability, as well as the flexibility of non-covalent dye labeling, suggest this method could be adopted by many research groups.

## References


Bowen, M. E., K. Weninger, et al. (2004). "Single molecule observation of liposome-bilayer fusion thermally induced by soluble N-ethyl maleimide sensitive-factor attachment protein receptors (SNAREs)." Biophys J **87**(5): 3569-3584.

Choi, U. B., P. Strop, et al. (2010). "Single-molecule FRET-derived model of the synaptotagmin 1-SNARE fusion complex." Nat Struct Mol Biol **17**(3): 318-324.

Clamme, J. P. and A. A. Deniz (2005). "Three-color single-molecule fluorescence resonance energy transfer." Chemphyschem **6**(1): 74-77.

Clark, A. B., M. E. Cook, et al. (1999). "Functional analysis of human MutSalpha and MutSbeta complexes in yeast." Nucleic Acids Res **27**(3): 736-742.

Dulubova, I., M. Khvotchev, et al. (2007). "Munc18-1 binds directly to the neuronal SNARE complex." Proc Natl Acad Sci U S A **104**(8): 2697-2702.

Eid, J., A. Fehr, et al. (2009). "Real-Time DNA Sequencing from Single Polymerase Molecules." Science **323**(5910): 133-138.

Friedman, L. J., J. Chung, et al. (2006). "Viewing dynamic assembly of molecular complexes by multi-wavelength single-molecule fluorescence." Biophys J **91**(3): 1023-1031.

Ha, T., A. Y. Ting, et al. (1999). "Single-molecule fluorescence spectroscopy of enzyme conformational dynamics and cleavage mechanism." Proc Natl Acad Sci U S A **96**(3): 893-898.

Heilemann, M., P. Tinnefeld, et al. (2004). "Multistep energy transfer in single molecular photonic wires." J Am Chem Soc **126**(21): 6514-6515.

Hohng, S., C. Joo, et al. (2004). "Single-molecule three-color FRET." Biophys J **87**(2): 1328-1337.

Kapanidis, A. N., Y. W. Ebright, et al. (2001). "Site-specific incorporation of fluorescent probes into protein: hexahistidine-tag-mediated fluorescent labeling with (Ni(2+):nitrilotriacetic Acid (n)-fluorochrome conjugates." J Am Chem Soc **123**(48): 12123-12125.

Kunkel, T. A. and D. A. Erie (2005). "DNA mismatch repair." Annu Rev Biochem **74**: 681-710.

Lata, S., M. Gavutis, et al. (2006). "Specific and stable fluorescence labeling of histidine-tagged proteins for dissecting multi-protein complex formation." J Am Chem Soc **128**(7): 2365-2372.

Lata, S., A. Reichel, et al. (2005). "High-affinity adaptors for switchable recognition of histidine-tagged proteins." J Am Chem Soc **127**(29): 10205-10215.

Lee, N. K., A. N. Kapanidis, et al. (2007). "Three-color alternating-laser excitation of single molecules: monitoring multiple interactions and distances." Biophys J **92**(1): 303-312.

Li, Y., G. J. Augustine, et al. (2007). "Kinetics of complexin binding to the SNARE complex: correcting single molecule FRET measurements for hidden events." Biophys J **93**(6): 2178-2187.

Lundquist, P. M., C. F. Zhong, et al. (2008). "Parallel confocal detection of single molecules in real time." Optics Letters **33**(9): 1026-1028.

Margittai, M., J. Widengren, et al. (2003). "Single-molecule fluorescence resonance energy transfer reveals a dynamic equilibrium between closed and open conformations of syntaxin 1." Proc Natl Acad Sci U S A **100**(26): 15516-15521.

McCann, J. J., U. B. Choi, et al. (2010). "Optimizing Methods to Recover Absolute FRET Efficiency from Immobilized Single Molecules." Biophys J **accepted**.

Munro, J. B., R. B. Altman, et al. (2010). "A fast dynamic mode of the EF-G-bound ribosome." Embo J **29**(4): 770-781.

Rhoades, E., E. Gussakovsky, et al. (2003). "Watching proteins fold one molecule at a time." Proc Natl Acad Sci U S A **100**(6): 3197-3202.

Rizo, J. and C. Rosenmund (2008). "Synaptic vesicle fusion." Nat Struct Mol Biol **15**(7): 665-674.

Ross, J., P. Buschkamp, et al. (2007). "Multicolor single-molecule spectroscopy with alternating laser excitation for the investigation of interactions and dynamics." J Phys Chem B **111**(2): 321-326.

Roy, R., A. G. Kozlov, et al. (2009). "SSB protein diffusion on single-stranded DNA stimulates RecA filament formation." Nature **461**(7267): 1092-1097.

Sass, L. E., C. Lanyi, et al. (2010). "Single-molecule FRET TACKLE reveals highly dynamic mismatched DNA-MutS complexes." Biochemistry **49**(14): 3174-3190.

Tessmer, I., Y. Yang, et al. (2008). "Mechanism of MutS searching for DNA mismatches and signaling repair." J Biol Chem **283**(52): 36646-36654.

Wang, H., Y. Yang, et al. (2003). "DNA bending and unbending by MutS govern mismatch recognition and specificity." Proc Natl Acad Sci U S A **100**(25): 14822-14827.

Webb, S. E., D. J. Rolfe, et al. (2008). "Simultaneous widefield single molecule orientation and FRET microscopy in cells." Opt Express **16**(25): 20258-20265.

Weninger, K., M. E. Bowen, et al. (2008). "Accessory proteins stabilize the acceptor complex for synaptobrevin, the 1:1 syntaxin/SNAP-25 complex." Structure **16**(2): 308-320.

Weninger, K., M. E. Bowen, et al. (2003). "Single-molecule studies of SNARE complex assembly reveal parallel and antiparallel configurations." Proc Natl Acad Sci U S A **100**(25): 14800-14805.

# Chapter 4

## CHARACTERIZATION OF HUMAN MSH2-MSH6 NUCLEOTIDE OCCUPANCY

### Introduction

An important aspect of the function of MutS(α) is the formation of the sliding clamp. Most data suggest that a MutS(α) sliding clamp forms in the presence of ATP. However, the circumstances that lead to formation of the sliding clamp remain unclear. Experimental evidence has shown that MutS(α) undergoes conformational changes in the presence of ATP (Allen, Makhov et al. 1997; Studamire, Quach et al. 1998; Gradia, Subramanian et al. 1999; Blackwell, Bjornson et al. 2001; Kato, Kataoka et al. 2001; Hess, Gupta et al. 2002; Joshi and Rao 2002; Jiang, Bai et al. 2005; Mendillo, Mazur et al. 2005; Gorman, Chowdhury et al. 2007; Pluciennik and Modrich 2007; Qiu, DeRocco et al. 2012). The ATPase activity and the nucleotide occupancy requirement for such a conformational change has been the focus of many studies (Haber and Walker 1991; Gradia, Acharya et al. 1997; Blackwell, Bjornson et al. 1998; Blackwell, Martik et al. 1998; Gradia, Subramanian et al. 1999; Gradia, Acharya et al. 2000; Drotschmann, Hall et al. 2002; Joshi and Rao 2002; Antony and Hingorani 2003; Selmane, Schofield et al. 2003; Lamers, Georgijevic et al. 2004; Antony, Khubchandani et al. 2006; Mazur, Mendillo et al. 2006; Jacobs-Palmer and Hingorani 2007; Cyr 2008; Zhai and Hingorani

2010; Heinen, Cyr et al. 2011). Progress has been made in understanding the role of nucleotide occupancy in the formation of MutS-MutL (prokaryotes) and MutSα-MutLα (eukaryotes) ternary complexes and signaling downstream repair. Studies have shown that while the presence of ATP is a requirement for MutS-MutL-mismatch DNA (mmDNA) complex formation, ATP hydrolysis by either protein is not necessary (Selmane, Schofield et al. 2003). Given the importance of ATP binding and hydrolysis in the activation of the MMR process, it is not surprising to note that many of the mutations in the ATPase domain of either subunit are part of the human nonpolyposis colorectal cancer (HNPCC) mutation spectrum.

Three models have been proposed to try to explain the MMR initiation mechanism: the translocation model, the molecular switch model, and the static modulation model. The translocation model suggests that upon recognizing a mismatch, ATP hydrolysis by MutS(α) drives the protein to travel along the DNA away from the mismatch (Allen, Makhov et al. 1997; Blackwell, Bjornson et al. 1998; Gradia, Subramanian et al. 1999; Blackwell, Bjornson et al. 2001; Acharya, Foster et al. 2003; Gorman, Chowdhury et al. 2007) to recruit other MMR proteins and the coordinate downstream repair events (Allen, Makhov et al. 1997; Blackwell, Bjornson et al. 1998; Gradia, Subramanian et al. 1999; Blackwell, Bjornson et al. 2001; Acharya, Foster et al. 2003; Gorman, Plys et al. 2010). The molecular switch model suggests that a combination of factors must occur prior to MutS(α) initiated repair. MutS(α) must recognize a mismatch and then bind a total of two ATP molecules, one into each subunit. The rate-limiting step is thought to be the exchange of ADP for ATP in MSH2 (or subunit 2 in Taq and *E.* coli) is the final step before MutS undergoes a conformational

change to form the sliding clamp, which would subsequently recruit MMR proteins and coordinate downstream repair (Gradia, Acharya et al. 1997; Gradia, Subramanian et al. 1999; Gradia, Acharya et al. 2000; Acharya, Foster et al. 2003). The static modulation model proposes that MutS(α) requires ATP binding and hydrolysis in order to control interactions with DNA while also remaining at the mismatch site (Habraken, Sung et al. 1998; Wang, Lawrence et al. 1999; Junop, Obmolova et al. 2001; Schofield, Nayak et al. 2001; Selmane, Schofield et al. 2003; Geng, Sakato et al. 2012). There is evidence to support each of the proposed MMR initiation models, but it unclear which model(s) is correct. It is important to determine the mechanism of MMR initiation as it may be useful for the development of targeted therapeutics or treatments.

Certain mutations in the ATPase domains of MSH2-MSH6 result in a separation-of-function mutant MutSα complex, which is deficient in MMR but able to participate in apoptotic responses due to DNA damage. For example, a mutation of the glycine residue in the Walker A motif of Msh2 (GXXXGK(S/T)) ($MSH2^{G674A}$-$MSH6^{WT}$ in mouse and human) results in a mutator phenotype due to a deficiency in MMR (Drotschmann, Topping et al. 2004; Lin, Wang et al. 2004; Lützen, de Wind et al. 2008; Ollila, Dermadi Bebek et al. 2008; Geng, Sakato et al. 2012). $Msh2^{G674A/G674A}$ mice exhibit the same mutagenic spectrum of cancer development as that of a MutSα null system (Lin, Wang et al. 2004). However, the $Msh2^{G674A/G674A}$ mice have a longer lifespan than that of the Msh2 null mice. Interestingly $Msh2^{G674A/G674A}$ mouse embryonic fibroblasts (MEFs) exhibit the same susceptibility to cisplatin treatment that $Msh2^{+/+}$ mice had (Yang, Scherer et al. 2004) which is contrary to studies showing cells deficient in Msh2 are resistant to chemotherapeutic treatments. This discrepancy suggests that the

$Msh2^{G674A/G674A}$ cells are inducing DNA damage dependent apoptosis in a similar manner to that of $Msh2^{+/+}$ cells (Lin, Wang et al. 2004).

Biochemical analyses suggest that the G674A mutation in MSH2 does not affect the protein stability. Mismatch binding by $MSH2^{G674A}$-$MSH6^{WT}$ is unaffected; however, ATP dependent release of a mismatch is inefficient compared to $MSH2^{WT}$-$MSH6^{WT}$ (Drotschmann, Topping et al. 2004; Lützen, de Wind et al. 2008; Ollila, Dermadi Bebek et al. 2008; Geng, Sakato et al. 2012). It has been hypothesized that due to the high binding affinity for a mismatch and slow ATP dependent release of the mismatch, that $Msh2^{G674A}$-$MSH6^{WT}$ mutant might prevent MMR by blocking access to the mismatch (Drotschmann, Topping et al. 2004; Ollila, Dermadi Bebek et al. 2008).

A second interesting separation-of-function mutant involves a point mutation in Msh6 at the interface between Msh2 and Msh6 near the p-loop of the Msh2 ATPase site ($Msh2^{WT}$-$Msh6^{G1067D}$ in *S. cerevisiae* and the homologous mutations $MSH2^{WT}$-$MSH6^{T1219D}$ in humans and $Msh2^{WT}$-$Msh6^{T1217D}$ in mice) (Berends, Wu et al. 2002; Hess, Gupta et al. 2002; Yang, Scherer et al. 2004). Similar cell survival studies of $Msh6^{T1217D/T1217D}$ mice to those performed with $Msh2^{G674A/G674A}$ mice yielded the same inability to activate MMR (observed by a higher occurrence of microsatellite instabilities (MSIs) which are a hallmark of cancer susceptibility) while maintaining wild type-like cellular vulnerability to DNA damage (Yang, Scherer et al. 2004). Studies of nucleotide binding for a homologous mutation in *Saccharomyces cerevisiae* (*S. cerevisiae*) ($yMsh2^{WT}$-$Msh6^{G1067D}$), suggest that the protein is deficient for nucleotide binding in the Msh2 subunit. However, the homologous mutation in the yeast system is not a conserved residue.

Interestingly, both $MSH2^{G674A}$-$MSH6^{WT}$ and $MSH2^{WT}$-$MSH6^{T1219D}$ mutants were shown *in vitro* to be able to bind mmDNA similar to wild type $MSH2^{WT}$-$MSH6^{WT}$. However, neither protein was unable to form the ternary complex with MutLα that is required for MMR initiation (Hess, Gupta et al. 2002; Hess, Mendillo et al. 2006; Geng, Sakato et al. 2012). Combined, these data support a role for the MutSα-MutLα ternary complex in MMR signaling and suggest some divergent function of MutSα in apoptotic response. To better characterize the conditions required for sliding clamp formation in hMutSα and potential differences in hMutSα induced apoptosis, we evaluated the nucleotide binding properties of wild type $hMSH2^{WT}$-$hMSH6^{WT}$ (WT), $hMSH2^{G674A}$-$hMSH6^{WT}$ (G674A), and $hMSH2^{WT}$-$hMSH6^{T1219D}$ (T1219D).

## Materials and Methods

### *Preparation of human MSH2-MSH6 and its mutants*

MSH2-MSH6 and its mutants were prepared and purified as described previously (Geng, Du et al. 2011; Geng, Sakato et al. 2012). Briefly, recombinant hMutSα was expressed in insect cells using the baculovirus system. Each protein was purified over a 6-ml Resource™ Q anion exchange column (GE Healthcare), a 5-ml HiTrap™ Heparin affinity column (GE Healthcare), and a HiLoad 16/60 Superdex 200 sizing column (GE Healthcare) as described in (Geng, Du et al. 2011; Geng, Sakato et al. 2012). Wild type hMutSα and $hMSH2^{G674A}$-$hMSH6^{WT}$ were eluted in buffer A (25 mM HEPES, pH 7.5, 0.1 mM EDTA, 10% glycerol, 1 mM DTT, 1× Complete proteinase inhibitor mixture (Roche Applied Science) and 0.1% PMSF) containing 100 mM KCl. $MSH2^{wt}$-$MSH6^{T1219D}$ was eluted in buffer A containing 300 mM KCl as described in (Geng, Du et

al. 2011; Geng, Sakato et al. 2012). Concentrations of MutSα were determined with a modified Bradford protein assay (Bio-Rad) using BSA as the standard.

*DNA substrates*

ssDNA oligonucleotides used to create DNA substrates were purchased from either Integrated DNA Technologies (IDT) (Coralville, IA) or TriLink Biotechnologies (San Diego, CA). Oligonucleotide (oligo) sequences used to make DNA substrates for DNA cross-linking experiments are given in Table 4.1. DNA substrates for cross-linking were previously used in biochemical studies by Geng *et al* (Geng, Sakato et al. 2012). Briefly, to create AT, GT, and $O^6$MeGT substrates, Oligo 1 was annealed to Oligo 2, Oligo 3, or Oligo 4 respectively. Appropriate oligonucleotides were annealed at ~70°C for 20 min and slowly cooled to room temperature at ~1°C $min^{-1}$.

*UV-crosslinking of Nucleotide*

Nucleotide occupancy was determined by UV cross-linking α or γ labeled $^{32}$P-ATP into the ATPase domains of hMSH2-MSH6 and resolving the two bound subunits on a 10% SDS-PAGE similar to previously performed experiments on *S. cerevisiae* and human MSH2-MSH6 (Hess, Gupta et al. 2002; Mazur, Mendillo et al. 2006; Hargreaves, Shell et al. 2010; Heinen, Cyr et al. 2011). UV-crosslinking experimental design is depicted in Figure 4.1. Reactions were performed in 96 well plates at 4°C. Each 20 μL reaction mixture contained 10 μCi of 3000 Ci/mmol [γ-$^{32}$P]-ATP or of 800 Ci/mmol [α-$^{32}$P]-ATP, reaction buffer with or without magnesium chloride (25 mM Tris HCl (pH 7.8), 100 mM sodium acetate, 5 mM magnesium chloride, 2 mM dithiothreitol (DTT), 200 μg/mL BSA, and 5% glycerol), 4 pmol hMSH2-MSH6 or appropriate mutant

**Table 4.1 - DNA oligonucleotide sequences used for cross-linking DNA substrate construction.**

| Oligonucleotide | Sequence (5' to 3') |
|---|---|
| **1** | CGG ATC CGA CTC ATT CCT GCA GCG ACT CCA TGG GA |
| **2** | TCC CAT GGA GTC GCT GCA GGA ATG AGT CGG ATC CG |
| **3** | TCC CAT GGA GTC GCT GCG GGA ATG AGT CGG ATC CG |
| **4** | TCC CAT GGA GTC GCT GC(meG) GGA ATG AGT CGG ATC CG |

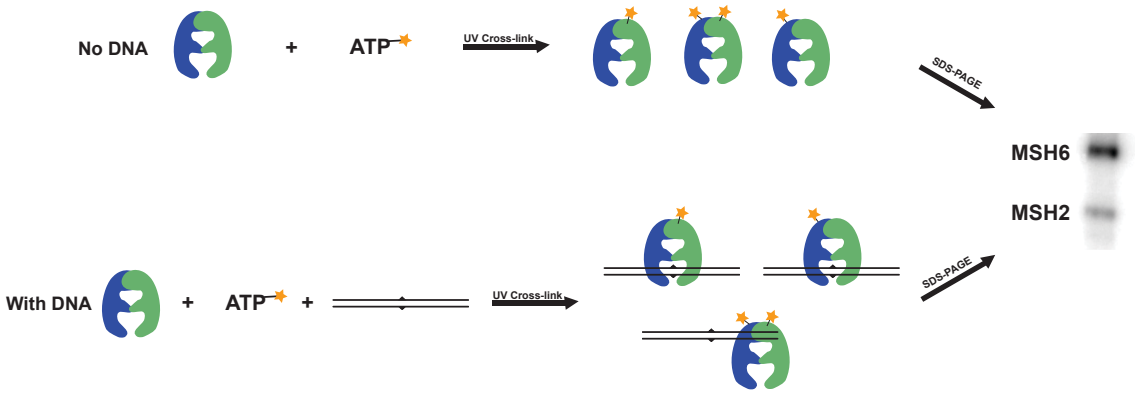


**Figure 4.1 – UV cross-linking experimental design.**

A cartoon representation of the UV-crosslinking experiments is shown with the MSH2 subunit represented in blue and the MSH6 subunit represented in green. Radiolabeled nucleotide is depicted in yellow. UV crosslinking was preformed at 254 nm for 20 min. Radiolabeled subunits of $MSH2^{WT}$-$MSH6^{WT}$, $MSH2^{G674A}$-$MSH6^{WT}$, or $MSH2^{WT}$-$MSH6^{T1219D}$ were resolved on a 10% SDS-PAGE. Experiments were performed in the presence and absence of DNA as well as the presence and absence of $Mg^{2+}$.

protein, and enough unlabeled ATP to bring the total ATP concentration to 100 μM. Reactants were incubated on ice 10 min prior to UV cross-linking. UV cross-linking was performed at 254 nm for 20 min in a Stratagene UV Crosslinker 1800. Samples were then boiled in SDS load dye and subunits were resolved on a 10% SDS-PAGE with a 4% stacking gel. Gels were Coomassie stained, destained, and exposed to phosopho-imaging screens overnight.

The intensities of phosphoimage bands were quantified using NIH ImageJ software (v1.46J) (Rasband 1997-2012). Nucleotide occupancy percentages are calculated as a percent of total radiation detected within the MSH2 and MSH6 bands of a particular lane.

**Results**

To better understand the mechanism by which the $MSH2^{WT}$-$MSH6^{T1219D}$ and the $MSH2^{G674A}$-$MSH6^{WT}$ behave as separation-of-function mutants, we evaluated the nucleotide occupancy for each protein in the presence and absence of DNA and $Mg^{2+}$. The absence of $Mg^{2+}$ has been previously used as a means to prevent ATP hydrolysis (Mazur, Mendillo et al. 2006). In addition, results in the absence of $Mg^{2+}$ are similar to those performed using γ-$S^{35}$-ATP in the presence of $Mg2^{+}$. The requirement of nucleotide binding (but not necessarily nucleotide hydrolysis) by hMutS(α) in order to initiate DNA mismatch repair has been a topic of much interest (Gradia, Acharya et al. 1997; Gradia, Subramanian et al. 1999; Gradia, Acharya et al. 2000; Junop, Obmolova et al. 2001; Kato, Kataoka et al. 2001; Jiang, Bai et al. 2005; Jacobs-Palmer and Hingorani 2007; Heinen, Cyr et al. 2011; Monti, Cohen et al. 2011; Geng, Sakato et al. 2012; Qiu, DeRocco et al. 2012). Evidence suggests that in the presence of a DNA mismatch, a

specific nucleotide occupancy combination may be involved in the signaling mechanism for repair. However, little is known regarding the behavior of the protein with respect to DNA damage and apoptotic signaling. The work presented here is an attempt to further understand the apoptotic signaling involvement of hMutSα by using mutant proteins shown to be deficient in the mismatch repair pathway, but retain their ability initiate apoptosis in response to DNA damaging agents. These particular proteins contain mutations in the ATPase domains.

Nucleotide cross-linking studies have been used previously to determine both nucleotide binding constants and differences between subunit affinity for nucleotide prior to binding and while bound to the mismatch DNA (Hess, Mendillo et al. 2006; Mazur, Mendillo et al. 2006; Heinen, Cyr et al. 2011). These studies in conjunction with traditional ATPase assays give further insight to the workings of the composite ATPase sites of MutS(α). Cross-linking ATP nucleotide into WT, G674A, and T1219D under hydrolyzing conditions in the absence of DNA yields similar occupancy results in WT and T1219D (Figure 4.2). Lanes containing [α-$^{32}$P]-ATP will display protein bands that are a combination of [α-$^{32}$P]-ATP and [α-$^{32}$P]-ADP given that hydrolysis will not affect the radioactivity present. Lanes containing [γ-$^{32}$P]-ATP will only display bands containing [γ-$^{32}$P]-ATP. By evaluating both [α-$^{32}$P]-ATP and [γ-$^{32}$P]-ATP, we can get a qualitative idea regarding binding of ADP vs. that of ATP in each subunit.

*WT and T1219D preferentially bind ATP into MSH2 over MSH6*

Both WT and T1219D exhibit a strong preference for nucleotide binding into MSH2 (93% and 99% respectively) in the absence of DNA and presence of $Mg^{2+}$ (Figure 4.2). Interestingly, while the WT protein has a clear preference for binding nucleotide

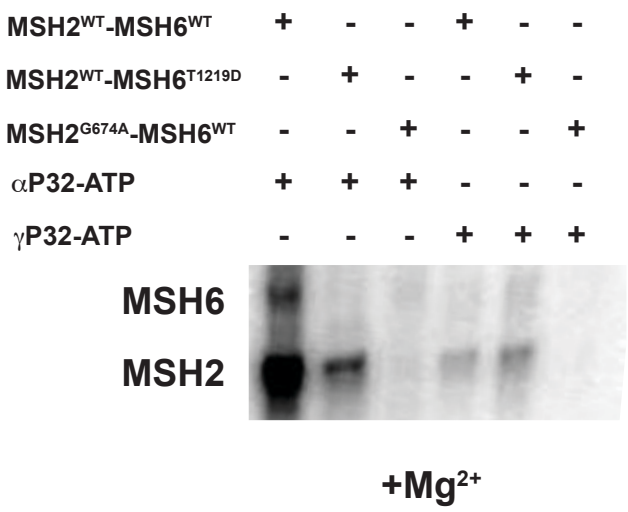


**Figure 4.2 – SDS-PAGE of UV cross-linked nucleotide into subunits of WT, G674A, and T1219D in the absence of DNA under hydrolyzing conditions.**

SDS-PAGE results of UV cross-linked [α-$^{32}$P]-ATP or [γ-$^{32}$P]-ATP into the MSH2 and MSH6 ATPase sites of WT, T1219D, or G674A in the presence of excess ATP (100 μM) and $Mg^{2+}$ (5 mM). Each 20 μL reaction contained 10 μCi of 3000 Ci/mmol [γ-$^{32}$P]-ATP or of 800 Ci/mmol [α-$^{32}$P]-ATP, reaction buffer (25 mM Tris HCl (pH 7.8), 100 mM sodium acetate, 5 mM magnesium chloride, 2 mM dithiothreitol (DTT), 200 μg/mL BSA, and 5% glycerol), and 4 pmol hMSH2-MSH6 or appropriate mutant protein. Cross-linking was performed on ice for 20 min at 254 nm. MSH2-MSH6 subunits were resolved on a 10% SDS-PAGE.

into MSH2 over MSH6, it still binds a measureable fraction of nucleotide into MSH6 (7%), and the majority of that nucleotide appears to be ADP not ATP (comparing [α-$^{32}$P]-ATP to [γ-$^{32}$P]-ATP lanes) (Figure 4.2). T1219D on the other hand, does not appear to bind any measureable amount of nucleotide into MSH6 (Figure 4.2). The majority of nucleotide bound into MSH2 appears to be ATP given the amount of [γ-$^{32}$P]-ATP bound into WT and T1219D (77% and 81% respectively). This result is consistent with *S. cerevisiae* studies (Mazur, Mendillo et al. 2006). The G674A mutant displays no detectable nucleotide binding into either subunit in the absence of DNA and presence of $Mg^{2+}$. In these experiments we observe little nucleotide binding to G674A, but the binding observed is 42% and 58% into MSH2 and MSH6 respectively in the [α-$^{32}$P]-ATP lanes. Due to the minimal detection, these measurements have a large error associated with them (±17%). We cannot, therefore, say that the protein does not bind nucleotide at all, but that if the protein is binding nucleotide, the bound complex may not be sufficiently stable for efficient cross-linking.

### *WT, T1219D, and G674A preferentially bind ATP into MSH6 over MSH2 under non-hydrolyzing conditions*

To gain some insight about the nucleotide occupancy in the absence of DNA and prior to hydrolysis, we evaluated the nucleotide cross-linking the absence of $Mg^{2+}$ (Figure 4.3). Because we are looking at non-hydrolyzing conditions, the inspection of [α-$^{32}$P]-ATP and [γ-$^{32}$P]-ATP would be redundant. We therefore evaluated ATP binding via [α-$^{32}$P]-ATP cross-linking and ADP binding by using unlabeled ADP as a competitor in an equimolar concentration to that of ATP.

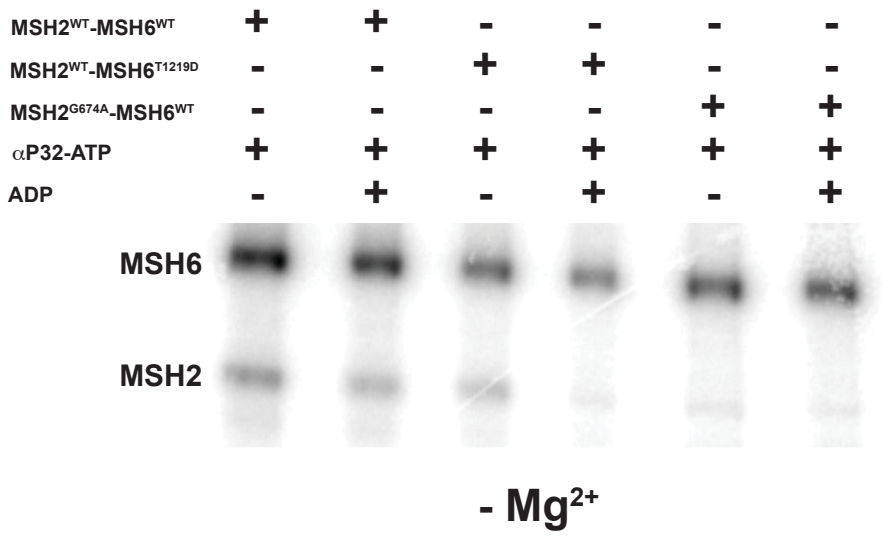


**Figure 4.3 - SDS-PAGE of UV cross-linked nucleotide into subunits of WT, G674A, and T1219D in the absence of DNA under non-hydrolyzing conditions.**

SDS-PAGE results of UV cross-linked [α-$^{32}$P]-ATP or [γ-$^{32}$P]-ATP into the MSH2 and MSH6 ATPase sites of WT, T1219D, or G674A in the presence of excess ATP (100 μM). $Mg^{2+}$ was not present in these reactions. Each 20 μL reaction contained 10 μCi of 3000 Ci/mmol [γ-$^{32}$P]-ATP or of 800 Ci/mmol [α-$^{32}$P]-ATP, reaction buffer without $Mg^{2+}$ (25 mM Tris HCl (pH 7.8), 100 mM sodium acetate, 2 mM dithiothreitol (DTT), 200 μg/mL BSA, and 5% glycerol), and 4 pmol hMSH2-MSH6 or appropriate mutant protein. Cross-linking was performed on ice for 20 min at 254 nm. MSH2-MSH6 subunits were resolved on a 10% SDS-PAGE.

Under non-hydrolyzing conditions, we observe a shift in the dominant nucleotide bound subunit (Figure 4.3). WT, T1219D, and G674A exhibit strong preferences for binding nucleotide into the MSH6 subunit over MSH2 (Figure 4.3; lanes 1, 3, and 5 respectively) with 83%, 87%, and 98% of nucleotide residing in MSH6 respectively. Interestingly, the addition of ADP does not appear to alter ATP binding significantly for WT (87%) or G674A (99%) (Figure 4.3, lanes 2 and 6 respectively). In contrast, ADP addition competes with ATP binding into MSH2 of the T1219D mutant (~three fold decrease in apparent binding into MSH2) (Figure 4.3, lane 4). This result suggests that the T1219D mutant has a higher affinity for ADP in MSH2 than either WT or G674A. The measureable binding of nucleotide into MSH6 of the G674A mutant in the absence of hydrolysis is in direct contrast with the lack of binding observed in the presence of hydrolysis. This difference suggests that the G674A mutant may bind and hydrolyze ATP so rapidly in MSH6 that the nucleotide cross-linking efficiency under hydrolyzing conditions is dramatically decreased. Consistent with ATP hydrolysis data, independent of hydrolyzing vs. non-hydrolyzing conditions, the G674A mutant appears to be impaired for nucleotide binding in MSH2 in the absence of DNA.

### *DNA induces equal nucleotide binding into MSH2 and MSH6 of WT under hydrolyzing conditions*

Geng *et al.* determined the steady state ATP hydrolysis rates for WT, G674A, and T1219D in the absence of DNA and presence of homoduplex and heteroduplex DNA (Geng, Sakato et al. 2012). The steady state hydrolysis rate of WT human MutSα in the absence of DNA was determined to be ~0.03 $s^{-1}$ and ~0.68 $s^{-1}$ in the presence of a GT mismatch. The steady state hydrolysis rates for the G674A and T1219D mutant proteins

exhibited an opposite trend in hydrolysis. G674A and T1219D exhibited hydrolysis rates of ~0.26 $s^{-1}$ and 0.39 $s^{-1}$ respectively in the absence of DNA. Similar hydrolysis rates were determined for G674A and T1219D in the presence of homoduplex DNA ($k_{cat}$ = 0.42 $s^{-1}$ and 0.89 $s^{-1}$ respectively). However, in the presence of a GT mismatch the hydrolysis rates of the two proteins decrease ~10-fold ($k_{cat}$ = 0.03 $s^{-1}$ and 0.02 $s^{-1}$ respectively) (Geng, Sakato et al. 2012). We therefore sought to characterize the nucleotide occupancy of WT, T1219D, and G674A in the presence of homoduplex (AT), base-base mismatched (GT), and damaged ($O^6$MeGT) DNA.

Under hydrolyzing conditions in the presence of DNA (Figure 4.4), WT no longer exhibits a preference for nucleotide binding into MSH2 over MSH6. In fact, the nucleotide occupancy in MSH2 and MSH6 of WT is about equal between the two subunits and quite similar when comparing AT, GT, and $O^6$MeGT (Figure 4.4 – Lanes 1, 5, 9 respectively) where we observe 47, 58, and 45% of nucleotide bound into MSH2 respectively. The addition of ADP to system does little to alter WT nucleotide occupancy for AT, GT, or $O^6$MeGT (50%, 48%, 46% binding into MSH2 respectively). These observations are consistent with a requirement for nucleotide binding into both subunits for MMR initiation (Acharya, Foster et al. 2003; Antony and Hingorani 2003; Antony, Khubchandani et al. 2006; Heinen, Cyr et al. 2011; Monti, Cohen et al. 2011; Qiu, DeRocco et al. 2012).

*DNA induces a preferential binding of nucleotide into MSH2 for T1219D but into MSH6 for G674A under hydrolyzing conditions*

In contrast to wild type, the T1219D and G674A mutants do not exhibit equal occupancy of ATP for each subunit. Under hydrolyzing conditions, T1219D maintains a

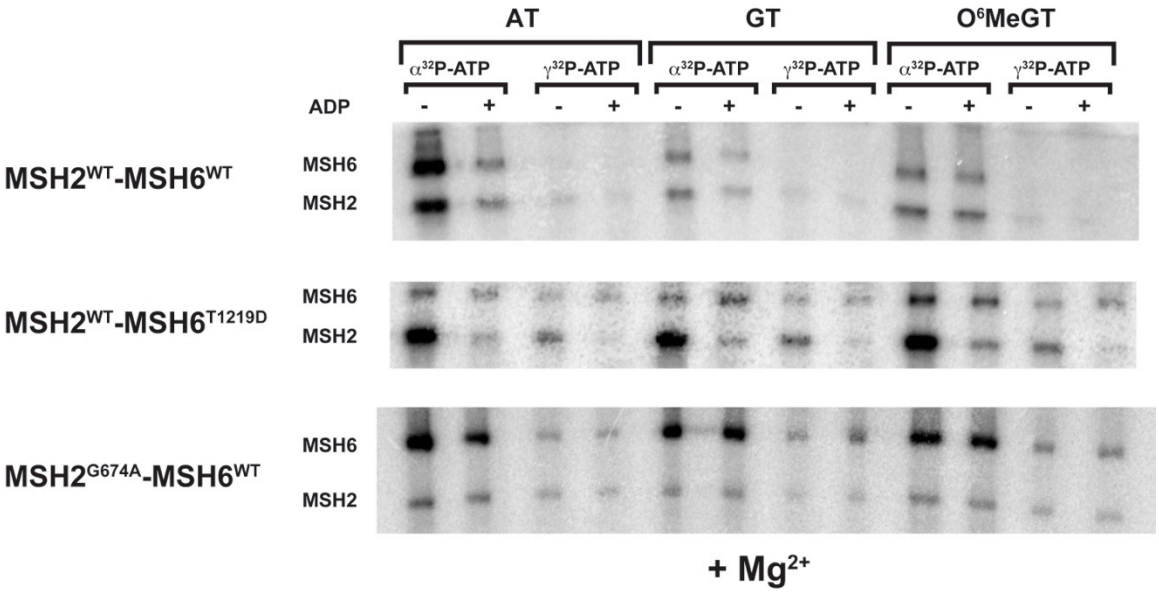


**Figure 4.4 - SDS-PAGE of UV cross-linked nucleotide into subunits of WT, G674A, and T1219D in the presence of 10 nM of the appropriate DNA under hydrolyzing conditions.**

SDS-PAGE results of UV cross-linked [α-$^{32}$P]-ATP or [γ-$^{32}$P]-ATP into the MSH2 and MSH6 ATPase sites of WT, T1219D, or G674A in the presence of excess ATP (100 μM), $Mg^{2+}$ (5 mM), and 10 nM of homoduplex, GT, or $O^6$MeGT DNA. Each 20 μL reaction contained 10 μCi of 3000 Ci/mmol [γ-$^{32}$P]-ATP or of 800 Ci/mmol [α-$^{32}$P]-ATP, reaction buffer (25 mM Tris HCl (pH 7.8), 100 mM sodium acetate, 5 mM magnesium chloride, 2 mM dithiothreitol (DTT), 200 μg/mL BSA, and 5% glycerol), 4 pmol hMSH2-MSH6, or appropriate mutant protein, and 10 nM DNA. Cross-linking was performed as described in Materials and Methods.

preference for binding nucleotide into MSH2 over MSH6 in the presence of homoduplex DNA (90% in MSH2), GT DNA (89% in MSH2), and $O^6$MeGT (80% in MSH2) (Figure 4.4 – Middle panel, Lanes 1, 5, and 9 respectively). Again there is very little difference in nucleotide preference for the different DNA substrates. The addition of ADP to the reaction alters the nucleotide binding occupancies in T1219D where AT, GT, and $O^6$MeGT exhibit nucleotide binding at 56%, 43%, and 46% respectively in the MSH2 subunit (Figure 4.4 – Middle panel, Lanes 2, 6, and 10 respectively). This occupancy is roughly half of the nucleotide binding in MSH2 observed in the absence of unlabeled ADP reinforcing the proposed affinity of MSH2 for ADP in contrast to WT and G674A.

Under hydrolyzing conditions, G674A exhibits nucleotide occupancies opposite from that of T1219D. In the presence of AT, GT, and $O^6$MeGT, G674A exhibits a preference for nucleotide binding into the MSH6 subunit over the MSH2 subunit (only 13%, 9%, and 9% respectively being bound into MSH2) (Figure 4.4- Bottom panel, Lanes 1, 5, and 9 respectively). The addition of ADP into the system does not alter the nucleotide occupancies in the presence of AT (19% in MSH2), GT (10% in MSH2), or $O^6$MeGT (10% in MSH2) (Figure 4.4- Bottom panel, Lanes 2, 6, and 10 respectively). In this respect, the lack of an ADP competitive effect on nucleotide occupancy is similar in WT and G674A.

### *WT, T1219D, and G674A bind ATP preferentially in MSH6 over MSH2 under non-hydrolyzing conditions*

Pre-steady state nucleotide occupancies were also probed in the presence of AT, GT, and $O^6$MeGT DNA substrates by withholding magnesium ($Mg^{2+}$), thereby preventing ATP hydrolysis. Under non-hydrolyzing conditions, WT (Figure 4.5 - Top

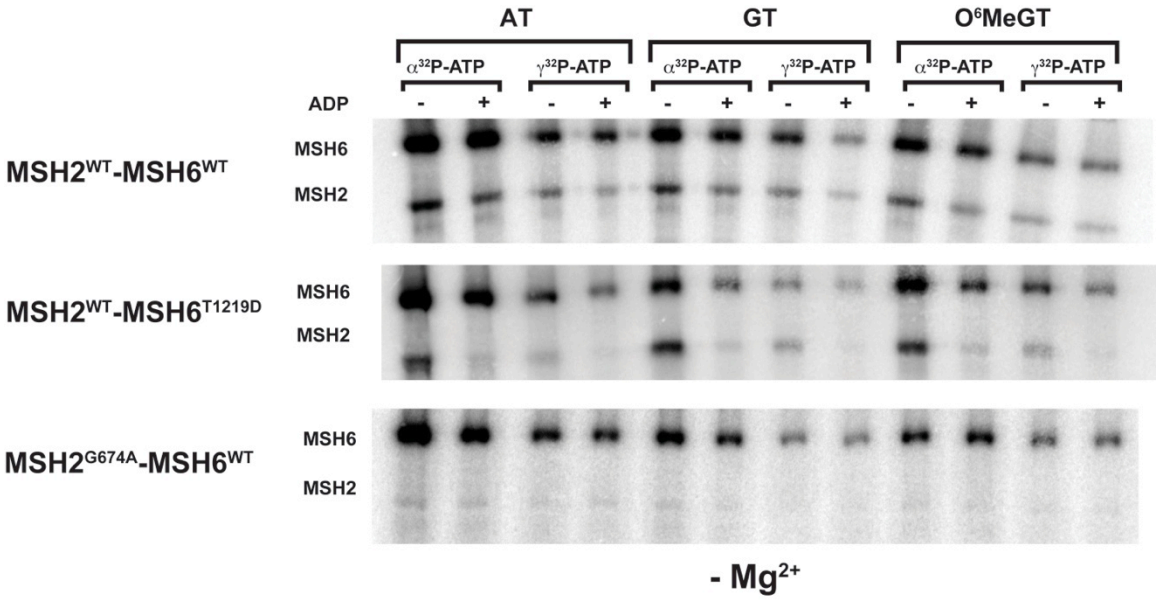


**Figure 4.5 - SDS-PAGE of UV cross-linked nucleotide into subunits of WT, G674A, and T1219D in the presence of 10 nM of the appropriate DNA under non-hydrolyzing conditions.**

SDS-PAGE results of UV cross-linked [α-$^{32}$P]-ATP or [γ-$^{32}$P]-ATP into the MSH2 and MSH6 ATPase sites of WT, T1219D, or G674A in the presence of excess ATP (100 μM) and 10 nM of homoduplex, GT, or O$^6$MeGT DNA. $Mg^{2+}$ was not present in these reactions. Each 20 μL reaction contained 10 μCi of 3000 Ci/mmol [γ-$^{32}$P]-ATP or of 800 Ci/mmol [α-$^{32}$P]-ATP, reaction buffer (25 mM Tris HCl (pH 7.8), 100 mM sodium acetate, 2 mM dithiothreitol (DTT), 200 μg/mL BSA, and 5% glycerol), 4 pmol hMSH2-MSH6, or appropriate mutant protein, and 10 nM DNA. Cross-linking was performed as described in Materials and Methods.

panel) and T1219D (Figure 4.5 - Middle panel) again behave similarly. In the presence of AT and $O^6$MeGT DNA substrates we observe a preference for nucleotide binding into MSH6 with WT binding into MSH2 at 23% and 24% respectively (Figure 4.5 - Top panel, Lanes 1 and 9) and T1219D binding into MSH2 at 20% and 28% respectively (Figure 4.5 - Middle panel, Lanes 2 and 10). There is some discrepancy between the binding affinities of WT and T1219D in the presence of a GT mismatch (25% and 47% respectively) (Figure 4.5 - Top panel, Lane 5 and Middle panel, Lane 5 respectively), however, given the error associated with each calculation, (±7% and ±17% respectively) there is no statistical difference between the two data sets using the student's T-Test ($T(4)=1.540$, $p>0.05$). Therefore, WT and T1219D share similarities in the presence of AT, GT, and $O^6$MeGT with a nucleotide binding preference for MSH6 over MSH2.

However, upon addition of ADP to the reaction, WT remains unaltered in its nucleotide binding properties with binding into MSH2 remaining at 17%, 23% and 16% for AT, GT, and $O^6$MeGT DNA substrates respectively (Figure 4.5 - Top panel, Lanes 2, 6, and 10). In contrast, T1219D binding into MSH2 decreases to 4%, 13%, and 10% for AT, GT, and $O^6$MeGT DNA substrates respectively (Figure 4.5 - Middle panel, Lanes 2, 6, and 10). This 2 to 4 fold change in nucleotide binding into MSH2 is consistent with the decreased nucleotide binding occupancy observed under hydrolyzing conditions in the presence of DNA and non-hydrolyzing conditions in the absence of DNA. Together, the data reinforce a higher affinity for ADP binding in MSH2 of the T1219D mutant.

Under non-hydrolyzing conditions, the G674A mutant maintains a preference for binding nucleotide into MSH6 in the presence of AT (3% MSH2), GT (4% MSH2), and $O^6$MeGT (4% into MSH2) DNA (Figure 4.5 - Bottom panel, Lanes 1, 5, and 9). Addition

of ADP does not alter this preference for MSH6 nucleotide binding with 4%, 5%, and 3% for AT, GT, and $O^6$MeGT DNA substrates respectively (Figure 4.5 - Bottom panel, Lanes 2, 6, and 10). Because these experiments were performed in the absence of hydrolysis, we can reasonably propose that the G674A mutant is defective for nucleotide binding into the MSH2 subunit.

**Discussion**

Our recent studies in collaboration with Geng *et al* revealed that the mechanism of action of WT hMutSα and the two mutant hMutSα proteins discussed here differ greatly in biochemical assays of MMR activity, ATPase activity, and ternary complex formation with hMutLα (Geng, Sakato et al. 2012). The G674A and the T1219D mutants were shown to be defective in initiation of both 3′ and 5′ nick-directed repair. Both mutants exhibit a strong binding affinity for the mismatch and block MMR-dependent excision. The two mutants have faster ATPase activities than wild type in the absence of DNA and much slower ATPase activities than WT in the presence of DNA. The two separation-of-function mutants were shown to both be competent for mismatch binding but defective in MMR at the mismatch. However, on closer inspection, it was shown that G674A mutant was able to form a ternary complex with MutLα to a lesser extent than that of WT while the T1219D mutant was shown to be completely defective in ternary complex formation with MutLα.

Overall, in our study we observe similar nucleotide occupancies for WT, T1219D, and G674A in non-hydrolyzing conditions regardless of the presence or absence of DNA. All proteins exhibit a higher affinity for MSH6 occupancy in the absence of hydrolysis. The extent of binding varies somewhat, but the general trend is clear. In fact, under

hydrolyzing conditions and in the absence of DNA, we again observe similarities in nucleotide occupancy between WT and T1219D where MSH2 is the subunit exhibiting the highest nucleotide occupancy. Given that the G674A mutant appears to be completely deficient in nucleotide binding in MSH2, it is not surprising that we do not observe the same nucleotide occupancy as WT and T1219D in the absence of DNA under hydrolyzing conditions. Interestingly, despite the separation-of-function behavior of the two mutants, we observe no differences in nucleotide occupancy in the presence of AT, GT, or $O^6$MeGT DNA for WT, T1219D, or G674A suggesting that the role of MutSα in apoptotic response to DNA damage is not dependent on nucleotide occupancy. However, the apoptotic role of MutSα may be dependent on conformational differences of the protein-DNA complex.

The mechanisms by which the three proteins act diverge under hydrolyzing conditions in the presence of DNA. WT exhibits almost equal nucleotide occupancy of the two subunits while T1219D occupancy resembles that of T1219D under non-hydrolyzing conditions and in the absence of DNA again exhibiting an MSH2 preference. The G674A mutant exhibits a clear nucleotide binding preference in MSH6 which is opposite of that of T1219D. Interestingly, under all conditions, the addition of ADP to the system only affects the nucleotide occupancy of the T1219D mutant resulting in decreased nucleotide occupancy of MSH2. These results reinforce the requirement for two functional ATPase domains for MMR to occur. We suggest that the G674A mutant is unable to induce MMR because it is completely unable to bind nucleotide into MSH2.

*T1219D is not deficient for nucleotide binding*

In our studies, the T1219D mutant appears to be competent for nucleotide binding in both subunits regardless of conditions. This result differs from the conclusions from similar cross-linking studies with the analogous mutations in *S. cerevisiae* (yMsh2$^{WT}$-Msh6$^{G1067D}$) (Hess, Gupta et al. 2002). Previous cross-linking results of yMsh2$^{WT}$-Msh6$^{G1067D}$ under non-hydrolyzing conditions suggested that the mutation eliminates ATP binding into Msh2. However, under non-hydrolyzing conditions we observe wild type-like cross-linking of ATP into MSH2 for T1219D in the absence of additional ADP. Because the analogous mutation in yeast is not of a conserved residue in human (glycine in yeast, threonine in human), the disparities between the nucleotide occupancy studies may be attributed to evolutionary differences between the two systems. Regardless, the T1219D mutant is able to bind nucleotide into both MSH2 and MSH6.

We observe a competitive effect of ADP suggesting that the T1219D mutant has a much higher affinity for ADP binding into MSH2. It has been proposed that the T1219D mutant is unable to undergo the ADP to ATP exchange required for conformational changes into the MutSα sliding clamp (Hess, Mendillo et al. 2006; Geng, Sakato et al. 2012). The inability of the T1219D protein to form the sliding clamp has been demonstrated in both yeast and human systems using SPR analyses (Hess, Mendillo et al. 2006; Hargreaves, Shell et al. 2010; Geng, Sakato et al. 2012). Our result is consistent with an inability to exchange ADP for ATP in MSH2. T1219D would therefore exist predominantly in an MSH2-ADP liganded state where only MSH6 would be able to hydrolyze ATP. It has also been suggested that the T1219D mutation prevents the formation of the sliding clamp either by altering the MSH2 nucleotide-binding pocket or by blocking conformational changes at the ATPase interface. The MSH2 binding pocket

could certainly be molded such that the binding of ATP is unlikely, but that of ADP is unaltered. The proximity of the T1219D mutation to the interface between the two ATPase domains suggests that conformation shifts around the domain may be inhibited. While we cannot rule out either of these hypotheses, we further suggest that the T1219D mutation prevents either an ADP to ATP exchange in MSH2 or an exchange of the MSH2-bound ADP for the MSH6-released ADP either of which could be required for sliding clamp formation. This liganded state is consistent with the proposed dead end complex of the molecular switch model (Heinen, Cyr et al. 2011).

*G674A is a nucleotide binding deficient in MSH2*

The G674A mutation appears to be somewhat more complicated. The data from these studies suggest that the G674A mutant is defective for nucleotide binding into MSH2. However, the data from Geng *et al* suggests that the G674A mutant has some ability to form a ternary complex with MutLα (Geng, Sakato et al. 2012). If nucleotide binding into MSH2 is necessary for sliding clamp formation, and therefore ternary complex formation, a population of G674A that forms the ternary complex with MutLα would not be observed. However, if this competent G674A population is short-lived upon addition of ATP, the nucleotide occupancy would not necessarily be observed, given the time frame of the experiments presented here. These results would be consistent with a predominantly defective population for sliding clamp formation. The inability of the G674A mutant to form the sliding clamp is therefore similar to that of the T1219D mutation. G674A cannot bind nucleotide into MSH2 and therefore has the same difficulty performing the ADP to ATP exchange or the MSH2-bound ADP to MSH6-released ADP as discussed for the T1219D mutation.

## Conclusions

The nucleotide binding defects observed for the G674A and T1219D mutants and the phenotypes observed in other studies (Berends, Wu et al. 2002; Lin, Wang et al. 2004; Yang, Scherer et al. 2004; Hess, Mendillo et al. 2006; Geng, Sakato et al. 2012) are consistent with an inability of either protein to undergo the conformational change to the sliding clamp required in MMR. The work presented here emphasizes the need for nucleotide binding capabilities in both ATPase domains of hMutSα. Specifically, we have shown that the inability of MSH2 to perform an ADP to ATP exchange or an MSH2-bound ADP to MSH6-released ADP exchange prevents the protein from forming the sliding clamp. Given the mismatch affinity of the G674A and T1219D mutants, the defective proteins remain at the mismatch and block excision and MMR. Because we do not observe differences between the nucleotide occupancies of the proteins in the presence of AT, GT, or $O^6$MeGT DNA substrates, we cannot speculate on the role of nucleotide occupancy in apoptotic response to DNA damage.

Given the similar mutagenic phenotypes of the G674A and T1219D mutants *in vivo*, it is interesting that the nucleotide binding properties of these mutants should be so different. The observations presented here have interesting implications for the points in the MutSα ATPase processing pathway these mutants may be trapped in. If these mutants are in fact being trapped in different stages of the ATP processing pathway, further characterization of each mutant may lead to a better understanding of both the MutSα mechanism of recognition and initiation and the involvement of MutSα in the DNA damage induced apoptosis.

## References


Acharya, S., P. L. Foster, et al. (2003). "The coordinated functions of the E. coli MutS and MutL proteins in mismatch repair." Mol Cell **12**(1): 233-246.

Allen, D., A. Makhov, et al. (1997). "MutS mediates heteroduplex loop formation by a translocation mechanism." The EMBO journal **16**(14): 4467-4476.

Antony, E. and M. M. Hingorani (2003). "Mismatch recognition-coupled stabilization of Msh2-Msh6 in an ATP-bound state at the initiation of DNA repair." Biochemistry **42**(25): 7682-7693.

Antony, E., S. Khubchandani, et al. (2006). "Contribution of Msh2 and Msh6 subunits to the asymmetric ATPase and DNA mismatch binding activities of Saccharomyces cerevisiae Msh2-Msh6 mismatch repair protein." DNA repair **5**(2): 153-162.

Berends, M. J., Y. Wu, et al. (2002). "Molecular and clinical characteristics of MSH6 variants: an analysis of 25 index carriers of a germline variant." Am J Hum Genet **70**(1): 26-37.

Blackwell, L. J., K. Bjornson, et al. (1998). "DNA-dependent activation of the hMutSalpha ATPase." The Journal of biological chemistry **273**(48): 32049-32054.

Blackwell, L. J., K. P. Bjornson, et al. (2001). "Distinct MutS DNA-binding modes that are differentially modulated by ATP binding and hydrolysis." The Journal of biological chemistry **276**(36): 34339-34347.

Blackwell, L. J., D. Martik, et al. (1998). "Nucleotide-promoted release of hMutSalpha from heteroduplex DNA is consistent with an ATP-dependent translocation mechanism." The Journal of biological chemistry **273**(48): 32055-32062.

Cyr, J. (2008). "Hereditary cancer-associated missense mutations in hMSH6 uncouple ATP hydrolysis from DNA mismatch binding." Journal of Biological Chemistry.

Drotschmann, K., M. C. Hall, et al. (2002). "DNA binding properties of the yeast Msh2-Msh6 and Mlh1-Pms1 heterodimers." Biol Chem **383**(6): 969-975.

Drotschmann, K., R. P. Topping, et al. (2004). "Mutations in the nucleotide-binding domain of MutS homologs uncouple cell death from cell survival." DNA Repair (Amst) **3**(7): 729-742.

Geng, H., C. Du, et al. (2011). "In vitro studies of DNA mismatch repair proteins." Analytical biochemistry.

Geng, H., M. Sakato, et al. (2012). "Biochemical Analysis of the Human Mismatch Repair Proteins hMutS MSH2G674A-MSH6 and MSH2-MSH6T1219D." The Journal of biological chemistry **287**(13): 9777-9791.

Gorman, J., A. Chowdhury, et al. (2007). "Dynamic basis for one-dimensional DNA scanning by the mismatch repair complex Msh2-Msh6." Mol Cell **28**(3): 359-370.

Gorman, J., A. J. Plys, et al. (2010). "Visualizing one-dimensional diffusion of eukaryotic DNA repair factors along a chromatin lattice." Nature structural & molecular biology **17**(8): 932-938.

Gradia, S., S. Acharya, et al. (1997). "The human mismatch recognition complex hMSH2-hMSH6 functions as a novel molecular switch." Cell **91**(7): 995-1005.

Gradia, S., S. Acharya, et al. (2000). "The role of mismatched nucleotides in activating the hMSH2-hMSH6 molecular switch." J Biol Chem **275**(6): 3922-3930.

Gradia, S., D. Subramanian, et al. (1999). "hMSH2-hMSH6 forms a hydrolysis-independent sliding clamp on mismatched DNA." Mol Cell **3**(2): 255-261.

Haber, L. T. and G. C. Walker (1991). "Altering the conserved nucleotide binding motif in the Salmonella typhimurium MutS mismatch repair protein affects both its ATPase and mismatch binding activities." The EMBO journal **10**(9): 2707-2715.

Habraken, Y., P. Sung, et al. (1998). "ATP-dependent assembly of a ternary complex consisting of a DNA mismatch and the yeast MSH2-MSH6 and MLH1-PMS1 protein complexes." J Biol Chem **273**(16): 9837-9841.

Hargreaves, V. V., S. S. Shell, et al. (2010). "Interaction between the Msh2 and Msh6 Nucleotide-binding Sites in the Saccharomyces cerevisiae Msh2-Msh6 Complex." Journal of Biological Chemistry **285**(12): 9301-9310.

Heinen, C. D., J. L. Cyr, et al. (2011). "Human MSH2 (hMSH2) Protein Controls ATP Processing by hMSH2-hMSH6." The Journal of biological chemistry **286**(46): 40287-40295.

Hess, M. T., R. D. Gupta, et al. (2002). "Dominant Saccharomyces cerevisiae msh6 mutations cause increased mispair binding and decreased dissociation from mispairs by Msh2-Msh6 in the presence of ATP." The Journal of biological chemistry **277**(28): 25545-25553.

Hess, M. T., M. L. Mendillo, et al. (2006). "Biochemical basis for dominant mutations in the Saccharomyces cerevisiae MSH6 gene." Proc Natl Acad Sci U S A **103**(3): 558-563.

Jacobs-Palmer, E. and M. M. Hingorani (2007). "The effects of nucleotides on MutS-DNA binding kinetics clarify the role of MutS ATPase activity in mismatch repair." J Mol Biol **366**(4): 1087-1098.

Jiang, J., L. Bai, et al. (2005). "Detection of high-affinity and sliding clamp modes for MSH2-MSH6 by single-molecule unzipping force analysis." Molecular cell **20**(5): 771-781.

Joshi, A. and B. J. Rao (2002). "ATP hydrolysis induces expansion of MutS contacts on heteroduplex: a case for MutS treadmilling?" Biochemistry **41**(11): 3654-3666.

Junop, M., G. Obmolova, et al. (2001). "Composite Active Site of an ABC ATPase:: MutS Uses ATP to Verify Mismatch Recognition and Authorize DNA Repair." Molecular cell.

Kato, R., M. Kataoka, et al. (2001). "Direct observation of three conformations of MutS protein regulated by adenine nucleotides." Journal of molecular biology **309**(1): 227-238.

Lamers, M. H., D. Georgijevic, et al. (2004). "ATP increases the affinity between MutS ATPase domains. Implications for ATP hydrolysis and conformational changes." The Journal of biological chemistry **279**(42): 43879-43885.

Lin, D. P., Y. Wang, et al. (2004). "An Msh2 point mutation uncouples DNA mismatch repair and apoptosis." Cancer Res **64**(2): 517-522.

Lützen, A., N. de Wind, et al. (2008). "Functional analysis of HNPCC-related missense mutations in MSH2." Mutation Research/ ….

Mazur, D. J., M. L. Mendillo, et al. (2006). "Inhibition of Msh6 ATPase activity by mispaired DNA induces a Msh2(ATP)-Msh6(ATP) state capable of hydrolysis-independent movement along DNA." Molecular cell **22**(1): 39-49.

Mendillo, M. L., D. J. Mazur, et al. (2005). "Analysis of the interaction between the Saccharomyces cerevisiae MSH2-MSH6 and MLH1-PMS1 complexes with DNA using a reversible DNA end-blocking system." The Journal of biological chemistry **280**(23): 22245-22257.

Monti, M. C., S. X. Cohen, et al. (2011). "Native mass spectrometry provides direct evidence for DNA mismatch-induced regulation of asymmetric nucleotide binding in mismatch repair protein MutS." Nucleic Acids Research **39**(18): 8052-8064.

Ollila, S., D. Dermadi Bebek, et al. (2008). "Mechanisms of pathogenicity in human MSH2 missense mutants." Human mutation **29**(11): 1355-1363.

Pluciennik, A. and P. Modrich (2007). "Protein roadblocks and helix discontinuities are barriers to the initiation of mismatch repair." Proceedings of the National Academy of Sciences of the United States of America **104**(31): 12709-12713.

Qiu, R., V. C. DeRocco, et al. (2012). "Large conformational changes in MutS during DNA scanning, mismatch recognition and repair signalling." The EMBO journal.

Rasband, W. S. (1997-2012). "ImageJ." from http://imagej.nih.gov/ij/.

Schofield, M. J., S. Nayak, et al. (2001). "Interaction of Escherichia coli MutS and MutL at a DNA mismatch." J Biol Chem **276**(30): 28291-28299.

Selmane, T., M. J. Schofield, et al. (2003). "Formation of a DNA mismatch repair complex mediated by ATP." J Mol Biol **334**(5): 949-965.

Studamire, B., T. Quach, et al. (1998). "Saccharomyces cerevisiae Msh2p and Msh6p ATPase activities are both required during mismatch repair." Molecular and Cellular Biology **18**(12): 7590-7601.

Wang, H., C. W. Lawrence, et al. (1999). "Specific binding of human MSH2.MSH6 mismatch-repair protein heterodimers to DNA incorporating thymine- or uracil-containing UV light photoproducts opposite mismatched bases." The Journal of biological chemistry **274**(24): 16894-16900.

Yang, G., S. J. Scherer, et al. (2004). "Dominant effects of an Msh6 missense mutation on DNA repair and cancer susceptibility." Cancer Cell **6**(2): 139-150.

Zhai, J. and M. M. Hingorani (2010). "Saccharomyces cerevisiae Msh2-Msh6 DNA binding kinetics reveal a mechanism of targeting sites for DNA mismatch repair." Proceedings of the National Academy of Sciences of the United States of America **107**(2): 680-685.

# Chapter 5

## CHARACTERIZATION OF THE PROTEIN-DNA INTERACTIONS OF HUMAN MSH2-MSH6

### Introduction

The crystal structures of both the prokaryotic MutS (*E. coli* and *T. aquaticus*) and human MSH2-MSH6 (hMutSα) suggests DNA binding by the protein is asymmetric (Lamers, Perrakis et al. 2000; Obmolova, Ban et al. 2000; Alani, Lee et al. 2003; Warren, Pohlhaus et al. 2007). This asymmetric nature is also observed in the ATP binding properties of the protein (Bjornson and Modrich 2003; Antony and Hingorani 2004; Martik, Baitinger et al. 2004; Antony, Khubchandani et al. 2006; Monti, Cohen et al. 2011). Biochemical data evaluating the nucleotide binding properties for human MSH2-MSH6 (or yeast Msh2-Msh6) consistently suggest a higher affinity for ATP in the MSH6 subunit and for ADP in the MSH2 subunit (Blackwell, Martik et al. 1998; Drotschmann, Yang et al. 2002; Antony and Hingorani 2003; Antony and Hingorani 2004; Martik, Baitinger et al. 2004; Antony, Khubchandani et al. 2006; Mazur, Mendillo et al. 2006).

The relationship between ATP processing and conformational changes in the MSH2-MSH6 protein has been evaluated using both biochemical and biophysical means. Most biochemical and biophysical data strongly suggests a requirement for an ATP:ATP ligand state in the two subunits of MutS or MutSα (MutS(α)) in order to induce the

protein conformational change believed to be the MutS(α) DNA sliding clamp (Acharya, Foster et al. 2003; Antony and Hingorani 2003; Antony, Khubchandani et al. 2006; Lebbink, Fish et al. 2010; Mendillo, Putnam et al. 2010; Heinen, Cyr et al. 2011; Monti, Cohen et al. 2011; Qiu, DeRocco et al. 2012). However the order of events leading up to the ATP:ATP ligand state have been a matter of debate. The conformations associated with the different ligand-state possibilities have been explored in a limited number of studies (Mendillo, Putnam et al. 2010; Qiu, DeRocco et al. 2012).

The work in Chapter 4 describes the nucleotide binding properties of human MSH2-MSH6 (WT) and two hereditary non-polyposis colorectal cancer (HNPCC) mutant proteins, $MSH2^{G674A}$-MSH6 (G674A) and MSH2-$MSH6^{T1219D}$ (T1219D). We have shown that the nucleotide binding properties for WT, G674A, and T1219D do not vary with DNA substrate (homoduplex, GT mismatch, or $O^6$MeGT DNA damage). The nucleotide binding data suggest that G674A is deficient for nucleotide binding into the MSH2 subunit. The T1219D mutant is competent for binding nucleotide in both MSH2 and MSH6 subunits; however, the MSH2 subunit of T1219D exhibits a strong binding preference for ADP over ATP. The observed nucleotide binding deficiencies in G674A and T1219D present an opportunity to explore potential MSH2-MSH6 protein-DNA conformations of proteins in two different trapped ligand states. Specifically, G674A appears to be trapped in an MSH2-empty:MSH6-ATP ligand state and T1219D appears to be trapped in an MSH2-ADP:MSH6-ATP liganded state. These mutants allow us to evaluate the protein-DNA conformations in different ligand states and compare with that of WT.

Previous smFRET experiments evaluating the protein-DNA interactions of Thermus *aquaticus* (*Taq*) MutS with a GT mismatch DNA substrate have shown that the interaction is dynamic in nature (DeRocco, Anderson et al. 2010; Sass, Lanyi et al. 2010; Qiu, DeRocco et al. 2012). We have also demonstrated dynamic conformational changes in the mismatch binding region (Domain I) of the *Taq* MutS homodimer that are dependent on the presence of a mismatch and the nucleotide conditions (Qiu, DeRocco et al. 2012). These results are consistent with deuterium exchange studies showing changes in solvent accessibility in the presence of ATP and a mismatch versus absence of ATP for both the mismatch binding region (Domain I) and DNA clamp region (Domain IV) of yMutSα (Mendillo, Putnam et al. 2010). Little has been demonstrated regarding the protein-DNA interactions of the eukaryotic form of MutS (Msh2-Msh6 in yeast and MSH2-MSH6 in human). While we have a thorough report of the nucleotide binding preferences for each protein, the DNA binding conformational properties of either WT or the mutants have not been characterized.

The single-molecule FRET (smFRET) study presented here demonstrates that the prokaryotic MutS and the eukaryotic MutSα-DNA complexes exhibit different conformational properties. In contrast to the prokaryotic MutS-DNA complexes, we observe few dynamic, MutSα dependent conformational changes in the presence of GT mismatch DNA for WT, T1219D, and G674A. However, we do observe differences in protein-dependent DNA bending conformations for WT-GT, T1219D-GT, and G674A-GT complexes, which depend on the nucleotide conditions. Specifically, the largest conformational differences are observed in nucleotide conditions that promote sliding clamp formation of MutSα. These data taken with the nucleotide binding data presented

in Chapter 4 suggest different mechanisms for MMR deficiency and potentially DNA apoptotic response in the two HNPCC mutants, G674A and T1219D.

## Materials and Methods

### *Preparation of human MSH2-MSH6 and its mutants*

MSH2-MSH6 and the HNPCC mutants were prepared and purified as described previously (Geng, Du et al. 2011; Geng, Sakato et al. 2012). Briefly, recombinant hMutSα was expressed in insect cells using the baculovirus system. Each protein was purified over a 6-ml Resource$^{TM}$ Q anion exchange column (GE Healthcare), a 5-ml HiTrap$^{TM}$ Heparin affinity column (GE Healthcare), and a HiLoad 16/60 Superdex 200 sizing column (GE Healthcare) as described in (Geng, Du et al. 2011; Geng, Sakato et al. 2012). Wild type hMutSα and hMSH2$^{G674A}$-hMSH6$^{WT}$ were eluted in buffer A (25 mM HEPES, pH 7.5, 0.1 mM EDTA, 10% glycerol, 1 mM DTT, 1× Complete proteinase inhibitor mixture (Roche Applied Science) and 0.1% PMSF) containing 100 mM KCl. MSH2$^{WT}$-MSH6$^{T1219D}$ was eluted in buffer A containing 300 mM KCl as described in (Geng, Du et al. 2011; Geng, Sakato et al. 2012). Concentrations of MutSα were determined with a modified Bradford protein assay (Bio-Rad) using BSA as the standard. Protein was generously provided to us by Dr. Peggy Hsieh (NIDDK, Bethesda, MD).

### *DNA Substrates*

The 500 bp DNA substrates were constructed as described previously (Qiu, DeRocco et al. 2012) by first PCR amplifying a 500 bp linear DNA strand from the pUC-19 VSR plasmid . The forward primer was labeled with biotin and the reverse primer unlabeled. Primer sequences used in PCR are shown in Table 5.1. The linear DNA was

**Table 5.1 - PCR primers used in 500mer DNA substrate construction.**

| Name | Pri | Sequence |
|---|---|---|
| pUC19-vsr FRET PROBE R1 | R1 | 5'-/GAG TCA GTG AGC GAG GAA GC-3' |
| FRET Probe F1- Biotin | F1- | 5'-/biotin/CGG CAT CAG AGC AGA TTC TA-3' |

nicked at four sites nick sites with *Nt Bbv CI* (New England Biolabs) at 37˚C overnight. A 37 bp gap in the PCR product was formed by heating the nicked DNA at 80˚C for 30 minutes. While still warm, small DNA fragments and enzymes were removed from the reaction using the PCR Clean-up Kit (Qiagen). An oligo containing the desired mismatch (GT) and the Forster dye pairs (Cy3 and Cy5) was mixed with the gapped DNA in 1:1 ratio and annealed to form complete double stranded DNA. The oligo sequence was TCA GCA ATC CTC A/iCy3/GC CAG GTC TCA GCT G/iCy5/GC CTC AGC G where the underlined base is the site of the generated GT mismatch and iCy5 and iCy3 denote the internal positions of the Cy3 and Cy5 dyes. Finally, the DNA was ligated using T4 DNA ligase. All oligos and primers were purchased from Integrated DNA Technologies (Coralville, IA).

*Fluorescence Anisotropy*

Anisotropy binding curves were acquired by titrating hMutSα or the appropriate mutant into a 3 mm quartz cuvette (Starna Cells, Inc., Atascadero, CA) containing 5 or 10 nM TAMRA labeled DNA, 20 mM Tris HCl pH 7.8, 100 mM sodium acetate, 5 mM magnesium chloride. Binding curves performed in the presence of ADP or ATP included 1 mM of the desired nucleotide in the binding buffer. Anisotropy was monitored using 553 nm excitation and 574 nm emission on a Horiba Yvon Fluorolog-3 fluorimeter. The DNA sequence used in these binding experiments was: 5′- TAC CTC ATC TCG AGC GTG CCG ATA- (TAMRA)-3′ and the corresponding complement oligonucleotide containing the mismatch site (noted as the underline base): 5′-TAT CGG CAC GTT CGA GAT GAG GTA–3′. All oligonucleotides were purchased from IDT (Coralville, IA). Curves were fit using a previously described equation (Yang, Sass et al. 2005).

*TIRF Microscope*

smFRET experiments were performed using a prism-type TIRM configuration described previously (Sass, Lanyi et al. 2010). Briefly the TIRM configuration consisted of an IX51 microscope with a 60x 1.2 NA PlanApo water immersion objective (Olympus, Tokyo, Japan) and 2 collinear lasers for illumination (green: 532nm, 100mW laser exciting Cy3 and red: 635nm, 40mW laser exciting Cy5). The lasers were individually shuttered to allow sequential illumination. The microscope image was split into 2 distinct spectral bands by a Dualview imager (Photometrics, Tucson, AZ) and relayed onto a Cascade 512B emCCD (Photometrics). The dualview contained one dichroic mirror (645dcxr Chroma, Brattleboro, VT) and band pass filters to define the spectral bands: green channel (585x70, Chroma) and red channel (700x75, Chroma). Movies were collected at 10 Hz. A mapping function to align the two distinct spectral images was derived from images of red fluorescent microspheres (Duke Scientific, Palo Alto, California), which were visible in both channels. This mapping function was used to extract the dye emission intensities from locations pre-identified to contain the acceptor. Data was analyzed with custom MatLab programs (Mathworks, Inc. Natick, MA).

Backgrounds and leakages between channels were corrected during analysis as described elsewhere (Hohng, Joo et al. 2004; Clamme and Deniz 2005; Lee, Kapanidis et al. 2007; Ross, Buschkamp et al. 2007). Gamma factors were determined from anti-correlated donor and acceptor photobleaching events using $\gamma=\Delta I_A/\Delta I_D$ (where $\Delta I_A=I_A^{\text{before bleach}} - I_A^{\text{after bleach}}$, and $\Delta I_D=I_D^{\text{after bleach}} - I_D^{\text{before bleach}}$) as described elsewhere (Ha, Ting et al. 1999; Choi, Strop et al. 2010; McCann, Choi et al. 2010). Gamma was determined

from the data to be 0.9 for the Dualview. We determined a 9% leakage of the Cy3 signal into the red channel.

## Results

### *Anisotropy binding constants support sliding clamp deficiency in T1219D and G674A*

In order to evaluate the DNA binding properties of WT, T1219D, and G674A, we began by first determining the DNA binding constants for each protein to a GT mismatch in the presence and absence of nucleotide (reported in Table 5.2). WT exhibits a high affinity for the GT mismatch in the absence of nucleotide ($K_D$ = 7.5 nM) and in the presence of ADP ($K_D$ = 8.9 nM) is consistent with similar results acquired by Martik *et al.* ($K_D$ = 19 nM and 27 nM respectively). WT exhibited a weaker affinity for the GT mismatch in the presence of ATP ($K_D$ = 107.9 nM) again consistent with similar results acquired by Martik *et al.* ($K_D$ = 109 nM) (Martik, Baitinger et al. 2004).

Similar to WT, T1219D and G674A exhibited high affinities for the GT mismatch in the absence of nucleotide ($K_D$ = 5.2 nM and 15.4 nM respectively) and in the presence of ADP ($K_D$ = 10.8 nM and 6.2 nM respectively) (Table 5.2). Unlike WT, however, both T1219D and G674A maintain a high affinity for the GT mismatch in the presence of ATP ($K_D$ = 6.3 nM and 6.6 nM respectively). The observed binding affinity for T1219D is consistent with results suggesting the analogous mutant in *Saccharomyces cerevisiae* is unable to adopt the sliding clamp conformation (Hess, Mendillo et al. 2006; Hargreaves, Shell et al. 2010), as well as our studies with the Hsieh lab (NIDDK, Bethesda) showing that both T1219D and G674A are unable to adopt the sliding clamp conformation in the presence of ATP (Geng, Sakato et al. 2012).

**Table 5.2 - Dissociation constants derived from anisotropy binding curves for WT hMutSα and the T1219D and G674A mutants.**

The error indicated is the standard deviation of at least three independent experiments.

| Protein | DNA | Nucleotide | $K_D$ (nM) |
|---|---|---|---|
| **wt hMutSα** | GT | ATP | 107.9 ± 26 |
| | | ADP | 8.9 ± 8.8 |
| | | None | 7.5 ± 7 |
| | $O^6$MeGT | ATP | 121.1 ± 92 |
| | | ADP | 24.8 ± 4 |
| **T1219D hMutSα** | GT | ATP | 6.3 ± 3 |
| | | ADP | 10.8 ± 3 |
| | | None | 5.2 ± 1 |
| | $O^6$MeGT | ATP | 21.8 ± 3 |
| | | ADP | 28.4 ± 6 |
| **G674A hMutSα** | GT | ATP | 6.6 ± 4 |
| | | ADP | 6.2 ± 8 |
| | | None | 15.4 ± 14 |
| | $O^6$MeGT | ATP | 42.8 ± 6 |
| | | ADP | 74.9 ± 72 |

We further measured the DNA binding affinities of WT for an $O^6$MeGT DNA substrate (Table 5.2). WT exhibited a three fold weaker binding affinity for the $O^6$MeGT in the presence of ADP ($K_D$ = 24.8 nM) than that observed for the GT mismatch in the presence of ADP ($K_D$ = 8.9 nM). However, the binding affinity of WT for the O6MeGT lesion in the presence of ATP ($K_D$ = 121 nM) was consistent with that of WT for the GT mismatch ($K_D$ = 107.9 nM). Differences in DNA binding affinities between the GT mismatch and the $O^6$MeGT DNA lesion may be linked to differences in recognition mechanisms.

Consistent with the GT mismatch results (Table 5.2), T1219D exhibits similar binding affinities for $O^6$MeGT in the presence of ADP and ATP ($K_D$ = 28.4 nM and 21.8 nM respectively). However, T1219D exhibits a 2-3 fold weaker binding affinity for $O^6$MeGT than for GT. Similarly G674A exhibits comparable binding affinities for $O^6$MeGT in the presence of ADP and ATP. G674A exhibits a 12 fold weaker affinity for $O^6$MeGT ($K_D$ = 74.9 nM) than for GT ($K_D$ = 6.2 nM) in the presence of ADP. G674A displays a six fold weaker affinity for O6MeGT ($K_D$ = 42.8 nM) than for GT ($K_D$ = 6.6 nM) in the presence of ATP. The weaker binding affinities for an $O^6$MeGT lesion than for a GT mismatch of both separation-of-function mutations may play a role in their ability to recognize DNA damage but not signal for repair.

*Single Molecule FRET*

After determining the differences in DNA binding between WT and the separation-of-function mutants, T1219D and G674A, we sought to determine if there were corresponding differences in protein-DNA interaction or dynamics. In order to better understand the conformational properties of WT, T1219D, and G674A, we utilized

smFRET to monitor MutS-induced DNA bending as we had done for *Taq* MutS (Chapters 2 and 3). Using donor and acceptor dyes on either side of a DNA mismatch we observe single molecule fluorescence emission intensities (Figure 5.1a). Fluorescent emission intensities of the acceptor ($I_A$) and donor ($I_D$) are used to calculate smFRET as a function of time shown as smFRET traces (Figure 5.1a). smFRET is calculated as shown in Eq. 5.1.

$$FRET = \frac{(I_A - \beta I_D)}{((I_A - \beta I_D) + \gamma I_D)}$$

**Eq. 5.1**

Where β accounts for leakage of the donor emission into the acceptor channel and γ is a factor used to correct for differences in quantum efficiencies between the donor and acceptor dyes as described previously (Mccann, Choi et al. 2010). A simplified version of Eq. 5.1 is shown in Figure 5.1A. Example smFRET traces of DNA in the absence of protein are shown in (Figure 5.1B). Free DNA traces typically exhibited FRET values centered on 0.2. FRET states deviating from that observed in the absence of protein are characteristic of DNA bend states induced by the protein upon binding the mismatch or lesion similar to the DNA bending analysis described in Chapters 2 and 3.

*WT binding to a GT mismatch induces static DNA bending*

We measured smFRET for WT hMutSα binding to a GT mismatch in the absence of nucleotide and presence of ADP, ATP, or ATPγS (example traces shown in Figure 5.2). In the absence of nucleotide, we observe FRET traces that do not appear to be dynamic in nature, which we have termed "constant" traces (92% of molecules evaluated were constant) (Figure 5.2). Only a small population of traces exhibited a transition. Histogram

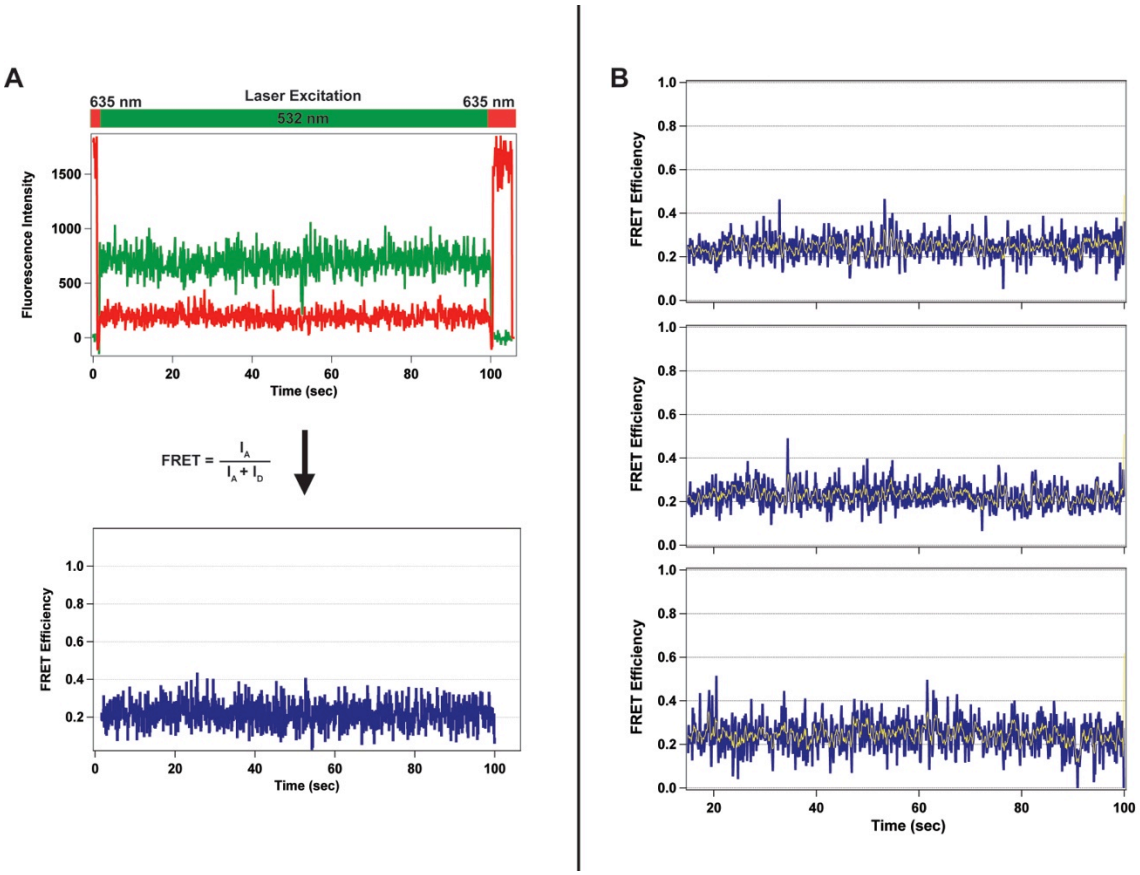


**Figure 5.1 - Example of single-molecule fluorescent intensities and FRET efficiencies.**

A) Fluorescent intensities for single molecule observation of an acceptor molecule (shown in red) and a donor molecule (shown in green). The laser excitation scheme for smFRET experiments is shown above the fluorescent emission trace. An example smFRET trace of a DNA molecule in the absence of protein is shown (in blue) and is calculated as $I_A/I_A+I_D$ as a function of time. B) Additional examples of smFRET traces in the absence of protein are shown (in blue) with a five point box smooth overlaid (yellow line)

distributions of the FRET values in the absence of nucleotide (Figure 5.3A) show a single population centered on a FRET value of 0.35. This value is clearly shifted away from the free DNA FRET value (shown in black cityscape in each histogram of Figure 5.3A) indicating that the protein is bound at the mismatch and is actively bending the DNA in the absence of nucleotide. This result is consistent with the high mismatch binding affinity WT has for a GT mismatch ($K_D$ = 7.5 nM) (Table 5.2).

Upon addition of ADP, WT exhibits a similar FRET profile where 81% of molecules evaluated are categorized as constant molecules (Figure 5.2). The histogram distribution of the FRET values for a GT mismatch in the presence of WT MutSα and ADP exhibits a single population centered on 0.35 (Figure 5.4A), which is similar to WT-GT in the absence of nucleotide. The dynamic traces we observed show FRET values consistent with the bent DNA conformation observed in the constant traces (0.35) and a FRET value consistent with our free DNA distributions (FRET 0.2) (Figure 5.2). Dynamic traces may be evidence for WT binding DNA and dissociation or DNA binding, bending, and unbending. As discussed in Chapter 3, we cannot distinguish between free DNA and DNA unbending in our experiments.

Similar to WT in the presence of a GT mismatch and ATP exhibits predominantly constant FRET traces (85%) (Figure 5.2). However, the FRET distribution of these traces exhibit a single population centered on FRET 0.23 (Figure 5.5A). This result is consistent with the free DNA population centered on FRET 0.2. WT in the presence of a GT mismatch and ATP is known to adopt a sliding clamp conformation. Again dynamic traces

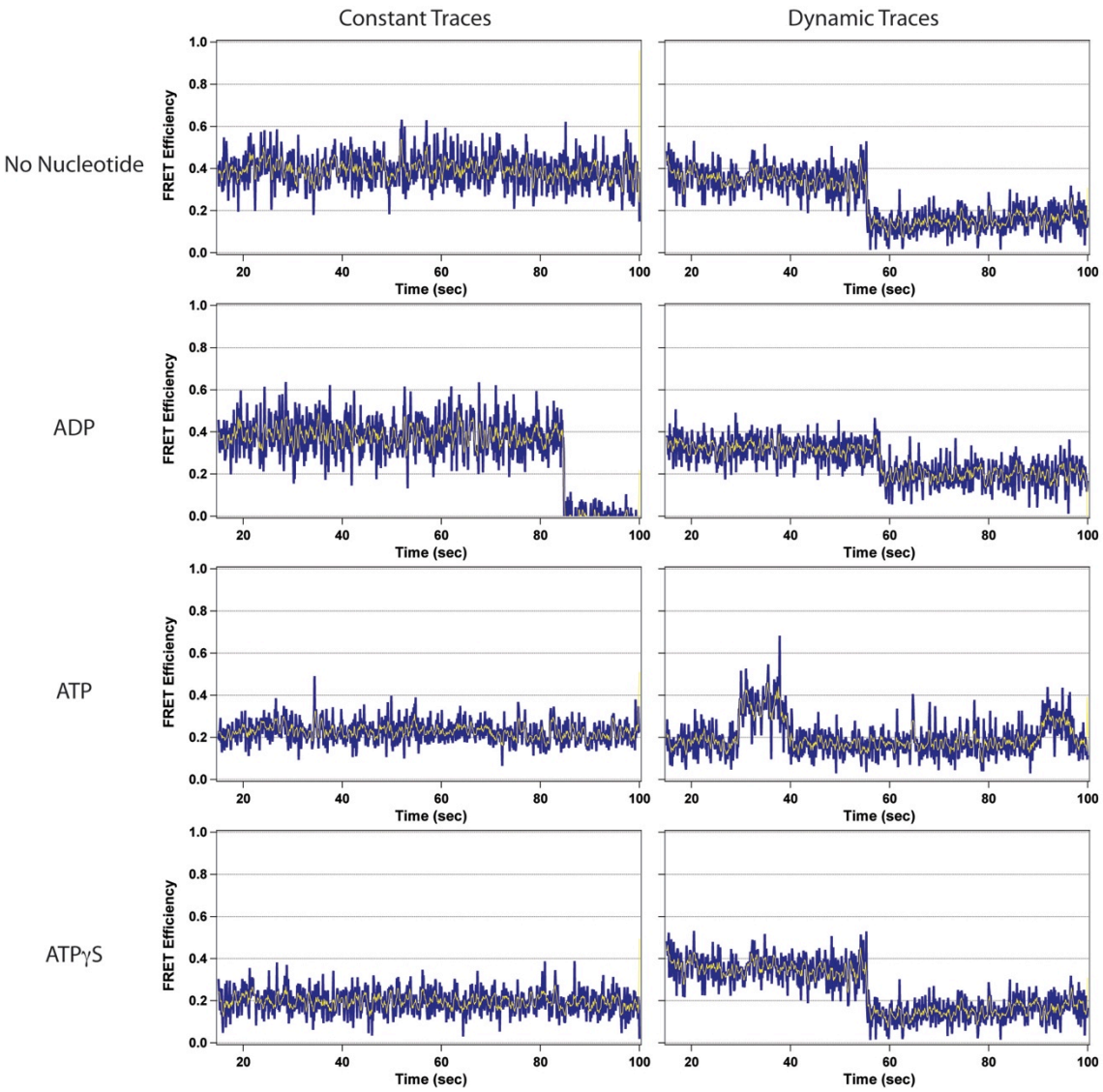


**Figure 5.2 - Example WT MutSα smFRET traces.**

FRET traces of MutSα in the presence of a 500mer bp DNA Cy3-Cy5 substrate in the absence of nucleotide and presence of ADP, ATP, or ATPγS. Raw FRET traces are shown in blue. A 5-point box smooth of the raw FRET data is shown in yellow for each trace.

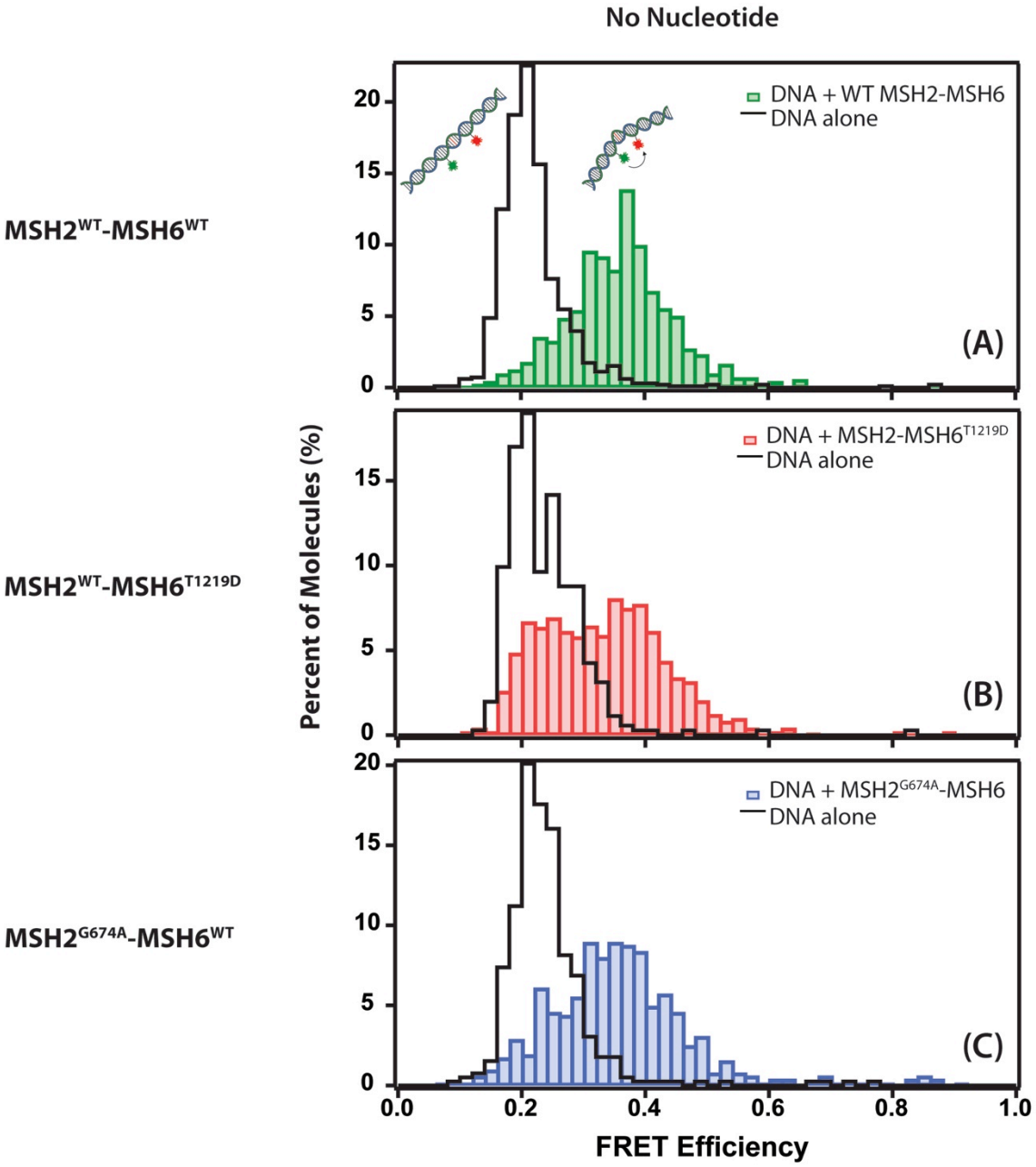


**Figure 5.3 - Histogram distributions of smFRET states for WT, T1219D, and G674A in the absence of nucleotide.**

Histogram distributions of the smFRET states (50 bins at a bin size of FRET 0.02) observed in single-molecule time-dependent traces are shown for (A) WT, (B) T1219D, and (C) G674A in the absence of nucleotide. Filled bars indicate the smFRET distribution of DNA in the presence of the appropriate protein (WT in green, T1219D in red, and

G674A in blue). The smFRET distribution of DNA in the absence of protein is shown (black cityscape) for each set of experiments. Cartoon representations for the DNA unbent and bent states are displayed above the corresponding FRET states.

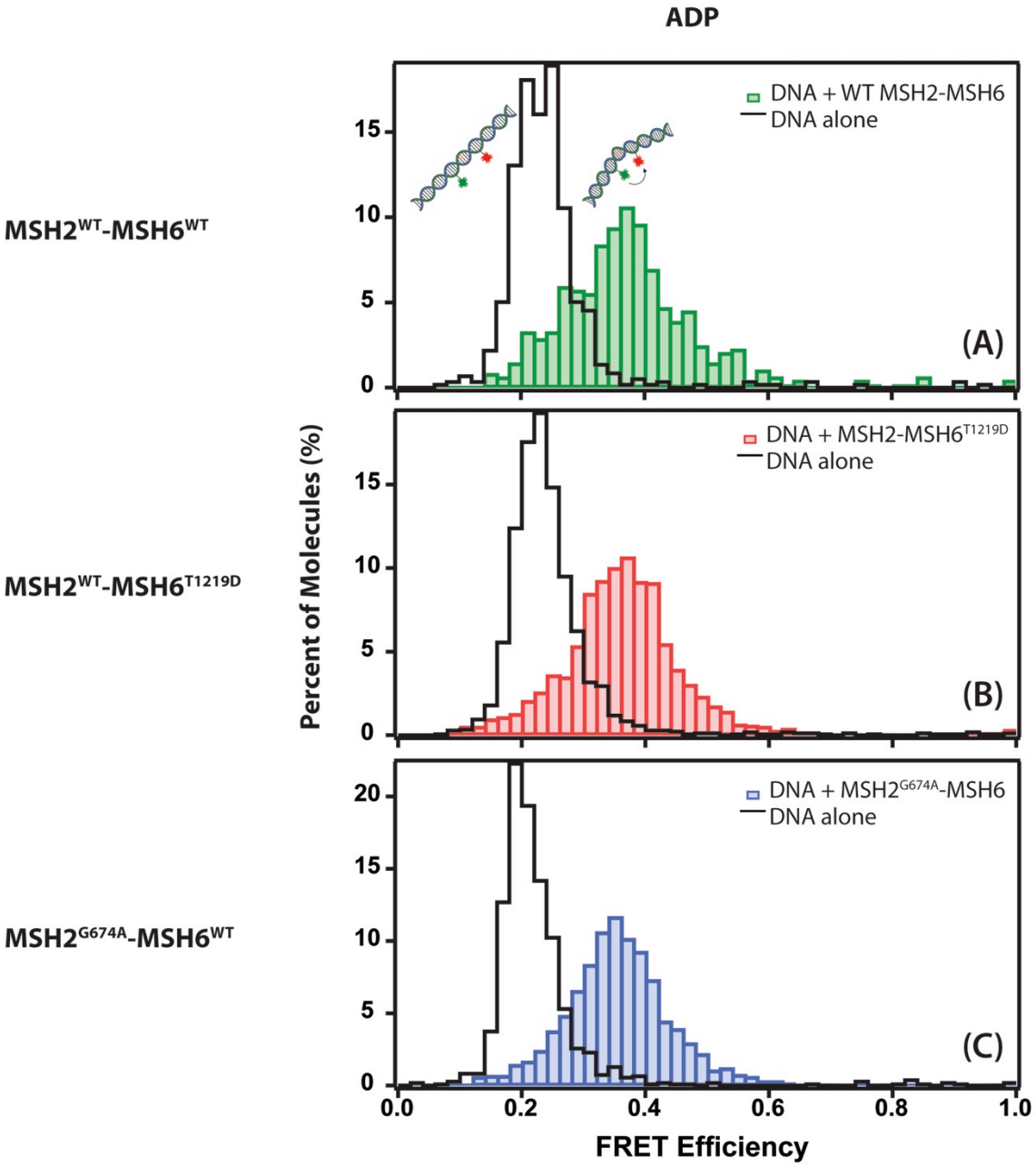


**Figure 5.4 - Histogram distributions of smFRET values for WT, T1219D, and G674A in the presence of 1 mM ADP.**

Histogram distributions of the smFRET states (50 bins at a bin size of FRET 0.02) observed in single-molecule time-dependent traces are shown for (A) WT, (B) T1219D, and (C) G674A in the presence of 1 mM ADP. Filled bars indicate the smFRET distribution of DNA in the presence of the appropriate protein (WT in green, T1219D in

red, and G674A in blue). The smFRET distribution of DNA in the absence of protein is shown (black cityscape) for each set of experiments. Cartoon representations for the DNA unbent and bent states are displayed above the corresponding FRET states.

resemble binding (FRET 0.35) and unbinding (0.2) FRET values. Because our DNA substrate is unblocked on the end, it is likely that the protein forms a sliding clamp and dissociates from the end of the DNA. We therefore measured the FRET of WT in the presence of a GT mismatch and ATPγS to prevent ATP hydrolysis and sliding clamp formation.

In the presence of ATPγS, WT again exhibits predominantly constant FRET traces (84% of measured molecules) (Figure 5.2). However, the histogram of FRET states results in a distribution that fits to two Gaussian populations. The first population centers on FRET 0.2 while the second population centers on FRET 0.32 (Figure 5.6A) consistent with an unbound population and the bound and bent population as observed in the absence of nucleotide and presence of ADP. Given the weaker binding affinity of WT for a GT mismatch in the presence of ATPγS ($K_D$ = 150 nM as determined previously (Martik, Baitinger et al. 2004)), it is not surprising to observe an unbound population.

*HNPCC mutant T1219D does not dissociate from a GT mismatch.*

We set out to determine if the differences in nucleotide binding between WT and the HNPCC mutants discussed in Chapter 5 had effects on the protein-DNA conformational states observed in smFRET. We performed smFRET bending experiments on the T1219D and G674A HNPCC separation-of-function mutant proteins in the absence of nucleotide and presence of ADP, ATP and ATPγS.

In the absence of nucleotide, T1219D traces maintain a similar trend to that of WT. We observed predominantly constant FRET traces (92% of molecules measured) (Figure 5.7). A histogram of the FRET values measured result in a distribution that fits to two Gaussian populations. The first population centers on FRET of 0.21 and the second

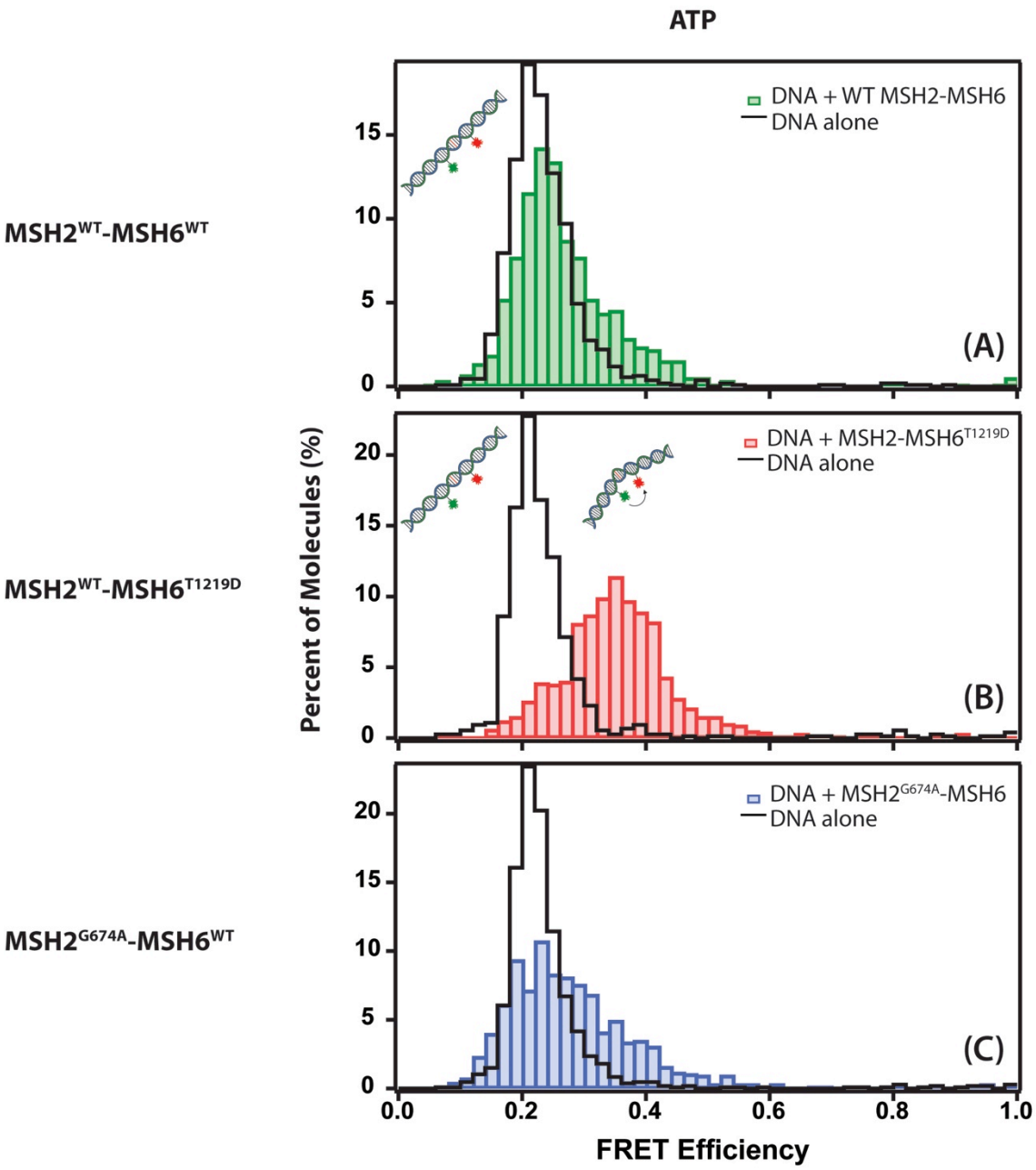


**Figure 5.5 - Histogram distributions of smFRET values for WT, T1219D, and G674A in the presence of 1 mM ATP.**

Histogram distributions of the smFRET states (50 bins at a bin size of FRET 0.02) observed in single-molecule time-dependent traces are shown for (A) WT, (B) T1219D, and (C) G674A in the presence of 1 mM ATP. Filled bars indicate the smFRET

distribution of DNA in the presence of the appropriate protein (WT in green, T1219D in red, and G674A in blue). The smFRET distribution of DNA in the absence of protein is shown (black cityscape) for each set of experiments. Cartoon representations for the DNA unbent and bent states are displayed above the corresponding FRET states.

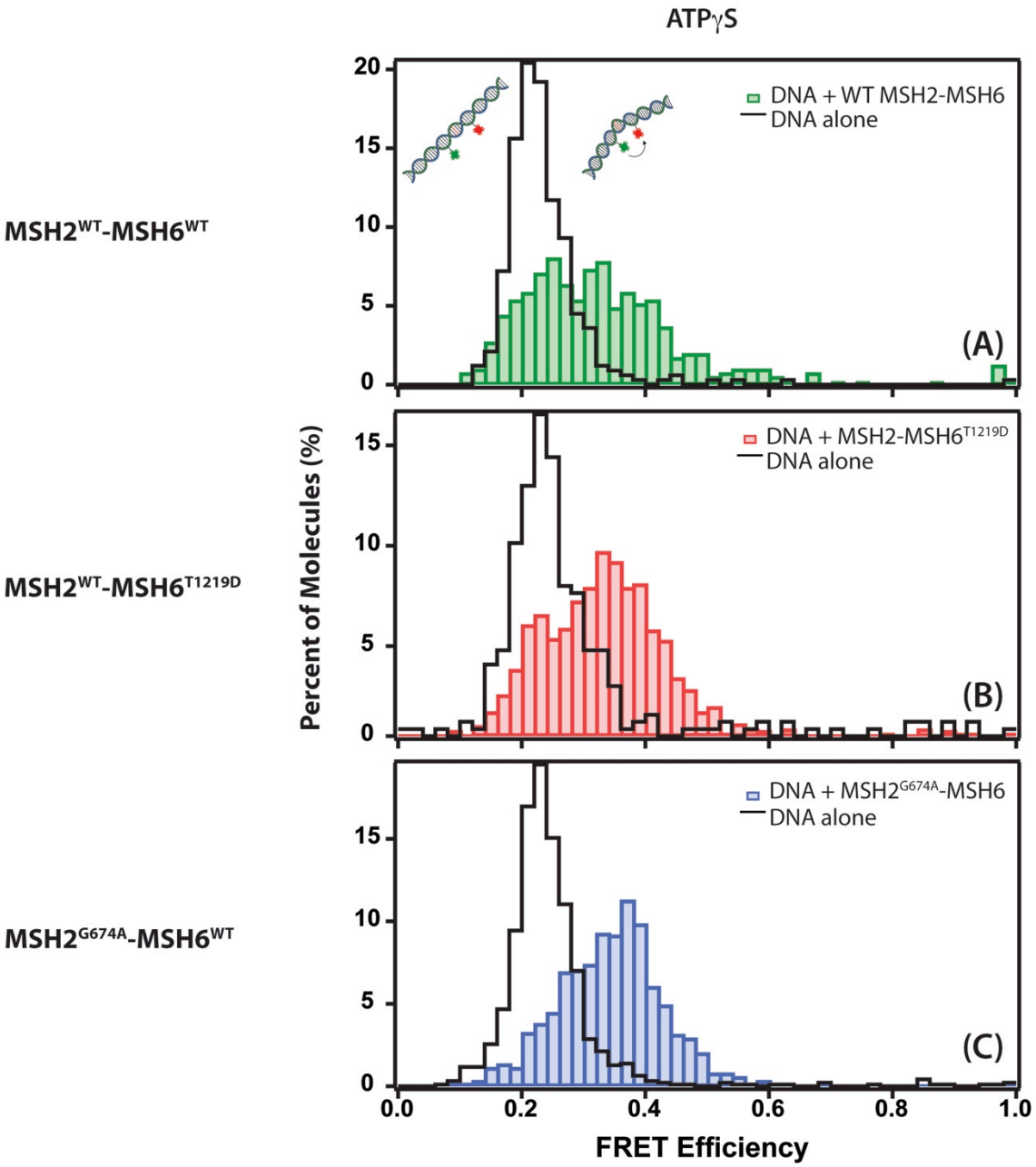


**Figure 5.6 - Histogram distributions of smFRET values for WT, T1219D, and G674A in the presence of 1 mM ATPγS.**

Histogram distributions of the smFRET states (50 bins at a bin size of FRET 0.02) observed in single-molecule time-dependent traces are shown for (A) WT, (B) T1219D, and (C) G674A in the presence of 1 mM ATPγS. Filled bars indicate the smFRET distribution of DNA in the presence of the appropriate protein (WT in green, T1219D in

red, and G674A in blue). The smFRET distribution of DNA in the absence of protein is shown (black cityscape) for each set of experiments. Cartoon representations for the DNA unbent and bent states are displayed above the corresponding FRET states.

population centers on FRET 0.35 (Figure 5.3B). This multiple population profile is similar to that observed for WT in the presence of the GT mismatch and ATPγS.

In the presence of ADP, we continued to observe predominantly constant FRET traces (93% of molecules measured) (Figure 5.7). The histogram of FRET values associated with a GT mismatch in the presence of T1219D and ADP shows a distribution of a single population centered on FRET of 0.35 (Figure 5.4B). This result is consistent with the shift in FRET states from free DNA (FRET 0.2) to a bent DNA conformation (FRET 0.35) observed for WT in the same conditions, suggesting that T1219D is bound in a similar conformation at the mismatch and actively bending the DNA.

In the presence of ATP, we again observe constant FRET traces (88% of molecules measured) (Figure 5.7). The histogram of FRET values measured shows a distribution of a single population centered on a FRET of 0.34 (Figure 5.5B). Under the same conditions, WT FRET traces exhibit distributions characteristic of sliding clamp formation and protein dissociation. In the presence of a GT mismatch and ATP, the T1219D mutant appears to remain stably bound at the mismatch with the DNA in a bent conformation despite being under conditions sufficient for sliding clamp formation for WT. This result is consistent with the high binding affinity T1219D maintains in the presence of ATP ($K_D$ = 6.3 nM) (Table 5.2) and with SPR results suggesting an inability for the T1219D mutant to form a sliding clamp (Hess, Mendillo et al. 2006; Hargreaves, Shell et al. 2010; Geng, Sakato et al. 2012). Our smFRET result demonstrates that T1219D remains stably bound to the mismatch site with the DNA conformed to a bent state in the presence of ATP.

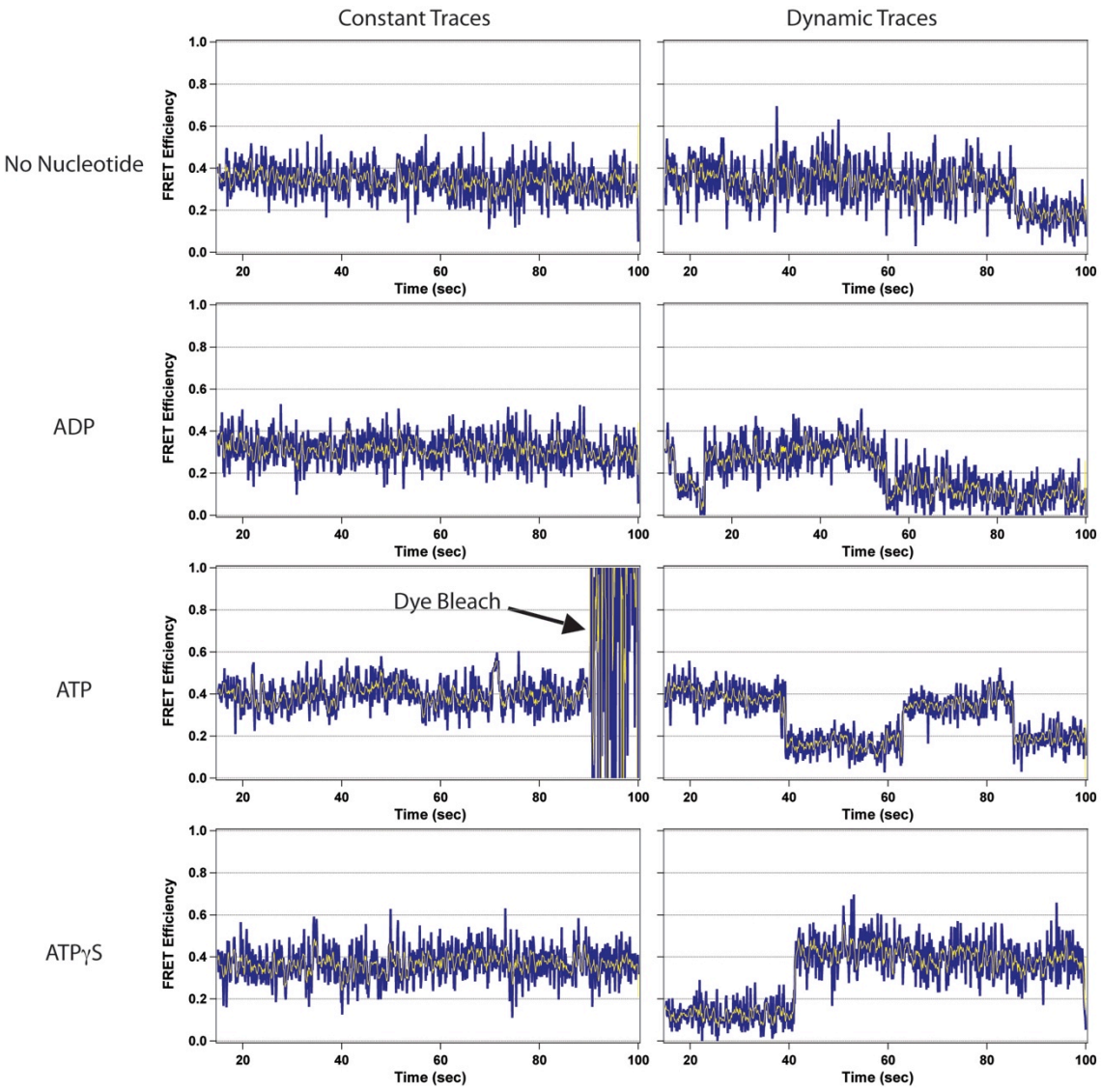


**Figure 5.7 - Example T1219D MutSα smFRET traces.**

FRET traces of T1219D MutSα in the presence of a 500mer bp DNA Cy3-Cy5 substrate in the absence of nucleotide and presence of ADP, ATP, or ATPγS. Raw FRET traces are shown in blue. A 5-point box smooth of the raw FRET data is shown in yellow for each trace. A dye bleach event is noted in the constant ATP example trace. The data from bleach events are not included in smFRET histogram distributions.

We further evaluated T1219D in the presence of a GT mismatch and ATPγS. The T1219D FRET traces were consistently constant in nature (89% of molecules measured) (Figure 5.7). The histogram of FRET values results in a distribution that fits to two Gaussian populations. The first conformational population centered on FRET 0.2 and the second population centered on FRET 0.33 (Figure 5.6B). These populations are consistent with a free DNA population and a bent DNA population. This result is also consistent with a similar distribution observed for WT in the presence on the GT mismatch and ATPγS.

Under all nucleotide conditions, the small population of dynamic traces observed for T1219D in the presence of a GT mismatch resembled those already discussed for WT under all nucleotide conditions. We consistently observed a state similar to free DNA (FRET 0.2) and a state comparable to bound and bent DNA (FRET ~0.35).

*HNPCC mutant G674A adopts a conformation similar to that of sliding clamp in WT in the presence of a GT mismatch*

In the absence of nucleotide, G674A exhibits predominantly constant FRET traces (93% of measured molecules) (Figure 5.8). A histogram of the FRET values results in a distribution of a single population centered on FRET 0.34 (Figure 5.3C). This is similar to the same FRET shift from free DNA (FRET 0.2) to bound and bent DNA (FRET 0.34) observed for both WT and T1219D in the absence of nucleotide.

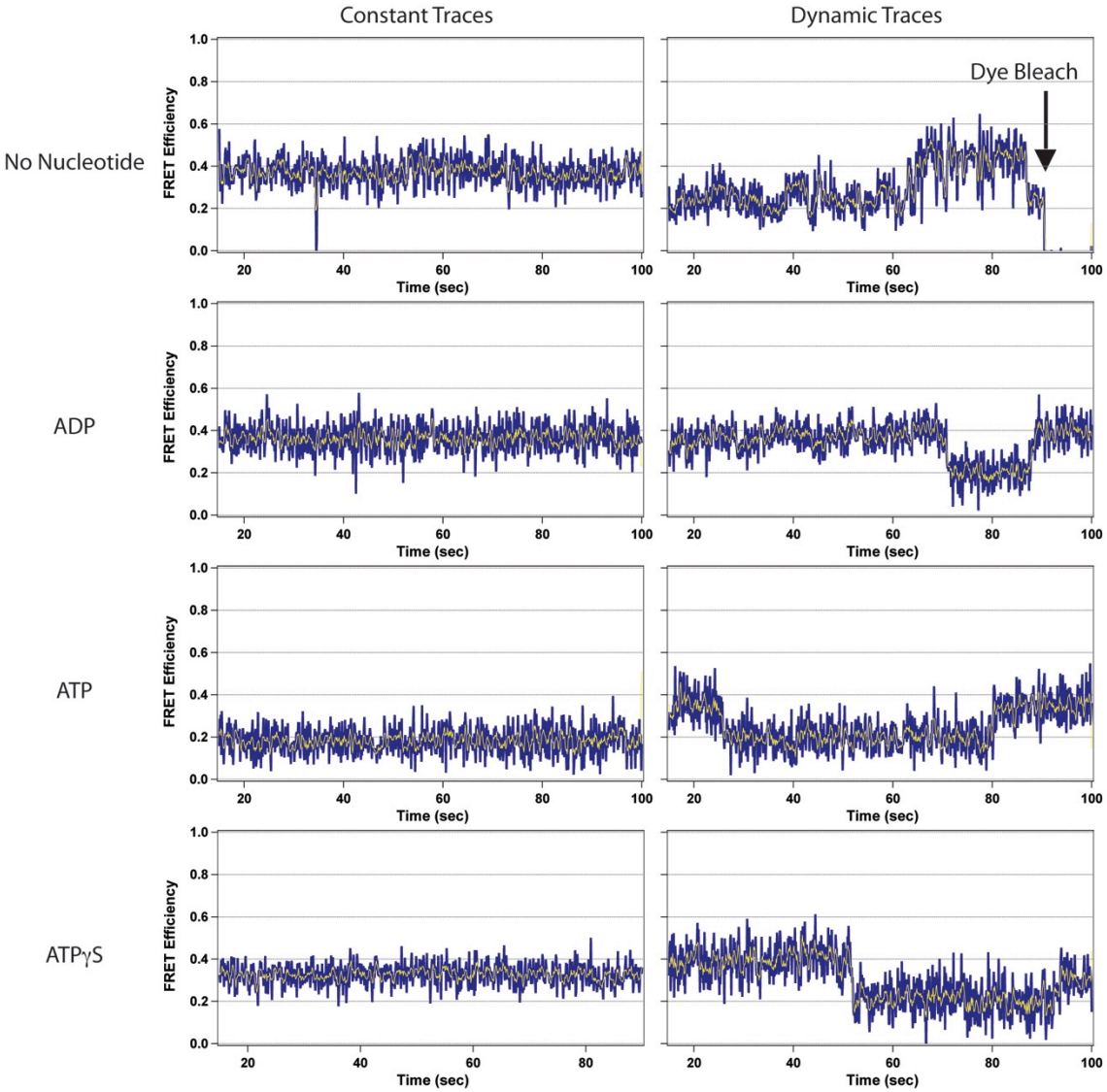


**Figure 5.8 - Example G674A MutSα smFRET traces.**

FRET traces of G674A MutSα in the presence of a 500mer bp DNA Cy3-Cy5 substrate in the absence of nucleotide and presence of ADP, ATP, or ATPγS. Raw FRET traces are shown in blue. A 5-point box smooth of the raw FRET data is shown in yellow for each trace. A dye bleach event is noted in the dynamic example trace for G674A in the absence of nucleotide. The data from bleach events are not included in smFRET histogram distributions.

FRET traces collected for G674A in the presence of a GT mismatch and ADP were predominantly constant (91% of measured molecules) (Figure 5.8). The histogram of FRET values results in a distribution of a single population centered on FRET 0.35 (Figure 5.4C). This result is consistent with a similar trend observed for both WT and T1219D in the presence of the GT mismatch and ADP. G674A therefore binds to the mismatch and actively bends the DNA as seen with both WT and T1219D.

Remarkably, G674A exhibited similar characteristics to WT in the presence of GT mismatch DNA and ATP. FRET traces were typically constant (86% of molecules measured) (Figure 5.8). The histogram of FRET values shows a distribution that fits to two Gaussian populations. The first population centers on FRET 0.21 and the second population centers on FRET 0.31 (Figure 5.5C). The larger of the two populations correlates with a free DNA population suggesting a larger proportion of G674A protein which is able to either adopt a specific conformation and slide off the end of the DNA, directly dissociate from the DNA, or alter the conformation of the protein on the DNA to an unbent conformation. Given the binding affinity of G674A for a GT mismatch in the presence of ATP (6.6 nM; Table 5.2), it is likely that the G674A mutant remains bound at the mismatch but adopts an unbent conformation because the G674A concentration is 150 nM in these experiments.

FRET traces for a GT mismatch in the presence of G674A and ATPγS are predominantly constant (85% of molecules measured) (Figure 5.8). This histogram of FRET values shows a distribution with a single population centered on FRET 0.34 (Figure 5.6C). Interestingly, this observation of a bent DNA conformational state in the

presence of a GT mismatch and ATPγS is not a two population distribution as seen for WT and T1219D under similar conditions. This may be due to the inability of G674A to bind nucleotide into the MSH2 ATPase site as demonstrated in Chapter 5.

**Discussion**

*Static DNA binding of wild type MSH2-MSH6 may be stabilized by the N-terminal region of MSH6*

In the crystal structure of WT human MSH2-MSH6, the protein is observed to bind mismatch DNA into a 45° bend angle (Warren, Pohlhaus et al. 2007). Based on our DNA substrate, we calculate a Förster distance of ~47Å for the Cy3-Cy5 dyes. The degree of DNA bending observed in our smFRET experiments results in a bent population centered on FRET 0.35. We calculate the bend angle observed in the smFRET data to be a ~46° bend. Our smFRET measurements are therefore consistent with the bend angle observed in the crystal structure.

Regardless of nucleotide condition, WT MSH2-MSH6 appears to maintain a stably bent DNA conformation when bound to a GT mismatch in conditions that prevent DNA sliding clamp conformation (no nucleotide, ADP, and ATPγS). We do not observe the DNA binding dynamics seen in similar smFRET based bending studies with WT *Taq* MutS in the absence of nucleotide (Sass, Lanyi et al. 2010). There may be several explanations for the discrepancy between the MutS proteins of the two organisms.

One possibility for the discrepancy lies in the sensitivity of the smFRET bending studies. Given the difference in the extent of bending observed in the crystal structures of *Taq* MutS and human MutSα (60° bend angle and 45° bend angle respectively) it is possible that the dye pair chosen do not have a Förster distance that allows sensitive

detection of small conformational changes in the DNA. However, our attempts to characterize this system using a dye pair (Alexa 568 as the donor and Cy5 as the acceptor) with a longer Forster distance (~63 Å) yielded similar results (data not shown). We were unable to observe dynamic conformational changes as seen with *Taq* MutS on the GT mismatch.

A second possibility for the discrepancy between *Taq* MutS and human MutSα dynamics may be evolutionary differences. The prokaryotic system may require MutS to undergo the series of conformational changes described by Sass *et al* to initiate the mismatch repair (Sass, Lanyi et al. 2010). The eukaryotic system may have evolved to eliminate the need for multiple conformational steps before signaling repair. The evolutionary variances between the prokaryotic and the eukaryotic systems have already been demonstrated in the varied mismatch repair efficiencies between organisms as well as the apparent role of the Phe-X-Glu mismatch-binding motif already discussed in Chapter 2. As previously discussed, the glutamate of the Phe-x-Glu motif appears to play different roles in *E. coli* where the alanine mutation (E38A) results in a mutator phenotype versus in *S. cerevisiae* where the alanine mutation in Msh6 (Msh2-Msh6$^{E339A}$) results in a reduction in MMR, but not completely abolishing it (Holmes, Scarpinato et al. 2007). The disparities in protein-DNA dynamics may be another result of evolutionary differences.

A third possibility may have to do with the role of the N-terminus of MSH6 in DNA binding. Approximately 300 amino acid residues at the N-terminus of MSH6 are truncated in the MutS variant that was used for the crystal structure of human MSH2-MSH6 (Warren, Pohlhaus et al. 2007). These residues share no homology with the

subunits of prokaryotic MutS. The N-terminal region (NTR) contains a proliferating cell nuclear antigen (PCNA) interaction peptide (PIP box) shown to be important in MMR (Chen, Merrill et al. 1999; Clark, Valle et al. 2000; Flores-Rozas, Clark et al. 2000; Clark, Deterding et al. 2007; Shell, Putnam et al. 2007). Previous studies suggest that the NTR of MSH6 also has the ability to independently bind DNA (Clark, Deterding et al. 2007). Evidence suggests that the NTR contributes to mismatch repair as well as DNA damage response to alkyl lesions such as $O^6$MeGT lesion. A portion of the NTR consists of a largely negatively charged region (49% of residues 192 to 230) which has been suggested to act as a DNA mimic (Clark, Deterding et al. 2007). In the context of our smFRET results, it is possible that the negative region of the NTR acts to stabilize DNA bending via charge repulsion. The regions of the NTR that bind DNA may act to stabilize the protein-DNA interactions such that the rapid conformational dynamics seen in *Taq* MutS without an NTR are prevented. Further characterization of the DNA binding properties of NTR deletion mutants using smFRET may confirm its importance in stabilizing MutSα-DNA interactions.

*G674A and T1219D are trapped in separate points in the nucleotide processing mechanism prior to sliding clamp formation.*

Conformational dynamics for both G674A and T1219D binding to a GT mismatch resemble that of WT. We consistently observe stable, non-dynamic smFRET traces regardless of the nucleotide conditions used in our experiments. We observe similar distributions of FRET states for G674A, T1219D, and WT in the absence of nucleotide and presence of ADP. Remarkably, G674A and WT exhibit similar smFRET distributions in the presence of ATP.

In the presence of ATP, WT is expected to adopt a DNA sliding clamp conformation and diffuse off of the DNA end. The smFRET distribution for G674A and WT both exhibit an overlap with the FRET values associated with unbound DNA consistent with a sliding clamp diffusing off the DNA. Given that G674A is unable to bind nucleotide stably into MSH2, it is somewhat surprising to observe a profile similar to that of WT sliding clamp in the presence of ATP. Evidence from multiple studies suggests that nucleotide binding into both subunits is required for sliding clamp formation (Acharya, Foster et al. 2003; Antony and Hingorani 2003; Antony, Khubchandani et al. 2006; Lebbink, Fish et al. 2010; Mendillo, Putnam et al. 2010; Heinen, Cyr et al. 2011; Monti, Cohen et al. 2011; Qiu, DeRocco et al. 2012). However, the smFRET distribution for G674A in the presence of ATP may be consistent with three different possibilities: 1) direct dissociation, 2) dissociation due to sliding off the end of the DNA, or 3) DNA unbending resulting in a FRET consistent with free DNA. Given the DNA binding affinity G674A has for a GT mismatch ($K_D = 6.6 \pm 4$ nM), it is unlikely that the conformational state being observed is that of unbound DNA. This observation eliminates both the direct dissociation and the sliding clamp formation scenarios. Therefore, the state being observed is likely to be G674A bound to the mismatch with the DNA in an unbent conformation. We plan further experiments to confirm this result.

Previous AFM and smFRET studies suggest a DNA binding and bending mechanism for MutS mismatch recognition and initiation of repair (Wang, Yang et al. 2003; Tessmer, Yang et al. 2008; Sass, Lanyi et al. 2010). MutS binds to the DNA and bends it as it scans for a mismatch. Upon locating a mismatch, MutS kinks the DNA and then unbends the DNA. The unbending of the DNA is the step before MMR initiation. In

this model, MutS only adopts an unbent DNA conformation in the presence of heteroduplex DNA substrates appropriate for MMR. G674A is able to adopt two of the DNA binding conformations associated with mismatch DNA recognition and MMR initiation (bent and unbent). Because G674A is deficient for nucleotide binding into MSH2, the $MSH2^{G674A}$-Empty:MSH6-ATP liganded protein is unable to further adopt the sliding clamp conformation required for downstream MMR initiation. The G674A bound-unbent DNA state has the potential to act as a replication block and thereby induce apoptosis via double strand breaks. This model would account for the separation-of-function phenotype observed with $Msh2^{G674A/G674A}$ mice and mouse embryonic fibroblasts (Lin, Wang et al. 2004).

The T1219D mutant consistently maintains a mismatch bound and bent DNA conformation regardless of nucleotide condition (no nucleotide, ADP, ATP, and ATPγS). The most striking difference between T1219D and WT is exhibited in the histogram distribution of smFRET states observed in the presence of the GT mismatch and ATP (Figure 5.5A and B). Unlike the WT and G674A proteins, the T1219D smFRET distribution in the presence of ATP remains centered on a FRET 0.34 (Figure 5.5B). The T1219D mutant, therefore, appears to remain stably bound at the mismatch with the DNA conformed to a bent state regardless of conditions suitable for sliding clamp formation. These smFRET results are consistent with anisotropy binding affinities determined for T1219D in the presence of a GT mismatch and ATP ($K_D = 6.3 \pm 3$ nM). Together, these results are consistent with biochemical data indicating that the T1219D (Geng, Sakato et al. 2012) and the analogous *S. cerevisiae* mutant (yMsh2-$Msh6^{G1067D}$) (Hess, Mendillo et al. 2006) are unable to form sliding clamp and dissociate from DNA.

Given the nucleotide binding data discussed in Chapter 4, T1219D is likely that it is bound in a MSH2-ADP:MSH6$^{T1219D}$-ATP liganded state for the smFRET traces in the presence of ATP. A similar MSH2-ADP:MSH6-ATP liganded state has previously been proposed as a "dead end" complex for WT human MSH2-MSH6 (Heinen, Cyr et al. 2011). The T1219D mutant may be a suitable mimic of the proposed dead end complex. The high binding affinity for ADP in MSH2 of T1219D may prevent ADP to ATP exchange resulting in a trapped T1219D-mismatch DNA complex.

Both G674A and T1219D appear to form trapped complexes at a mismatch. We have previously proposed a model for MutS(α) nucleotide processing as it relates to the steps in MMR initiation (searching, recognition of a mismatch, and downstream MMR initiation). Figure 5.9 (adapted from (Qiu, DeRocco et al. 2012) displays a variation on the proposed model including the positions of the G674A and T1219D trapped states. The formation of either the T1219D or the G674A trapped conformation results in a protein-DNA complex unable to proceed to the last step of MutS(α) ATP processing: the sliding clamp formation. Interestingly, the conformations of each trapped complex differ while the observed phenotypes for each mutant are similar. Both G674A and T1219D separation-of-function mutants exhibit phenotypes where MMR is defective but MutSα dependent apoptotic response is maintained (Lin, Wang et al. 2004; Yang, Scherer et al. 2004). The trapped protein-complexes are likely to remain bound at the mismatch forming a block to MMR and additional replicative and repair processes. Such a block would result in double stranded break, which would in turn signal for apoptotic response. Hence, the two separation-of-function mutants would be defective for MMR, but able to induce apoptosis.

## Conclusions

Overall, the smFRET data presented here indicate clear differences between the protein-DNA interaction dynamics of the prokaryotic homodimer, MutS, and the eukaryotic heterodimer, MSH2-MSH6. Previous *Taq* MutS smFRET studies suggest a complex, rapidly fluctuating, dynamic protein-DNA interactions. However, smFRET traces for hMutSα in the presence of a GT mismatch display few transitions between FRET states indicating a stable protein-DNA complex. Given the striking similarities between the proteins seen in the crystal structures, these differences in protein-DNA dynamics are unexpected. However, the two proteins appear similar in the absence of the NTR of MSH6 in the hMSH2-MSH6 crystal structure. We propose the stable hMutSα-DNA interactions observed in smFRET traces to be a function of the NTR of MSH6. Future smFRET characterization of the protein-DNA interactions for the crystallized hMutSα protein (truncation of 300 residues of the MSH6 NTR) will test this hypothesis.

The nucleotide binding data presented in Chapter 4 in conjunction with smFRET data suggests separate mechanisms of MutSα induced apoptosis for the two HNPCC separation-of-function mutants, G674A and T1219D. Nucleotide binding studies suggest difference ligand states to be likely for the G674A and the T1219D mutants. Both G674A and T1219D appear to form trapped complexes. However, smFRET data suggests G674A binds a mismatch and forms an unbent protein-DNA complex in the presence of ATP. Given the nucleotide binding data, this complex is likely to be in a $MSH2^{G674A}$-empty:MSH6-ATP ligand state. smFRET data suggests T1219D binds a mismatch and maintains a stably bent protein-DNA complex in the presence of ATP. Given the nucleotide binding data, this complex is likely to be in a MSH2-ADP:$MSH6^{T1219D}$-ATP

ligand state. The two mutants, therefore, become trapped at separate steps in the MutSα nucleotide processing mechanism (Figure 5.9). Both trapped protein-complexes are likely to remain bound at the mismatch forming a block to MMR and additional replicative and repair processes resulting in apoptotic response. In this way the two separation-of-function mutants are defective for MMR, but able to induce apoptosis.

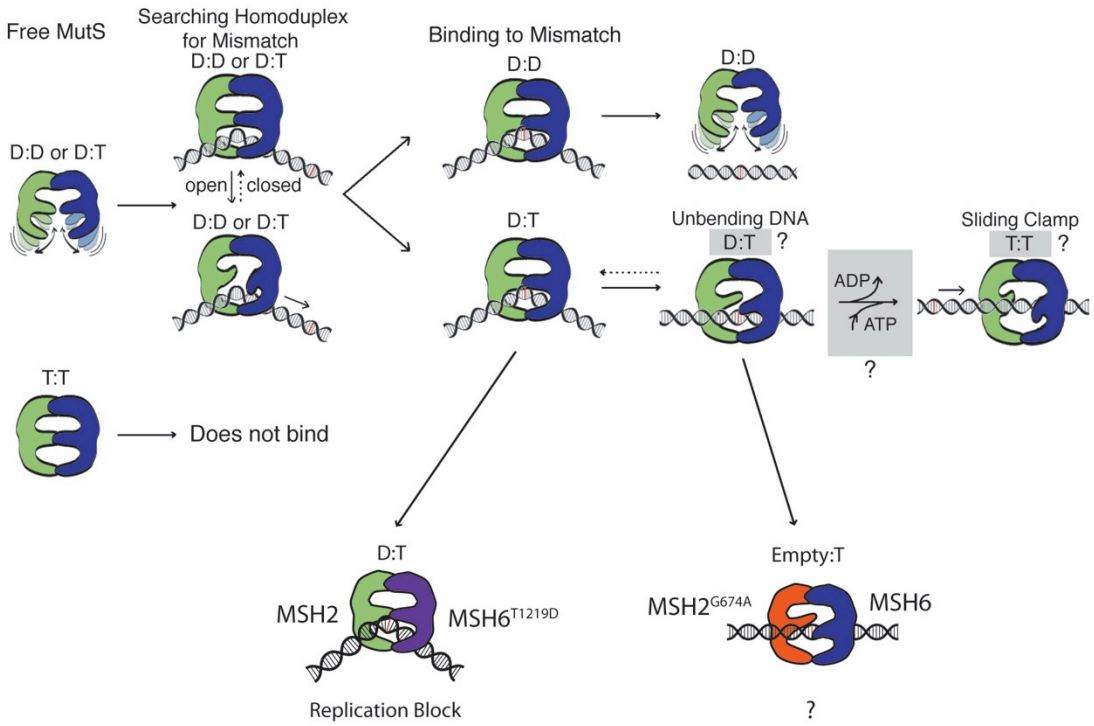


**Figure 5.9 – MutS(α) MMR initiation model with trapped G674A and T1219D states (Adapted from (Qiu, DeRocco et al. 2012)).**

Schematic representation indicates states addressing each step in MutS(α) nucleotide processing as they relate to the MMR activities of MutS(α) including scanning homoduplex DNA, recognizing mismatches, and adopting the mismatch activated sliding clamp. The proposed steps where G674A and T1219D mutant protein become trapped are displayed (T1219D in green and violet, G674A in orange and blue) with their respective liganded stated noted.

# APPENDIX A

## SINGLE-MOLECULE FRET DATA ANALYSIS PROTOCOL

We typically generate large quantities of smFRET data in any given data set. The key to efficiency with the data is organization. It's better to organize your data when you have relatively few data files to deal with. Each step of the analysis will amplify the number of data files exponentially.

The first thing to do is to keep your movie files (.pma files) and later .traces files in separate folders based on: 1. Date of experiment, 2. Lane, and 3. Experimental conditions (DNA vs. DNA + Protein…or whatever the case may be for your experiments).

### Part 1 – Conversion of .pma files to .traces files

In this part of the analysis, we are taking the movie files collected on the EMCCD camera, mapping the acceptor and donor molecules, and saving only the time traces associated with the molecules of interest. The .traces files are much smaller and more portable than .pma because you are eliminating of all of the background/surface information contained in the pixels between the molecules of interest in your .pma files.

1.) Open MatLab

2.) Call mapping program: complexingui2

   a. PMA viewer will open as a separate window. (As seen below)

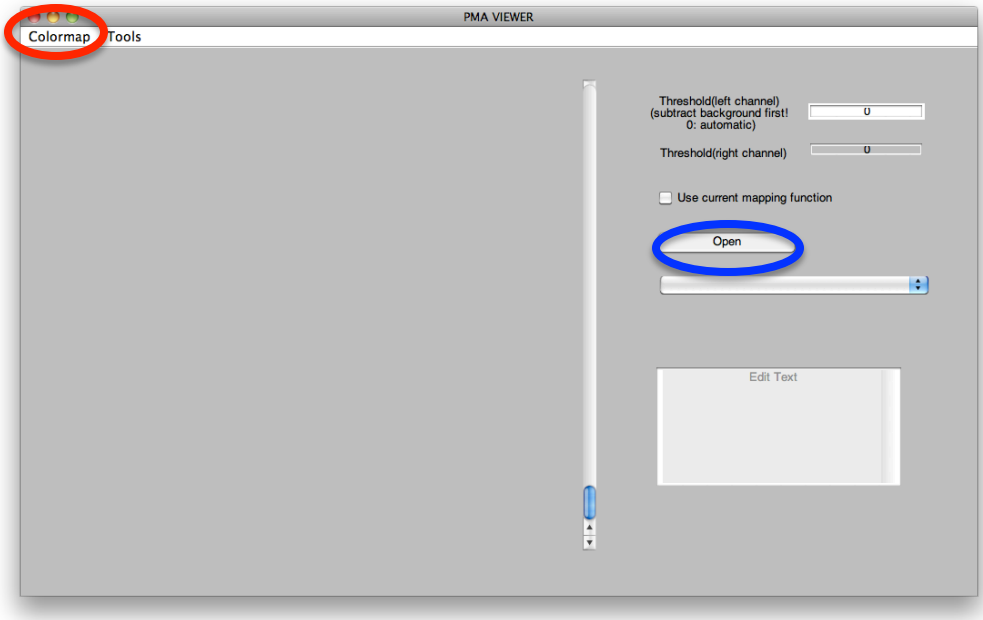


3.) Click the "OPEN" button (circled in blue)

a. Select a mapping bead movie collected on the day of data collection

i. VERY important to have collected bead movies on the day of data collection for accurate data analysis

1. Different users touch/use different optics

a. This will affect day-to-day pixel mapping

ii. You want to have the most accurate map for the data you collected

b. After selecting bead movie, click "open"

i. An image of your beads will show up in the PMA viewer

ii. You can adjust the brightness of the image with the slider on the right side of the image.

iii. You can also choose different color maps using the Colormap option on the top menu (circled in red).

1. I personally like the contrast between molecule and background that I get using the "Jet" colormap adjusted until the molecules are red and background is yellow.

4.) Click drop down menu on the right (shown below)

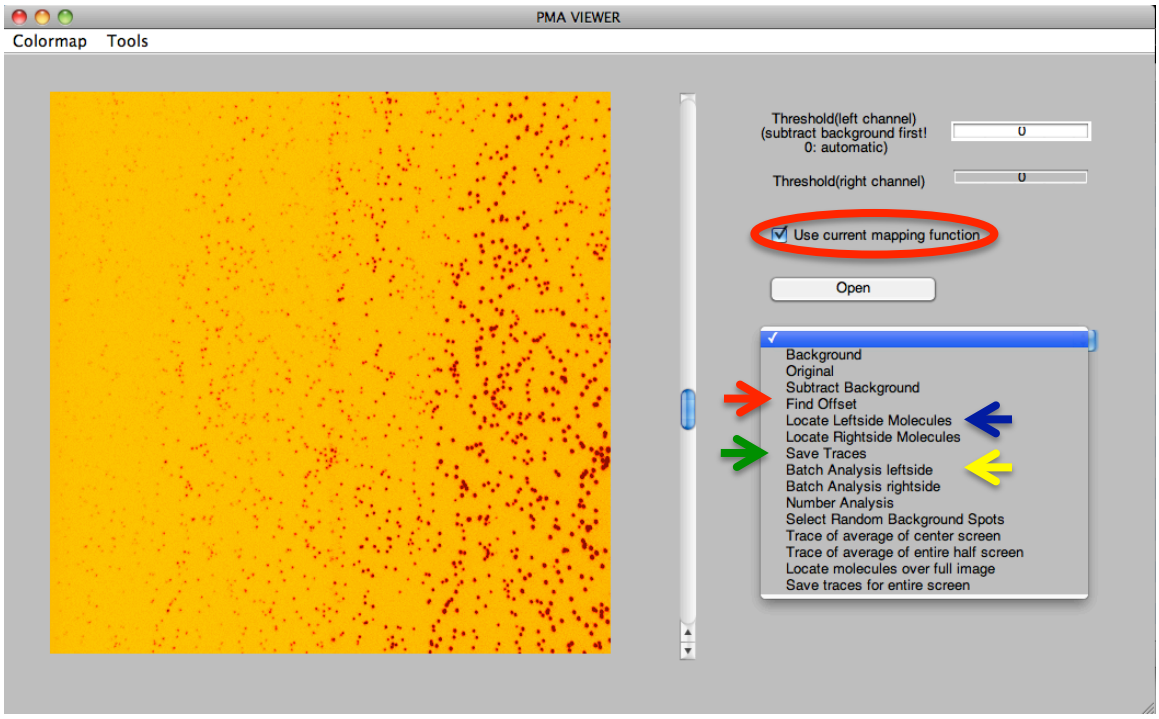


a. Select "Find Offset" (noted by red arrow)

   i. An (x,y) pixel offset will a appear in the command menu

      1. I usually check all my beads to make see if I'm getting a consistent x,y pixel offset.

b. Select "locate left side molecules" (noted by blue arrow)

   i. The program will encircle each molecule on the left-hand side of the movie (red/acceptor channel) in yellow and the corresponding molecules on the right-hand side (green/donor channel) in white

1. Note that the molecule on the outer area of the field of view are not included in this function
    a. This is to avoid partial molecules being included in the data analysis
2. Clumps of molecules (within 5 pixels of one another) are also left out of this calculation.
    a. To limit number of multiple molecules in the data analysis.

ii. Confirm that each molecule is located in the center or at least very close to the center of each circle
1. Verify across entire field of view.

c. If you are satisfied with the map, continue to Step 5
d. If you are not satisfied with the map REPEAT STEPS 3 and 4 with a new bead movie.

5.) Check the "Use current mapping function" box. (circled in red)

6.) Click "Open" button again

a. Open another bead movie
    i. We're checking the mapping offset that the program is holding
b. On drop-down menu
    i. Select "Locate left-side" molecules
        1. DO NOT select "Find Offset" button again
            a. You will have to start over again if you do this.
    ii. Verify that map is good on second movie.

1. Move on to Step 7.

7.) If saving only a single movie

   a. On drop-down menu select "Save Traces" (noted by green arrow)

      i. This will only generate the .trace file for the movie you're currently mapping.

8.) If doing a large batch of movie analyses

   a. On drop-down menu select "Batch analysis left-side" (noted by yellow arrow)

      i. This will go through and perform a left-side batch analysis for each movie in the directory and the sub-directories

9.) Type ctrl-c to exit the mapping program.

   a. You're done generating your .traces files.

   b. I would suggest moving your .pma files into their own folder. You're done working with them.

**Part 2 – Conversion of .trace files to an .itx file**

Your .trace file contains the donor and acceptor intensities over time for all molecules regardless of quality. The next step is to go through your molecules and only save those of good quality. Parts of this program have been altered by Cherie Lanyi to allow us to organize the molecules you save *while* you're weeding out the bad traces rather than having to do the weeding and organizing as two separate steps. This is a priceless improvement!

1.) Create four new folders named as follows for each of your experimental conditions:
    a. Constant
    b. Switching
    c. Other
    d. Junk
2.) In Matlab
    a. Call the program: new_keith_folder_view_tir
        i. It would be a good idea to check your gamma values and leakage values used in the script of this program.
            1. Make sure these values are appropriate for the dyes that you are using in your experiments.
    b. A browser window will pop up (see below)
        i. Select a .trace file

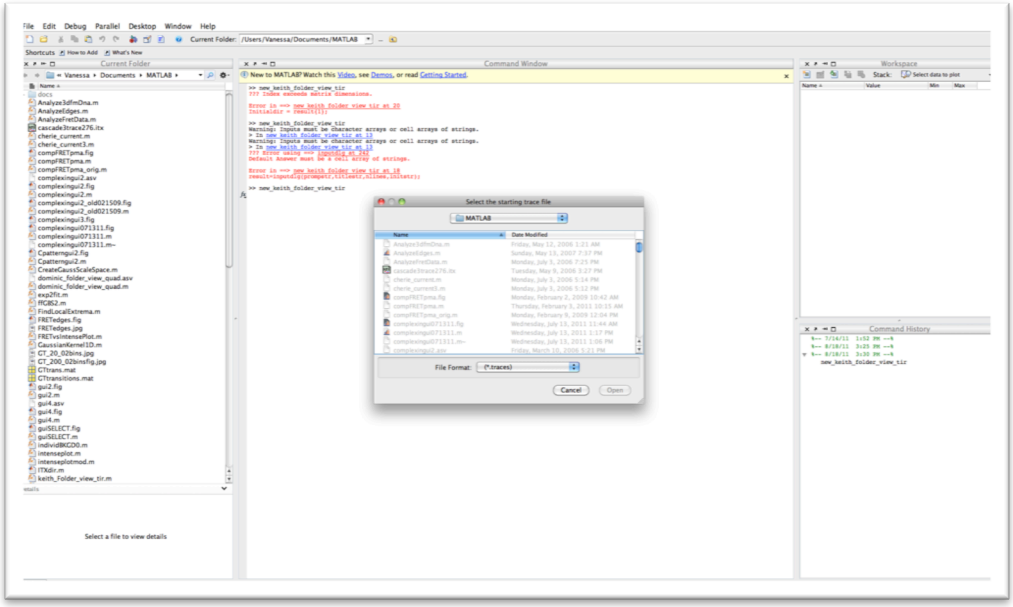

c. A GUI will pop up (as shown below):

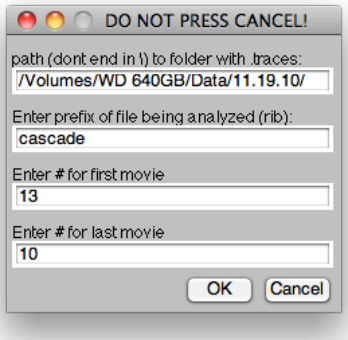


d. The directory information should reflect the directory of the .traces file you have chosen

e. Leave the prefix of file as “cascade” unless you have changed the naming of your .traces file to something besides cascade#.trace

f. Enter the number for the first movie you will be analyzing…that would the # in Cascade#.trace

g. Enter the number for the last movie in the folder

i. Make sure that this is a number larger than that of the movie you're starting on…even if you have no higher number in your folder. The program will error otherwise.

h. Click OK

i. The following will appear in your command window and a Figure will pop up (shown next page).

i. The command window will show

1. The directory
2. A counter
    a. Keeps track of how many molecules you've gone through (this can be deceiving because if you go backwards and then forwards through the molecules…you'll be counting twice.)
3. Working on – whichever trace file you've opened.
4. The length of the trace file – in frames
5. Ntraces – number of total traces (acceptor and donor)
6. Number of molecules – total number of molecules in the trace file.
7. Leakage – this is the leakage value set in the program…make sure this corresponds with your dye pair.

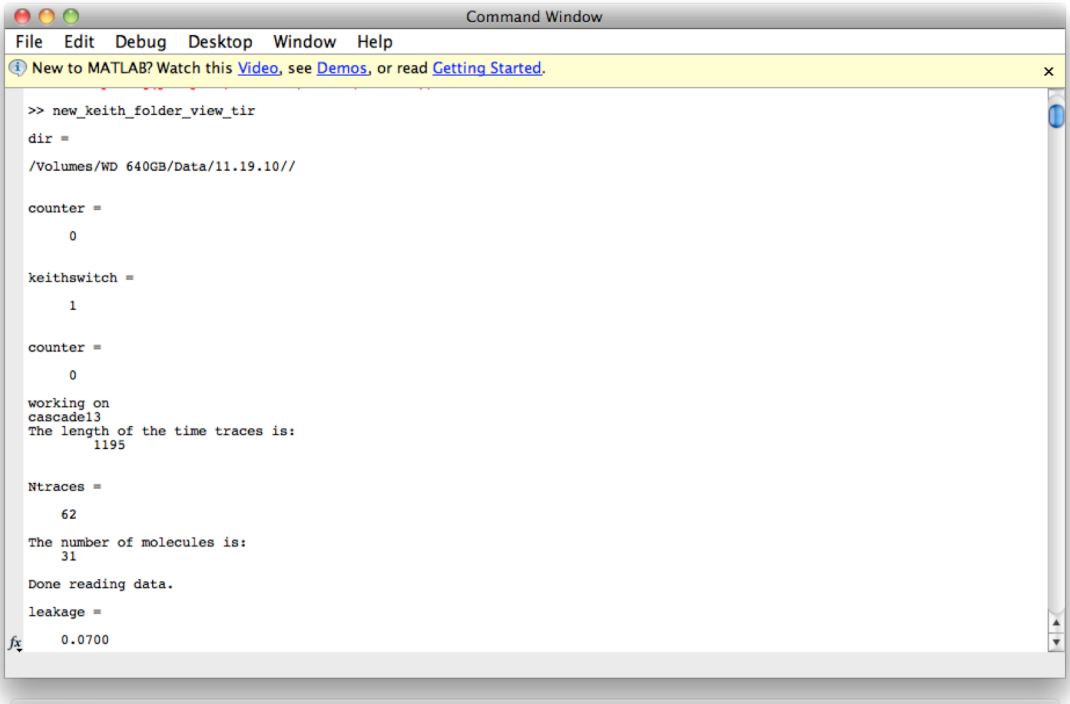


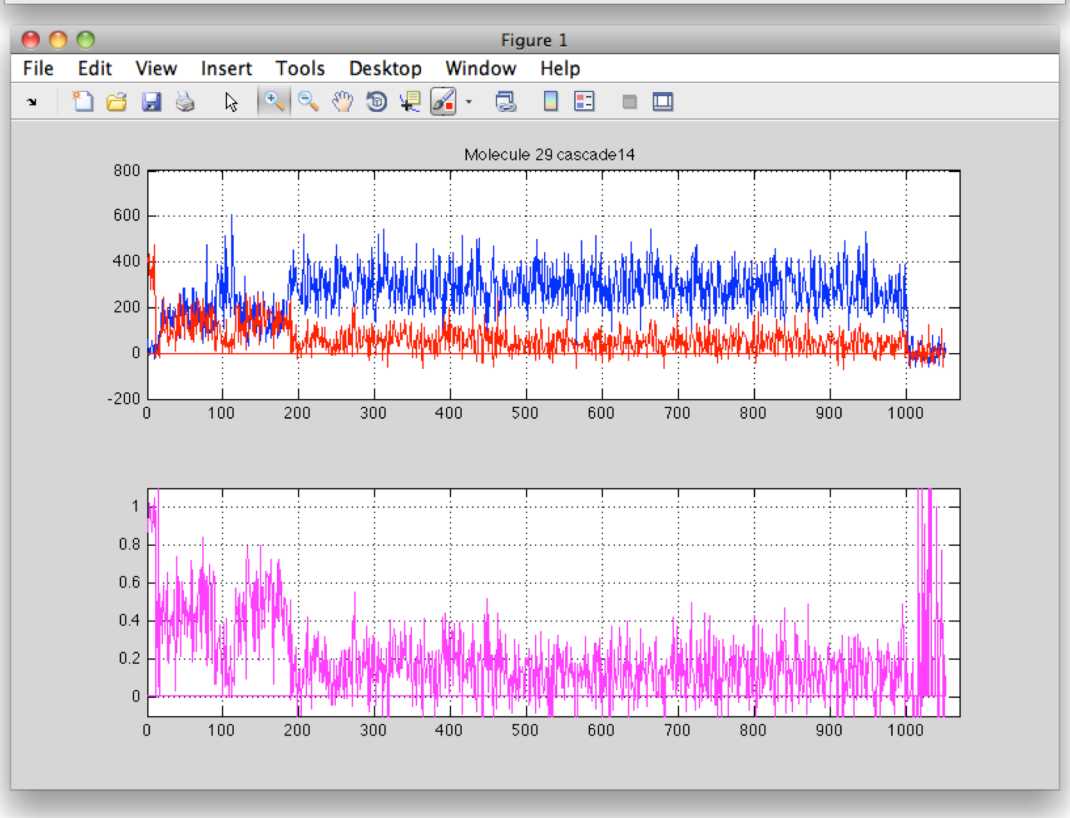


j. Now you will save and sort through your molecules

i. Press “s” and enter to save a molecule you deem good quality

1. The program will prompt you asking where you want to save the molecule.
    a. Press “c” and enter if the molecule is constant
    b. Press “s” and enter if the molecule is switching
    c. Press “o” and enter if you are unsure how you want to classify the molecule but think it is interesting. (other)
    d. Press “j” and enter if you didn’t mean to save. (junk)
2. This function will place your .itx files directly into the folder within the directory that you’ve selected.

ii. Press enter to pass on a molecule and go onto the next one.

iii. Press “b” if you need to go back to the previous molecule.
    1. Depending on which version you are using…the back command will either go back one molecule or two molecules. Just be aware.

3.) Go through each molecule for all of the .trace files in your folder in this way.

4.) Exit MatLab when done.

***Tips on saving molecules:***

1.) Determine a cutoff for high intensities. Each day of experiments will be different, but by going through your molecules you get a feel for what intensities are reasonably single molecules and what intensities constitute multiples. Typically

you'll see anywhere from 500 to 1500 as a single molecule. The variation depends on the laser intensity and TIRF spot density on the day of experimentation.

2.) Determine a cutoff for low intensities. This will be based on the noise in the data. I will typically not use molecules whose excited intensities are below 200. Use your best judgment.

3.) Switching molecules are only those molecules that undergo ANTI-CORRELATED changes in their signals. This is a REQUIREMENT for your molecules. If the green signal increases, a corresponding decrease in the red signal must be observed and vice versa. If you are not seeing anti-correlated changes then something is very wrong with that molecule or you are observing an artifact like a lint particle. Don't save that molecule.

4.) Dye blinks and photobleaches are NOT switches. You will typically see blinks and bleaches in the red channel the most. IF the red molecule goes to zero and then recovers, that is more than likely a blink. Keep in mind that blinks will also have an anti-correlated change in the donor channel. If the molecule goes to zero and does not recover, you have observed a bleach.

5.) Don't bother saving molecules that bleach in less than 100 frames. The amount of useful data there is not worth it. You're bound to have better molecules.

6.) If the Donor is excited when only the red laser is on (the beginning and the end of the trace) the molecule is probably just a fluorescent contaminant. Don't save.

7.) If you observe what appear to be switches buried in the noise of the data, be careful. I would personally find it more worthwhile to repeat the experiment at a

faster collection rate to temporally resolve those events rather than clump questionable noisy data in with good data.

8.) The program is NOT built so that you can leave off on a molecule, close out of the program, and pick up where you left off. Make sure that you note which molecule you leave off on if you have to stop analysis before the last molecule in the .trace file. Then you can open the .trace file and skip through to where you left off.

**Part 3 – Analyzing the .itx files**

Now your data is in its most useful format. The .itx files can be used for both the constant and the switching analyses.

1.) Constant Molecule analysis

   a. Open Igor Pro

      i. Open the .itx files you are in interested in analyzing

         1. Opening more than 150-200 files at once is not advisable…unless Igor improves significantly from the time this protocol was written.

         2. Your computer will start to lag with large numbers of files.

      ii. Click "Windows" on your top menu. (circled in red)

      iii. Scroll down to "Panel Macros" (circled in green)

      iv. Select "FRETprocessPANEL" (circled in blue)

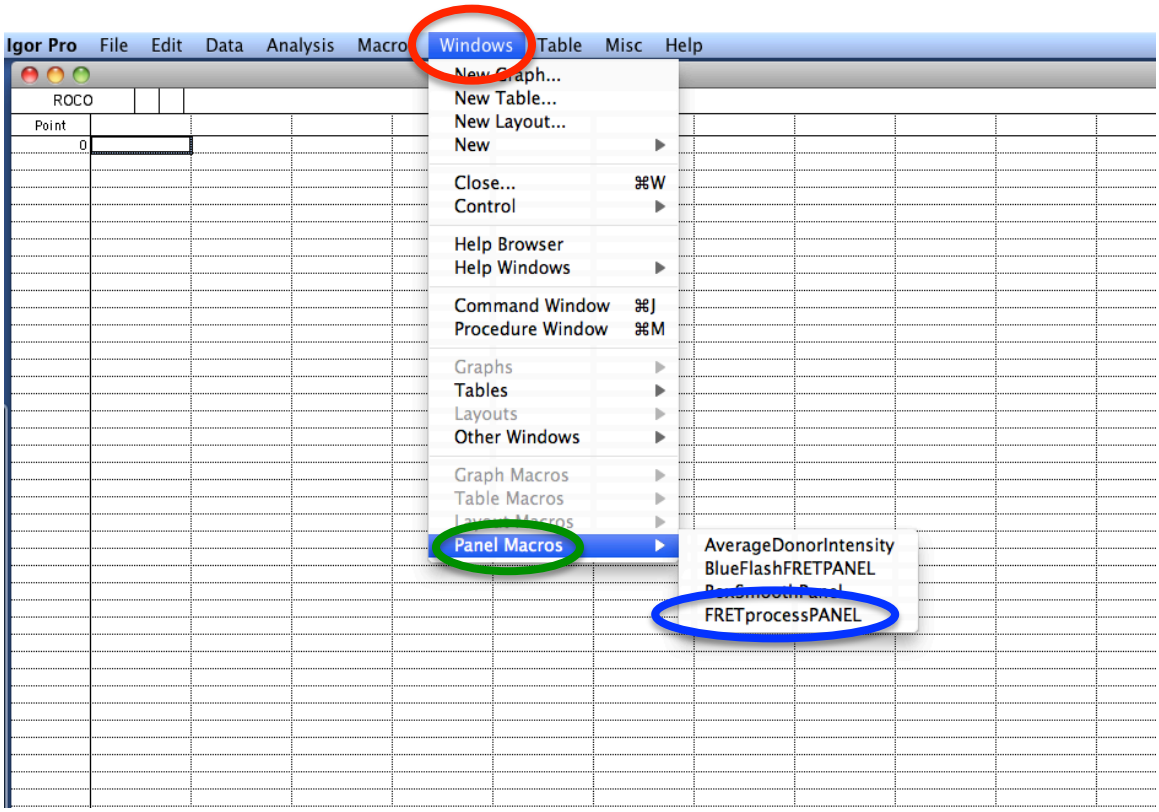


v. A Panel GUI will pop up on your screen (shown below)

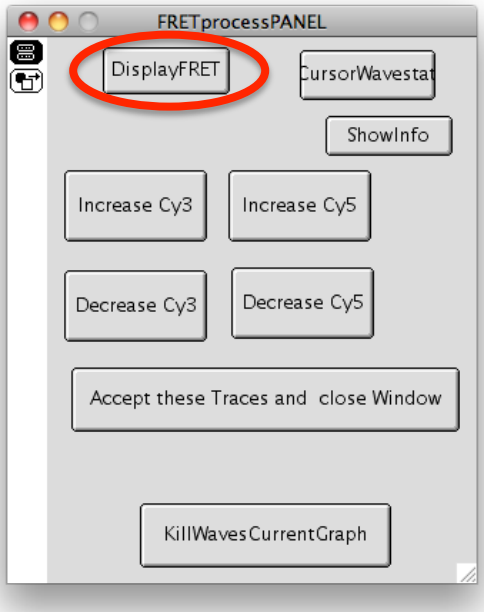

vi. Click “Display FRET” (circled in red)

    1. A program will run and do each of the following:

        a. Open each set of traces (acceptor and donor)

        b. Plot the traces in a graph

        c. Calculate the FRET efficiency for each Acceptor/Donor trace

        d. Average the first 15 or 50 frames (after the switch from red to green excitation) of the FRET trace.

        e. Generate a histogram of 50 bins with a 0.02 bin size.

vii. Assuming you have little to no background issues…the files generated by the program are suitable for further analysis.

    1. FretHist

        a. The histogram file containing the y values for each bin of your histogram

    2. 15frameAvgfret or 50frameAvgfret (depending on the number of frames you’ve decided to average)

        a. Contains the 15 or 50 frame average of each FRET trace you’ve opened.

        b. This is the most useful data file generate by the program

        c. 15Frettime

i. Used when converting frames to time in seconds. Usually commented out so the data file should be empty.

3. CorCy5 and CorCy3

a. Both are used as a temporary data files

i. The intensity values for acceptor and donor are temporarily loaded into these files for the frame averaging. They are overwritten with the intensity values of the next trace being opened.

viii. Select “Data” from the top menu (circled in red)

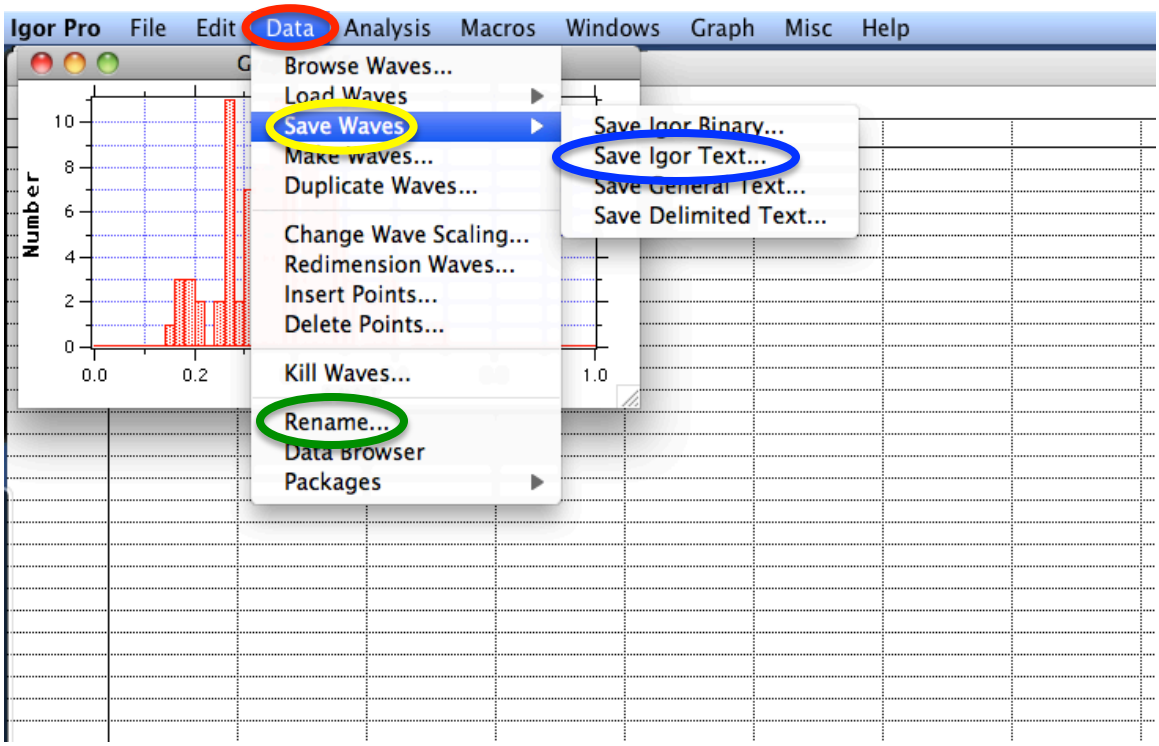


ix. Select “Rename…” (circled in green)

x. Select the 15frameAvgfret or 50frameAvgfret file

1. Rename the file
    a. I like to rename the file based on the day, lane, and movie
        i. Let's say you've opened all .itx files for Cascade1, which was in Lane 1 of your experiments on 08/10/11. I would name the file "081011_L1C1".
2. Click "Do it"

xi. Select "Data" from the top menu again (circled in red)

xii. Select "Saves Waves" (circled in yellow)

xiii. Select "Save Igor Text" (circled in blue)

1. Save the renamed file.
    a. It is more useful to save the Avgfret files rather than the histogram files because you can play with bin sizes readily.
        i. You can also use this file to re-generate the histogram and plot the data with the free DNA or DNA + Protein complement.
        ii. You can combine multiple Avgfret files and then generate a histogram of a much larger data set without bogging down the computer.

xiv. Repeat these steps for all movies within an experimental condition. You will be combining the Avgfret files.

b. Combining Avgfret files

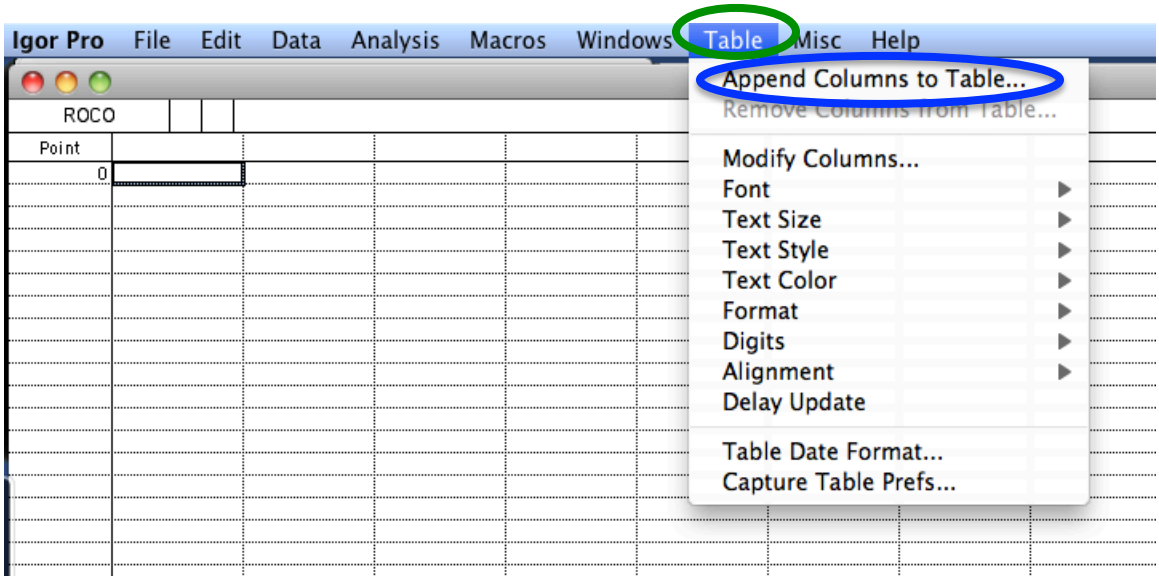


i. Open each of the saved Avgfret files that you generated according to the previous section.

ii. Select "Table" on the top menu (circled in green)

iii. Select "Append Columns to Table…" (circled in blue)

iv. Select all of your Avgfret files and select "Do it"

1. All of the files should be added to the columns of your table.

v. To combine the Avgfret files you will individually add each data set to a single column.

1. Be sure to rename that column (wave) appropriately

c. Histogram distributions (see image below)

i. Select "Analysis" (circled in red)

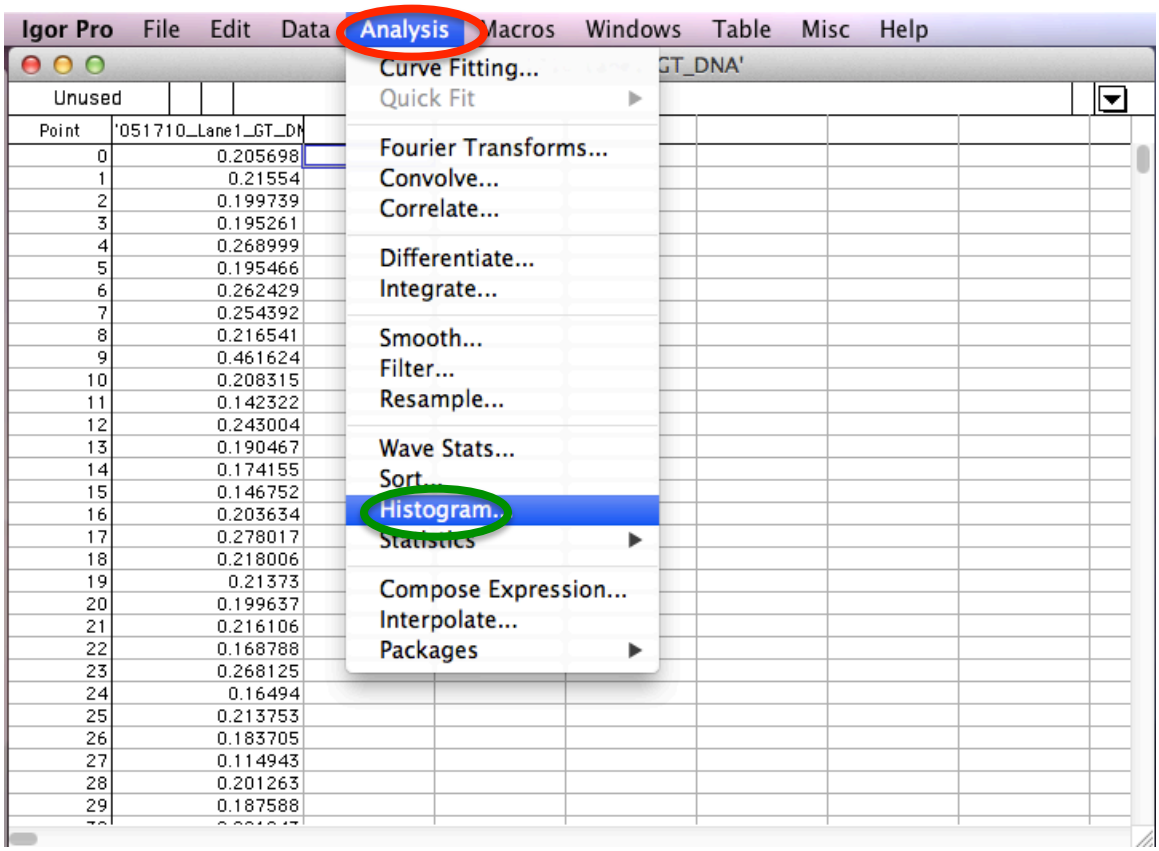


ii. Select “Histogram” (circled in green above)

iii. The histogram menu will pop up (shown below)

1. Select the source wave you wish to generate a histogram of
    a. This is the combined Avgfret wave
    b. An example wave is circled in red.
2. The default for histogram generation is manual set bins.
    a. Typically, we generate histograms of 50 bins (circled in green) with a bin size of FRET 0.02 (circled in yellow).
    b. Bin sizes and number of bins will depend on the data set you are working on.

c. Select “Display Output Wave” (circled in blue)

i. The program will automatically generate a graph with your histogram data.

d. Click “Do It”

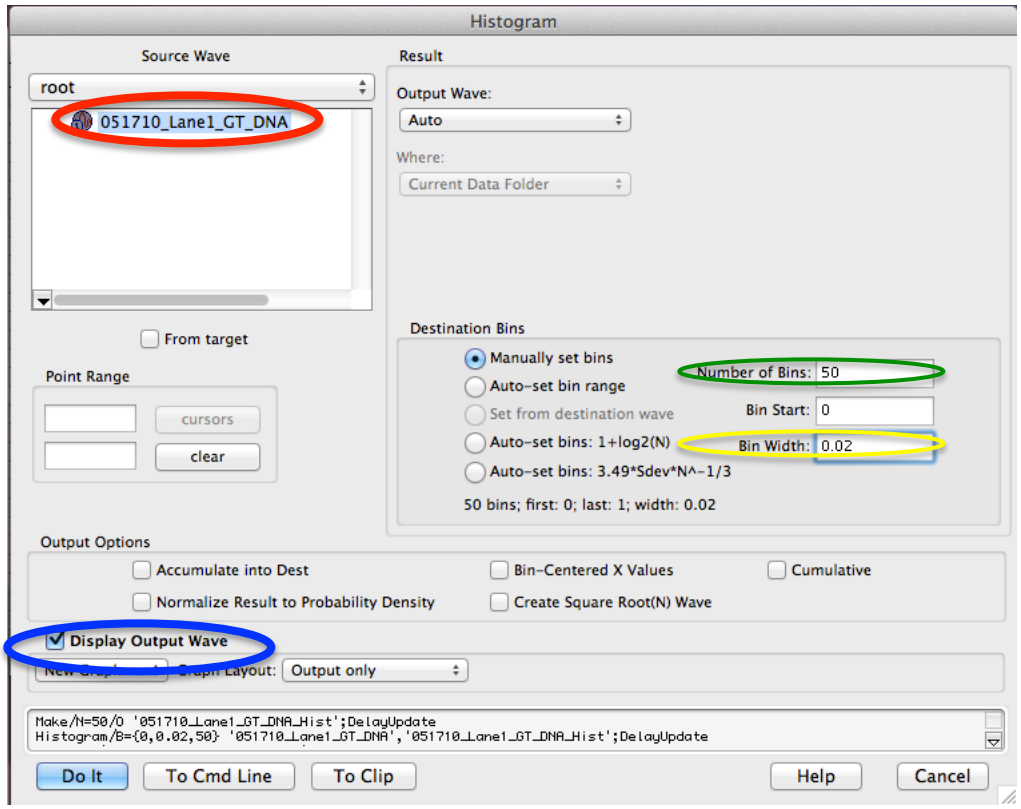


You have successfully generated a histogram of smFRET values for your experiment. Compare the histogram distribution to that of free DNA for a frame of reference.

# References


Acharya, S., P. L. Foster, et al. (2003). "The coordinated functions of the E. coli MutS and MutL proteins in mismatch repair." Mol Cell **12**(1): 233-246.

Alani, E., J. Y. Lee, et al. (2003). "Crystal structure and biochemical analysis of the MutS.ADP.beryllium fluoride complex suggests a conserved mechanism for ATP interactions in mismatch repair." J Biol Chem **278**(18): 16088-16094.

Antony, E. and M. M. Hingorani (2003). "Mismatch recognition-coupled stabilization of Msh2-Msh6 in an ATP-bound state at the initiation of DNA repair." Biochemistry **42**(25): 7682-7693.

Antony, E. and M. M. Hingorani (2004). "Asymmetric ATP binding and hydrolysis activity of the Thermus aquaticus MutS dimer is key to modulation of its interactions with mismatched DNA." Biochemistry **43**(41): 13115-13128.

Antony, E., S. Khubchandani, et al. (2006). "Contribution of Msh2 and Msh6 subunits to the asymmetric ATPase and DNA mismatch binding activities of Saccharomyces cerevisiae Msh2-Msh6 mismatch repair protein." DNA repair **5**(2): 153-162.

Bjornson, K. P. and P. L. Modrich (2003). "Differential and simultaneous adenosine di- and triphosphate binding by MutS." The Journal of biological chemistry **278**(20): 18557-18562.

Blackwell, L. J., D. Martik, et al. (1998). "Nucleotide-promoted release of hMutSalpha from heteroduplex DNA is consistent with an ATP-dependent translocation mechanism." The Journal of biological chemistry **273**(48): 32055-32062.

Chen, C., B. J. Merrill, et al. (1999). "Saccharomyces cerevisiae pol30 (proliferating cell nuclear antigen) mutations impair replication fidelity and mismatch repair." Mol Cell Biol **19**(11): 7801-7815.

Choi, U. B., P. Strop, et al. (2010). "Single-molecule FRET-derived model of the synaptotagmin 1-SNARE fusion complex." Nat Struct Mol Biol **17**(3): 318-324.

Clamme, J. P. and A. A. Deniz (2005). "Three-color single-molecule fluorescence resonance energy transfer." Chemphyschem **6**(1): 74-77.

Clark, A. B., L. Deterding, et al. (2007). "Multiple functions for the N-terminal region of Msh6." Nucleic Acids Res **35**(12): 4114-4123.

Clark, A. B., F. Valle, et al. (2000). "Functional interaction of proliferating cell nuclear antigen with MSH2-MSH6 and MSH2-MSH3 complexes." The Journal of biological chemistry **275**(47): 36498-36501.

DeRocco, V., T. Anderson, et al. (2010). "Four-color single-molecule fluorescence with noncovalent dye labeling to monitor dynamic multimolecular complexes." BioTechniques **49**(5): 807-816.

Drotschmann, K., W. Yang, et al. (2002). "Evidence for sequential action of two ATPase active sites in yeast Msh2-Msh6." DNA repair **1**(9): 743-753.

Flores-Rozas, H., D. Clark, et al. (2000). "Proliferating cell nuclear antigen and Msh2p-Msh6p interact to form an active mispair recognition complex." Nat Genet **26**(3): 375-378.

Geng, H., C. Du, et al. (2011). "In vitro studies of DNA mismatch repair proteins." Analytical biochemistry.

Geng, H., M. Sakato, et al. (2012). "Biochemical Analysis of the Human Mismatch Repair Proteins hMutS MSH2G674A-MSH6 and MSH2-MSH6T1219D." The Journal of biological chemistry **287**(13): 9777-9791.

Ha, T., A. Y. Ting, et al. (1999). "Single-molecule fluorescence spectroscopy of enzyme conformational dynamics and cleavage mechanism." Proc Natl Acad Sci U S A **96**(3): 893-898.

Hargreaves, V. V., S. S. Shell, et al. (2010). "Interaction between the Msh2 and Msh6 Nucleotide-binding Sites in the Saccharomyces cerevisiae Msh2-Msh6 Complex." Journal of Biological Chemistry **285**(12): 9301-9310.

Heinen, C. D., J. L. Cyr, et al. (2011). "Human MSH2 (hMSH2) Protein Controls ATP Processing by hMSH2-hMSH6." The Journal of biological chemistry **286**(46): 40287-40295.

Hess, M. T., M. L. Mendillo, et al. (2006). "Biochemical basis for dominant mutations in the Saccharomyces cerevisiae MSH6 gene." Proc Natl Acad Sci U S A **103**(3): 558-563.

Hohng, S., C. Joo, et al. (2004). "Single-molecule three-color FRET." Biophys J **87**(2): 1328-1337.

Holmes, S. F., K. D. Scarpinato, et al. (2007). "Specialized mismatch repair function of Glu339 in the Phe-X-Glu motif of yeast Msh6." DNA Repair (Amst) **6**(3): 293-303.

Lamers, M. H., A. Perrakis, et al. (2000). "The crystal structure of DNA mismatch repair protein MutS binding to a G x T mismatch." Nature **407**(6805): 711-717.

Lebbink, J. H. G., A. Fish, et al. (2010). "Magnesium coordination controls the molecular switch function of DNA mismatch repair protein MutS." The Journal of biological chemistry **285**(17): 13131-13141.

Lee, N. K., A. N. Kapanidis, et al. (2007). "Three-color alternating-laser excitation of single molecules: monitoring multiple interactions and distances." Biophys J **92**(1): 303-312.

Lin, D. P., Y. Wang, et al. (2004). "An Msh2 point mutation uncouples DNA mismatch repair and apoptosis." Cancer Res **64**(2): 517-522.

Martik, D., C. Baitinger, et al. (2004). "Differential specificities and simultaneous occupancy of human MutSalpha nucleotide binding sites." The Journal of biological chemistry **279**(27): 28402-28410.

Mazur, D. J., M. L. Mendillo, et al. (2006). "Inhibition of Msh6 ATPase activity by mispaired DNA induces a Msh2(ATP)-Msh6(ATP) state capable of hydrolysis-independent movement along DNA." Molecular cell **22**(1): 39-49.

McCann, J. J., U. B. Choi, et al. (2010). "Optimizing Methods to Recover Absolute FRET Efficiency from Immobilized Single Molecules." Biophys J **accepted**.

Mccann, J. J., U. B. Choi, et al. (2010). "Optimizing Methods to Recover Absolute FRET Efficiency from Immobilized Single Molecules." Biophysical Journal **99**(3): 961-970.

Mendillo, M. L., C. D. Putnam, et al. (2010). "Probing DNA- and ATP-mediated conformational changes in the MutS family of mispair recognition proteins using deuterium exchange mass spectrometry." The Journal of biological chemistry **285**(17): 13170-13182.

Monti, M. C., S. X. Cohen, et al. (2011). "Native mass spectrometry provides direct evidence for DNA mismatch-induced regulation of asymmetric nucleotide binding in mismatch repair protein MutS." Nucleic Acids Research **39**(18): 8052-8064.

Obmolova, G., C. Ban, et al. (2000). "Crystal structures of mismatch repair protein MutS and its complex with a substrate DNA." Nature **407**(6805): 703-710.

Qiu, R., V. C. DeRocco, et al. (2012). "Large conformational changes in MutS during DNA scanning, mismatch recognition and repair signalling." The EMBO journal.

Ross, J., P. Buschkamp, et al. (2007). "Multicolor single-molecule spectroscopy with alternating laser excitation for the investigation of interactions and dynamics." J Phys Chem B **111**(2): 321-326.

Sass, L. E., C. Lanyi, et al. (2010). "Single-molecule FRET TACKLE reveals highly dynamic mismatched DNA-MutS complexes." Biochemistry **49**(14): 3174-3190.

Shell, S. S., C. D. Putnam, et al. (2007). "The N terminus of Saccharomyces cerevisiae Msh6 is an unstructured tether to PCNA." Molecular cell **26**(4): 565-578.

Tessmer, I., Y. Yang, et al. (2008). "Mechanism of MutS searching for DNA mismatches and signaling repair." J Biol Chem **283**(52): 36646-36654.

Wang, H., Y. Yang, et al. (2003). "DNA bending and unbending by MutS govern mismatch recognition and specificity." Proc Natl Acad Sci U S A **100**(25): 14822-14827.

Warren, J. J., T. J. Pohlhaus, et al. (2007). "Structure of the Human MutSalpha DNA Lesion Recognition Complex." Mol Cell **26**(4): 579-592.

Yang, G., S. J. Scherer, et al. (2004). "Dominant effects of an Msh6 missense mutation on DNA repair and cancer susceptibility." Cancer Cell **6**(2): 139-150.

Yang, Y., L. E. Sass, et al. (2005). "Determination of protein-DNA binding constants and specificities from statistical analyses of single molecules: MutS-DNA interactions." Nucleic Acids Res **33**(13): 4322-4334.